METHODS FOR INCREASING THE SENSITIVITY AND THROUGHPUT OF SOLID-STATE NMR SPECTROSCOPY OF PHARMACEUTICAL SOLIDS

By

Loren J. Schieber

B.A., St. Olaf College, 2002
M.S., University of Kansas, 2005

Submitted to the graduate degree program in Pharmaceutical Chemistry
and the Graduate Faculty of University of Kansas
in partial fulfillment of the requirements for the degree of
Doctor of Philosophy.

Dissertation Committee:

_____
Chairperson

_____

_____

_____

_____

Date defended: December 9, 2009

The Dissertation Committee for Loren J. Schieber certifies that this is the approved version of the following dissertation:

METHODS FOR INCREASING THE SENSITIVITY AND THROUGHPUT OF SOLID-STATE NMR SPECTROSCOPY OF PHARMACEUTICAL SOLIDS

Dissertation Committee:

_____
Chairperson

_____

_____

_____

_____

Date approved: January 21, 2010

Abstract

Solid-state nuclear magnetic resonance (SSNMR) spectroscopy has been demonstrated to be a powerful technique for investigating solid dosage formulations. SSNMR has the ability to determine physical form, molecular structure, and dynamics of a pure or formulated active pharmaceutical ingredient (API).

To overcome two of the major shortcomings of SSNMR, acquisition time and sensitivity, a two-sample solids probe was designed, developed, and tested. The prototype was designed according to traditional probe technology. The probe allowed for two samples to be acquired simultaneously while being shuttled through the magnet bore with a stepper motor. The probe exhibited signal to noise ratio (SNR) values comparable to current probes. Pharmaceutical relevance was demonstrated by acquiring a spectrum of ibuprofen and a spectrum of aspirin simultaneously.

^{19}F SSNMR was used to examine low-level amorphous impurities in crystalline physical mixtures. A search for a pharmaceutically relevant fluorine-containing compound was performed. The model compound was chosen for amorphous form stability, cost, and ^{19}F SSNMR spectral resolution between the crystalline and amorphous solid forms. The search included over 20 compounds. Triamcinolone, a corticosteroid, was selected for quantitation studies using ^{19}F SSNMR.

Pure forms of amorphous and crystalline triamcinolone were generated to prepare physical mixtures of varying percentages. The physical mixtures were

studied by SSNMR through two quantitation techniques: spectral acquisition of five times the relaxation time and the difference-NMR technique. The difference-NMR technique exploited the vast ^{19}F relaxation time differences between the amorphous and crystalline forms. With the difference-NMR technique, low levels (<1%) of amorphous triamcinolone were detected.

The effects of paramagnetic oxygen were studied on different pharmaceutical samples. In the presence of oxygen, the ^{19}F relaxation times were significantly lower than in the absence of oxygen. A similar effect was shown on the ^{1}H relaxation times of dextran. Conversely the effect was not demonstrated on a crystalline form of dexamethasone. The relaxation times of cryoground aspirin were compared to bulk as-received material when exposed to oxygenated and deoxygenated conditions. The bulk material had a negligible change in relaxation time. The cryoground material exhibited a large change in relaxation time. Both forms were the same crystalline form and had no discernible differences in SSNMR spectral qualities.

Dedicated to:

Jan Schieber

Acknowledgements

I must thank my graduate advisor, Dr. Eric Munson. Eric has provided me a tremendous amount of personal and professional support during my stay at the University of Kansas. He has instilled in me many qualities that help me to be a better writer, scientist, and person. One of the strongest traits that I will take from him is his ability to take a seemingly complex problem or process and break it down into more simple and intuitive steps. This helped me to be a more effective writer and more capable scientist at troubleshooting hurdles. This is something that I will carry to all aspects of my life. I want to wish him the best on his move to the University of Kentucky.

Next, I would like to thank the previous members of the Munson laboratory: Drs. Tom Offerdahl and Joe Lubach. Tom mentored me in the early stages of my graduate career and helped me to form an appreciation for probe repair, soldering, and bad movies. Joe and I spent a great deal of time together in the lab troubleshooting NMR breakdowns, taking probes apart, and playing yahtzee. I will always appreciate the friendship that Joe and I forged in the basement of McCollum. The current lab members, Ben Nelson, Bob Berendt, Eric Gorman, Diana Sperger, Sarah Pyszczynski, and Elodie Dempah, have all made the Munson laboratory an extremely enjoyable and professional environment. Without these people, I would not be receiving my degree. Ben was instrumental in developing the multiple-sample solids prototype probe. Diana and Bob have been a great source of friendship and

professional motivation. I would like to thank Bob and Sarah for reading and editing a great deal of this dissertation. Most importantly, I must thank Dr. Dewey Barich. Without Dewey, I would still be converting files from xwinNMR to Spinsight for data analysis. Dewey has filled helped fill large holes that have allowed me to perform my research.

Thanks to my dissertation committee member, Drs. Steve Gehrke, Sue Lunte, John Stobaugh, and Cory Berkland for serving on my committee. Thanks to Drs. Lunte and Gehrke for being my dissertation *readers* and providing extremely valuable feedback. Thanks to the entire Department of Pharmaceutical Chemistry. The world-renowned faculty has afforded me a solid scientific foundation to start my career. The women in the office, Ann Heptig, Karen Hall, Nicole Brooks, and Nancy Helm have helped make life a lot less stressful. My fellow students past and present have been a great source of friendship.

Drs. Ales Medek, Mike Perlman, Evgenyi Shalaev, and Ken Waterman of Pfizer Global R&D provided me financial and scientific support. Our scientific talks helped me through a great deal of my scientific hurdles. Ales and Mike acted as surrogate advisors during my time at Pfizer Global. I will always appreciate how diligently Mike prepares for a meeting and the scientific candor of Ales. It has been a privilege work under their guidance and tutelage.

I have been blessed with having a large support group that has helped me through the anxiety of graduate school. In no particular order I want to thank Ben Toht, Andy Eklund, Lee Clark, Anthony Camastro, Meghan Herndon, Katie Sullivan,

Kaci McCall, Kristin Overton, Melanie Pendleton, Leo and Bridgett Zavarse, Case Collard, Justin Pennington, Maulik Trivedi, Jadh Kerr, Brianna Matzke, Raja, Bethany Erickson, Sara Erb, Jenny Kochsiek, Anne Hensley, Melissa Greer, Tracy Hall, Abigail Betts, Emily Marotta, Chriisty Fogleman, Teresa Owens, Sarah Noulles,, Tasha Parman, The Betty's, Natalie Aaron, Team Fun, and everybody else that has made my time in Lawrence amazing.

I would like to specifically thank the *Breakfast Club*, past present, and future. I don't think that you could ever find a better group of storytellers, laughers, and smilers. The original members: Grace Boudewyns, Molly Gaeckle, Steph Horner, and Maggee VanSpeybroeck. These women can perform some of the best impressions and can dissolve an immense amount of stress with the power of laughter. The new members: Jing Jian, Eileen Remley, Jenna Walenga, Maddie Webbe, Ryan Bigley, and future additions.

There have also been lifelong friends and surrogate family that I would like to recognize. The Nanas and Rhoades families have been extremely important in filling in for me as family when my own faltered. To each of them, I'm forever indebted.

Lastly, I'd like to thank my family. My siblings, Craig, *Becky,* Joan, *Andy,* Aaron, Ellen, and Annette. We weren't always very close to each other but in the past few years that has completely changed. The times we get to spend together get more and more enjoyable. I'm very proud of each one of them. The *Adventure Club* (Emma, Chase, Sarah, Will, Andrew, and future members). The nieces and nephews have helped bring our family closer together. This is something that they won't be

aware of for a very long time. My dad. I forgive you. My mom. She has been an inspiration for me throughout my life. Her life has shown me that you can endure some of the hardest times and still come out on top. Everything that I accomplish I owe to you.

Table of Contents

Abstract iii

Dedication v

Acknowledgements vi

Table of Contents x

Chapter 1. Pharmaceuticals in the Solid State 1

1.1 Introduction 2

1.2 Crystalline State 3

1.2.1 Polymorphism 4

1.2.2 Solvates, salts, and co-crystal 8

1.3 Amorphous State 10

1.3.1 Definition of the amorphous state 10

1.3.2 Characterization of the amorphous state 11

1.3.3 Preparation of amorphous solids 14

1.4 Overview of Thesis Research 16

1.4.1 Motivations 16

1.4.2 Importance of solid-state NMR spectroscopy 17

1.4.3 Multiple-sample NMR probe 17

1.4.4 Production of amorphous small-molecule drugs 18

1.4.5 Using ^{19}F SSNMR to study amorphous drugs 19

1.4.6 Effects of oxygen-induced relaxation effects 20

1.5 References 21

Chapter 2. Pharmaceutical Analysis Using Solid-State NMR Spectroscopy 25

2.1 Introduction 26

2.2 Basics of NMR 26

2.2.1 Spin and Resonance 26

2.2.2 NMR Relaxation 29

2.3 Solid-State NMR Spectroscopy 33

2.3.1 NMR spectroscopy for pharmaceutical analysis 33

2.3.2 High-power proton decoupling 34

2.3.3 Magic-angle spinning 35

2.3.4 Cross polarization 38

2.4 Characterization of Bulk Drugs Using SSNMR 40

2.4.1 Background on physical forms 40

2.4.2 Identification of physical form 41

2.4.3 Quantitation of forms 42

2.5 Pharmaceutically Relavant NMR-Observable Nuclei 50

2.6 ^{19}F SSNMR Spectroscopy 51

2.6.1 Comparison to ^{13}C SSNMR spectroscopy 51

2.6.2 Pharmaceutical applications 53

2.6.3 Pharmaceutical applications of 19F SSNMR spectroscopy 55

2.7 Conclusions 57

2.8 References 59

Chapter 3. Multiple-Sample Probe for Solid-State NMR Spectroscopy 62

3.1 Introduction 63

3.2 Probe Concept and Design Considerations 68

3.2.1 Probe concept 68

3.2.2 Magnetic field strength along the magnet bore 72

3.2.3 Objectives 72

3.3 Experimental 72

3.3.1 Samples 72

3.3.2 Solid-state NMR spectroscopy 74

3.4 Results 74

3.5 Conclusions 84

3.6 References 85

Chapter 4. Model Compound Selection 90

4.1 Introduction 91

4.1.1 Background 91

4.1.2 Generating stable amorphous compounds 92

4.2 Selecting a Model Amrophous Compound as Quantitation Standard 93

4.3 Experimental 96

4.3.1 Materials 96

4.3.2 Sample preparation 96

4.3.2.1 Cryogrinding 97

4.3.2.2 Spray drying 97

4.3.3 Sample analysis 98

4.3.3.1 Differential scanning calorimetry (DSC) 98

4.3.3.2 Solid-state NMR spectroscopy 98

4.3.3.3 Polarized-light microscopy 100

4.4 Results 100

4.4.1 Introduction to sample selection 100

4.4.2. Initial compound selection 101

4.4.3 Partial amorphous generation 104

4.4.4 Lack of chemical shift resolution 106

4.4.5 Crystallization of the amorphous material 109

4.4.6 Model compound – triamcinolone 112

4.4.7 Uniform mixing of standards 118

4.4.8 Temperature effects on chemical shifts of triamcinolone 123

4.5 Conclusions 127

4.6 References 128

Chapter 5. Quantitation of a Low-Level Amorphous Impurity 132

5.1 Introduction 133

5.1.1 Presence of amorphous materials in formulation 133

5.1.2 Analytical methods for quantitation of amorphous solids 134

5.1.3 ^{13}C SSNMR spectroscopy 137

5.1.4 ^{19}F SSNMR spectroscopy 139

5.1.5 Prevalence of fluorine in pharmaceuticals 141

5.1.6 NMR quantitation 142

5.1.7 Triamcinolone as a model compound 151

5.1.8 Strategy for quantitation mixtures using ^{19}F SSNMR 151

5.2 Experimental 153

5.2.1 Materials 153

5.2.2 Cryogrinding 155

5.2.3 Spray drying 156

5.2.4 SSNMR spectroscopy 156

5.2.5 Data conversion XWin-NMR to Spinsight 159

5.3 Results 160

5.3.1 Solid forms of triamcinolone 160

5.3.2 Quantitation attempt one 164

5.3.3 Quantitation attempt two 166

5.3.4 Quantitation attempt three 170

5.4 Conclusions 189

5.5 References 191

Chapter 6. Effect of Gaseous Oxygen on Solid-State NMR Relaxation times 195

6.1 Introduction 196

6.1.1 Background 196

6.1.2 Relaxation time changes 197

6.2 Experimental 200

6.2.1 Materials 200

6.2.2 Sample preparation and handling 200

6.2.3 Solid-state NMR spectroscopy 201

6.3 Results 203

6.3.1 Observation of changing NMR relaxation times 203

6.3.2 Testing the cause of the relaxation change 209

6.3.3 Dextran 215

6.3.4 Dexamethasone 216

6.4 Other Applications 219

6.4.1 Difference-NMR technique 219

6.4.2 Processing of aspirin 220

6.5 Conclusions 223

6.6 References 224

Chapter 1

Pharmaceuticals in the Solid State

1.1 Introduction

A solid formulation is the preferred delivery method for pharmaceuticals for several reasons. First, drugs tend to be more chemically stable in the solid state than in solution. Second, solid dosage forms are much more convenient for patients, which improves patient compliance. Third, solid dosage forms are easier to store, transport, and manufacture.

Solid drug formulations such as tablets are mixtures of the active pharmaceutical ingredient (API) and excipients, coatings, and other components. Solid formulations are complex because of the need to process the drug into a uniform dosage form that has a predictable dissolution rate. Because the physical form of the drug in the solid state plays such an important role in the dissolution of the drug, it is important to know which physical forms are present in solid drug formulations during different stages of manufacturing and upon storage.

Aqueous solubility of the API is an important concern during formulation, because it limits the overall bioavailability of the drug. Different solid forms may have different solubilities. In many cases, the solubility of the individual crystalline forms is not sufficient to proceed with formulation. Sometimes amorphous solids are selected over their crystalline counterparts as the desired form because of their increased solubility.[1] Although the dissolution rate may be faster, the amorphous form is metastable to the crystalline form. The balance between having increased

stability (chemical and physical) but a lower dissolution rate is a common dilemma in solid-state drug development.

Identification of which solid forms of an API are present in a formulation is critical to determining if a solid dosage form will perform properly. The focus of much of this dissertation is on the characterization of solid API in crystalline and amorphous forms using primarily solid-state NMR spectroscopy. A basic description of crystalline and amorphous states is described in the following sections.

1.2 Crystalline State

A crystalline solid is a material in which the atoms and/or molecules are arranged in a highly ordered and repeating fashion.[2] The basic repeating unit of a crystalline solid is the unit cell. The unit cell is the building block for a larger particle, and the conformation and packing of molecules within the unit cell is optimized to minimize void space or free volume while maximizing the favorable intermolecular interactions, including both ionic and non-covalent forces. These interactions can lead to different solid-state forms, morphologies, and crystal habits. A crystalline material can exhibit polymorphism and/or pseudopolymorphism (solvates and hydrates), and can exist as a salt and co-crystal. Each crystalline form may have unique physicochemical properties. A solid form that is selected for development must be physically and chemically stable but with sufficient solubility and bioavailability. If the incorrect crystalline form is chosen during development,

there is a risk of conversion between forms. If conversion could occur during formulation, manufacturing, or storage, then the drug may need to be reformulated.[3] Due to the importance of stability and solubility on the success of a drug product, a thorough selection process should occur to select the best solid form for the most robust and successful formulation. The differences in crystalline and amorphous solid forms will be discussed further below.

1.2.1 Polymorphism

The ability of a compound to adopt two or more crystalline states that differ in the conformation and/or arrangement of molecules in the crystal lattice is termed polymorphism.[2] The presence of multiple polymorphic forms is very common for small organic molecules, especially pharmaceuticals. Depending on which source is cited, polymorphism occurs in 32-57% of small organic molecules, and if solvates are included, the range rises to 56-87%.[4-6] Despite the wide approximated estimations, it is evident that polymorphism is extremely prevalent. Each polymorphic form has a different free energy and can be relatively more or less stable when compared to another polymorph at a given temperature. Differences in packing structure and thermodynamics between polymorphic forms give rise to differences in physicochemical properties such as melting point, density, hygroscopicity, solubility, and overall chemical and physical stability of the solid. If the physical form of an API changes during processing or manufacturing, the physicochemical properties might be different, and the intended dose may not be delivered due to an altered

dissolution profile. These properties are all important to consider when developing a safe and efficacious solid drug product.[2,7-9] Therefore, it is necessary to screen a drug candidate for polymorphs, and, in most cases, select the most thermodynamically stable form for development. The thermodynamically stable form will not spontaneously crystallize into a less stable polymorph, so formulating and developing the most stable polymorphic form helps limit physical conversions of the drug substance.

Polymorphs can be either monotropically or enantiotropically related. When one crystal form is always thermodynamically less stable than another form, the two polymorphic forms have a monotropic relationship. Figure 1.1 illustrates the thermodynamics of a montropic relationship between two polymorphic forms, A and B. At any temperature below the melting temperature of either form, the Gibb's free energy of polymorphic form A (G_A) is always lower than the free energy of form B (G_B). A theoretical inversion of free energy does exist between the two forms; however, the inversion occurs above the melting temperatures of both forms and will not be observed. Figure 1.2 shows the energy-temperature diagram for enantiotropically-related polymorphic forms A and C. The difference between the two energetic relationships is the presence of a transition temperature, T_t.[10] At the T_t, the Gibbs free energy relationship between forms A and C inverts. Below T_t, form A is thermodynamically more stable, and above T_t, form C is more stable. The T_t must

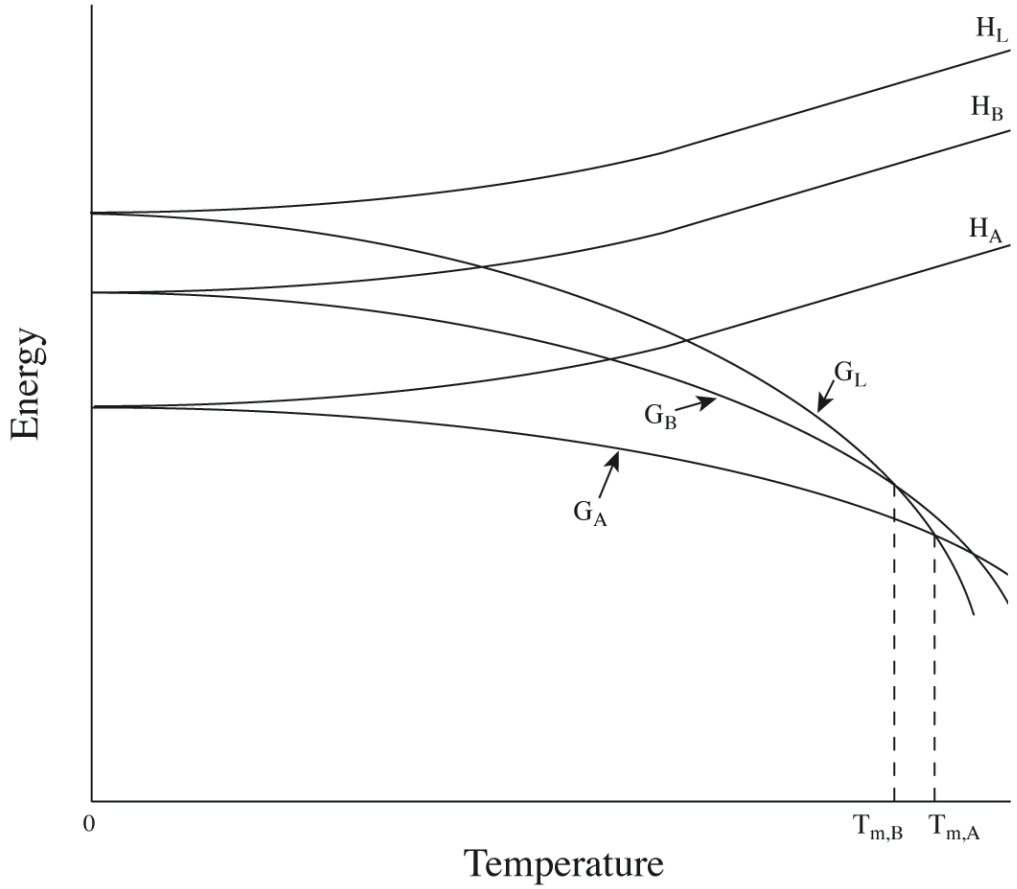

Figure 1.1. Theoretical energy versus temperature diagram of a monotropic system. G_A and G_B are the free energies of two monotropically related polymorphs (Forms A and B), and G_L is the free energy of the liquid. H_A, H_B, and H_L are the respective enthalpies for each form. The melting temperatures of Forms A and B are denoted by $T_{m,A}$ and $T_{m,B}$, respectively. Adapted from reference 11.

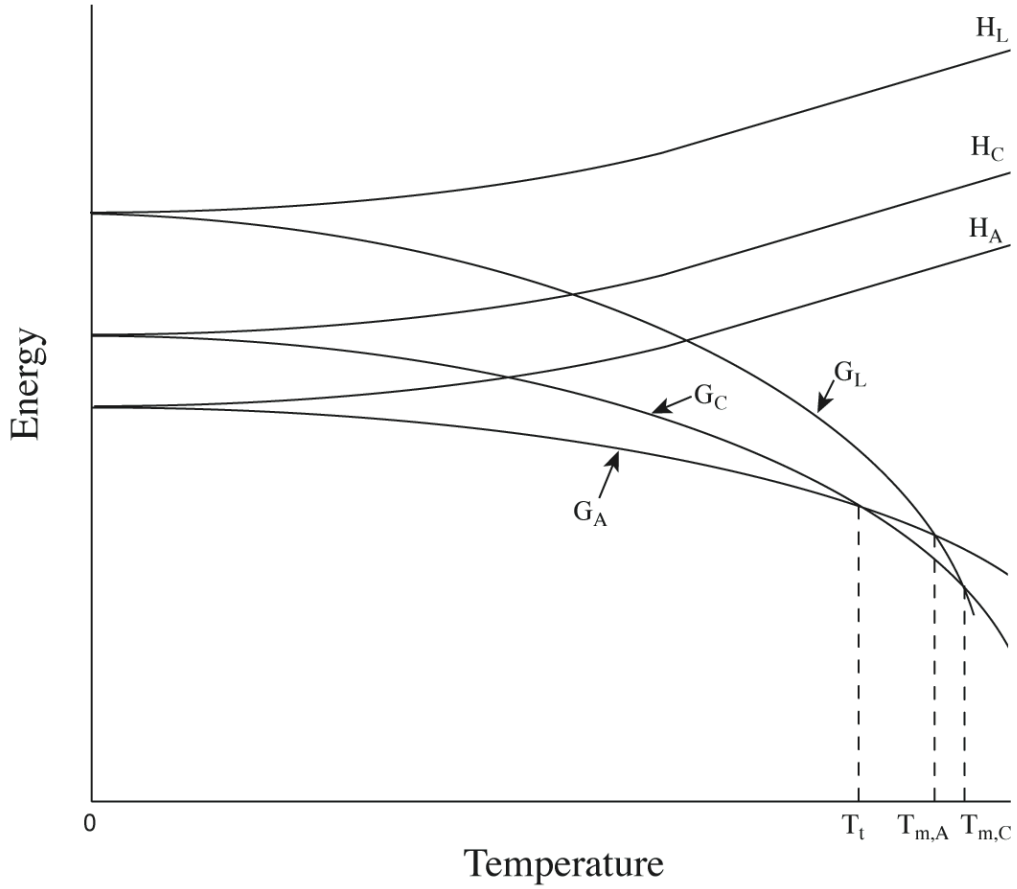

Figure 1.2. Theoretical energy versus temperature diagram of an enantiotropic system. G_A and G_C are the free energies of two enantiotropically related polymorphs (Forms A and C), and G_L is the free energy of the liquid. H_A, H_C, and H_L are the respective enthalpies for each form. The melting temperatures of Forms A and C are denoted by $T_{m,A}$ and $T_{m,C}$, respectively. The thermodynamic inversion of two enantiotropically related polymorphs occurs at a transition temperature, T_t. Adapted from reference 11.

occur prior to the melting point of either form, $T_{m,A}$ and $T_{m,C}$.

Monotropic and enantiotropic polymorphic systems can be determined by plotting the log of solubility versus temperature for two polymorphic forms. If the system is monotropic, the solubility profiles will not intersect below the melting temperature of either form. If the system is enantiotropic, the lines will cross, and the energetic relationship will invert at the T_t.

Additionally, the energetic relationship between polymorphs can be determined by the "heat of transition" and "heat of fusion" rules constructed by Burger and Ramberger.[11,12] The *heat of transition rule* states that two forms are related enantiotropically if an endothermic transition is observed between two forms at some temperature. On the other hand, if an exothermic transition is observed between two forms at some temperature it may be assumed that the two forms are monotropically related. The *heat of fusion rule* states that if the lower melting polymorphic form has the higher heat of fusion, then the two forms are related enantiotropically.[13]

1.2.2 Solvates, salts, and co-crystals

In addition to polymorphs, a compound can also crystallize as a solvate, salt, or a co-crystal.[2] The crystal form is termed a solvate when a solvent molecule is incorporated into the crystal lattice. If the solvent of interest is water, then the solvate is designated a hydrate. Solvates are also referred to as pseudopolymorphs and solvatomorphs in the literature.[13-15] The ratio of solvent to the molecule of interest

can occur in stoichiometric or non-stoichiometric ratios. When the solvent is incorporated into the crystal lattice in an orderly manner, typically in integer or half-integer ratios, it is referred to as stoichiometric. When the solvent is incorporated in a less defined manner, the solvate is non-stoichiometric. An example of a non-stoichiometric is a channel hydrate, where water molecules can move with relative ease through channels in the crystal lattice. Like polymorphs, solvates have different free energies, which will result in different physico-chemical properties in relation to the desolvated forms.

If a compound has a low aqueous solubility, stability issues, permeability, or other undesirable properties, a salt form can be prepared.[16] Salts of a compound can be formed when the compound has acidic or basic ionizable functional groups. A salt form is generated by crystallization of the drug substance with a complementary counterion forming a strong ionic interaction. Salts often have more favorable physicochemical properties than the free-base or free-acid form, which makes them good options for solid dosage formulations. Common acidic negative, anions for basic drugs are hydrochloride, sulfate, and acetate, whilst the common alkaline positive, cations for acidic drugs are sodium, magnesium, and potassium.[17] Approximately 50% of drugs used in medicinal therapy are administered as salts, which justifies preformulation salt screening.[17]

The last crystalline form to discuss is the co-crystal, which is formed when two compounds that are solids at room temperatures crystallize stoichiometrically in the same crystal lattice.[18] The changes in structure and composition of a co-crystal

could affect the bioavailability and intellectual property of the drug.[18] Formation of a co-crystal occurs when two different molecules have complementary functional groups that interact, typically through hydrogen bonds, more favorably than either molecule by itself. Co-crystals are most commonly formed from solution, yet grinding, milling, and growth from a melt are also possible methods of crystal formation.[18]

In the solid state, form selection is extremely important and should be performed early in development to identify potential issues with bioavailability and stability early. With the exception of co-crystals, high-throughput screening is typically performed for each crystalline form. In some cases, the crystalline form of the API cannot be formulated because the form has extremely poor solubility and bioavailability. For these compounds, the amorphous state of the API could be used as an alternative to enhance the solubility.

1.3 Amorphous State

1.3.1 Definition of the amorphous state

The word "amorphous" originated from the Greek word "αμορφος," which means "shapeless."[19] Amorphous materials are highly disordered systems that lack the long-range order that is characteristic of crystalline solids. However it should be noted that amorphous solids might maintain some short-range order on the molecular level.[20] The amorphous form is thermodynamically metastable compared to the

crystalline form. As compared to the crystalline forms, the amorphous form will likely have different physicochemical properties such as increased solubility and hygroscopicity, which generally lead to enhanced bioavailability and decreased stability.[1]

The amorphous state can be used as the desired solid form in a drug product to enhance the solubility of the API. However, the amorphous state is examined more often as a physical impurity that was produced during development or manufacturing. Undesired amorphous material can be generated in low levels from heat, pressure, or other high-energy manufacturing processes. The physical degradation of the solid form can lead to changes in solubility and bioavailability of the API. Additionally, the lack of stability of the amorphous material could raise a drug's susceptibility to chemical degradation. The physical and/or chemical degradation of the amorphous form can affect the therapeutic integrity of the solid dosage form. Thus it is important to monitor amorphous content at low levels in a formulation.

1.3.2 Characterization of the amorphous state

Basic identification of the amorphous state of a compound is most commonly determined by the lack of microscopic birefringence, and/or a broad (or no) powder pattern by powder X-ray diffraction. Additionally, the peaks in a solid-state NMR spectrum of an amorphous solid can be 10 times broader than the peaks of its crystalline counterpart.[21] The increased breadth of the NMR peaks is attributed to the lack of long-rage order in the amorphous state.

To further characterize the amorphous state, it is helpful to understand the thermodynamic relationship between the crystalline and amorphous forms as well as the liquid state. Shown in Figure 1.3 is a graphical depiction of the change in enthalpy with temperature of the three states (crystalline, amorphous, and liquid).[20] At lower temperatures, the enthalpy of a crystalline solid experiences small changes in enthalpy with respect to temperature. When the crystalline solid reaches the melting temperature, T_m, there is a pronounced jump in enthalpy (ΔH_m) that corresponds to a solid-liquid phase transition. If the liquid state is cooled rapidly below the T_m, there may not be sufficient time to allow the material to crystallize. When this occurs, the material is defined as an amorphous solid or *supercooled liquid*, maintaining the structural characteristics of a liquid with increased viscosity. If the enthalpy of the supercooled liquid continued to decrease at the same rate at lower temperatures, the supercooled liquid would eventually have a lower enthalpy than the crystalline solid. The theoretical intersection is a critical temperature referred to as the Kauzmann temperature (T_K). Below this temperature, the supercooled liquid theoretically would have a lower enthalpy then the crystalline solid. Therefore, a transition, or change in slope, could be considered a thermodynamic requirement for the system.[20]

Prior to reaching the enthalpy of the crystalline state, the slope of the enthalpy-temperature relationship of the supercooled liquid changes significantly. This change occurs at the glass transition temperature (T_g). Above the T_g, the amorphous material is highly mobile and termed the *rubbery state*, and at

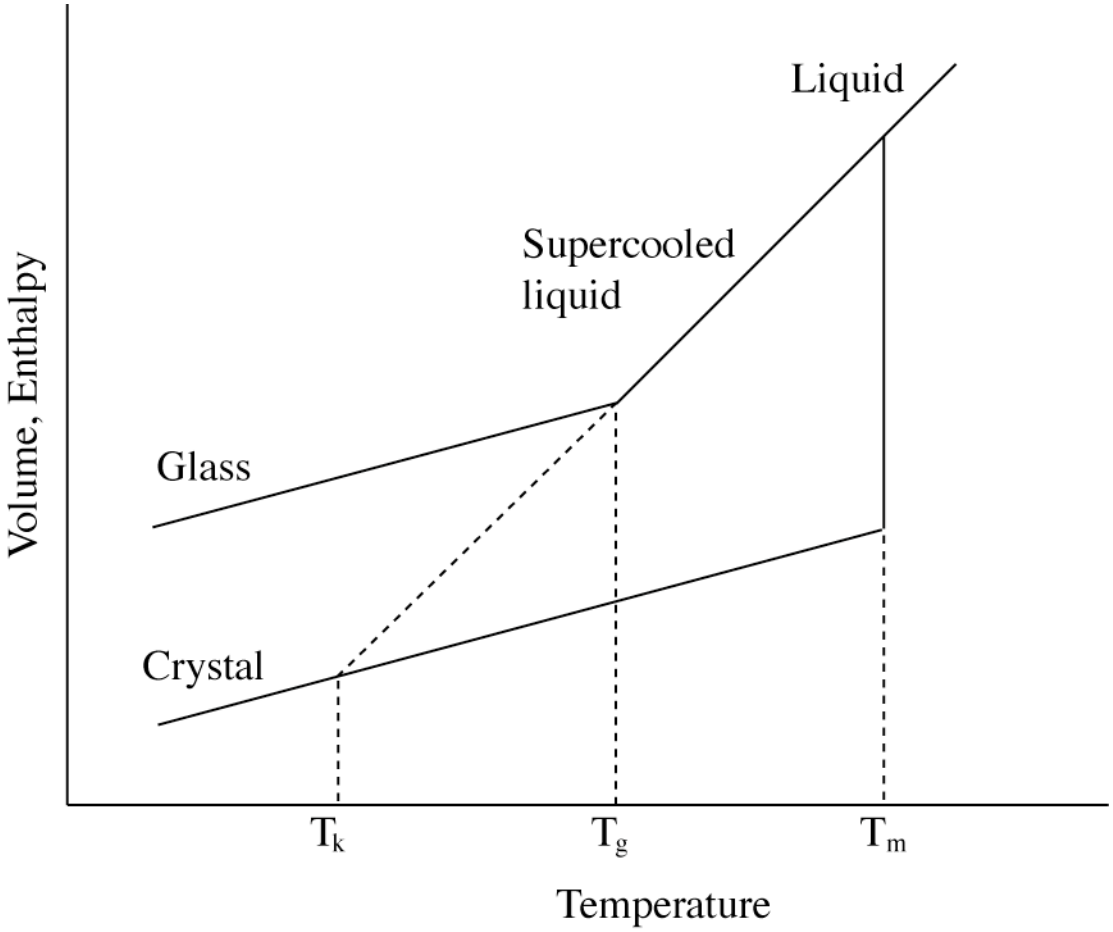

Figure 1.3. Graphical relationship of variation of enthalpy with temperature for amorphous and crystalline solids.

temperatures below the T_g, the material is termed the *glassy state*. The change in mobility is a contributing factor to why the T_g is the primary defining characteristic of an amorphous solid. Despite being the primary characteristic of an amorphous solid, the T_g can be difficult to detect and can change with thermal history and water content. Ahlneck et al. noted that water plasticized the glass transition of amorphous solids, lowered the glass transition temperature, which increased the rate of crystallization.[22]

The amorphous state can be characterized through a wide variety of instrumental techniques. The techniques can be classified in four main categories: thermal methods, dissolution techniques, crystallographic techniques, and spectroscopy. Thermal (e.g. DSC, TGA, hot stage microscopy) and dissolution techniques provide bulk information of the material such as the glass transition temperature, birefringence (or lack thereof), and dissolution rate. Crystallographic and spectroscopic techniques can yield information on the molecular level for a material. Using powder X-ray diffraction (PXRD), the amorphous state will be observed as a diffuse "halo." The peaks of the amorphous state in a solid-state NMR spectrum are much broader than its crystalline counterpart. Because NMR spectroscopy detects changes in the local environment, the chemical shifts of NMR peaks in a solid-state spectrum can be different between amorphous and crystalline forms.

1.3.3 Preparation of amorphous solids

The amorphous state of small-molecule organic solids is commonly generated by four techniques: quench cooling a melt, milling, spray drying, and lyophilization.[23]

Quench cooling a melt involves rapidly cooling a melted drug typically by immersion in liquid nitrogen. Ideally, the molecular disorder in the liquid state is frozen before the molecules can rearrange into a crystal lattice. This technique is often the first method used to prepare the amorphous form. However, many small-molecule organic compounds degrade upon melting.

Another process for generating an amorphous form is milling or grinding the compound. The material is subjected to a high amount of mechanical stress, which reduces the particle size until the order of the crystal lattice is destroyed. At times, milling can induce thermal degradation from the heat generated during the process. To reduce the likelihood of thermal degradation, grinding can be performed in a liquid nitrogen bath. This process is referred to as cryomilling or cryogrinding.

Another process for generating the amorphous state is by controlled removal of the solvent from a solution of the compound. Lyophilization and spray drying are two techniques that employ this process. During lyophilization, the material is dissolved in a solvent (typically water) that exhibits a triple point. The solution is frozen and exposed to a vacuum. The frozen solution goes through two drying processes: primary and secondary. During primary drying, the water sublimes from the lyophilization matrix. In the secondary phase, the residual, bound water is removed. When frozen, the material is locked in the random disorder of the liquid state. As the water sublimes, the material may maintain the structural disorder of the

liquid state. In contrast, during spray drying, the solution of drug and solvent is sprayed through a heated nozzle at a temperature higher than the boiling point of the solvent. The solvent evaporates rapidly, leaving behind small particles of highly disordered solid. Lyophilization is generally limited to samples with a fairly high aqueous solubility, whereas spray drying can be performed with organic solvents under the proper conditions.

The amorphous state can also be generated by dehydrating crystalline hydrates and solid dispersions. Solid dispersions are used to enhance the bioavailability of a drug product by creating a matrix of the amorphous form of the drug and a carrier, usually an excipient. This is commonly used for drugs that are too insoluble to provide an efficacious dose.

1.4 Overview of Thesis Research

1.4.1 Motivations

Understanding the solid-state properties of a drug substance is paramount to the success of a solid drug product. The amorphous state is a very important topic because of the regulatory concerns regarding low-level presence in a formulation. Current instrumentation and techniques are very limited in the ability to study low levels of drugs in formulation. Solid-state NMR spectroscopy has the potential to differentiate between the API and the excipients. However, the low sensitivity of the ^{13}C nucleus means that SSNMR can be time and cost prohibitive, which limits the

feasibility for some applications, particularly quantitation of low-levels of amorphous material. The research presented in this thesis is aimed at ways to increase the sensitivity of solid-state NMR spectroscopy for studying solid-state pharmaceuticals through two approaches: 1) the design, construction and testing of a multiple-sample NMR probe and 2) the detection and quantitation of low levels of an amorphous drug in a crystalline physical mixture using ^{19}F SSNMR spectroscopy.

1.4.2 Importance of solid-state NMR spectroscopy

Although there is no single characterization technique that can garner all the necessary information on a solid drug or drug product, solid-state NMR spectroscopy (SSNMR) is emerging as a valuable technique for determining the state of the API in a formulated product. The technique is non-invasive, non-destructive, inherently quantitative, and has the ability to discriminate between different crystalline and amorphous forms as well as excipients. In Chapter 2, the theory and applications of SSNMR will be presented. Several articles that highlight the application of SSNMR will be reviewed. Additionally, the ^{19}F nucleus will be closely examined as a high-sensitivity alternative to ^{13}C, when applicable. A brief review of literature pertaining to ^{19}F SSNMR of pharmaceuticals will be presented.

1.4.3 Increasing sensitivity and throughput with a multiple-sample NMR probe

SSNMR is a powerful analytical technique, but there are a few drawbacks. The inherent lack of sensitivity of the ^{13}C nucleus and long NMR relaxation times

require extensive signal averaging and long (hours to days) data acquisition times. These long acquisition times hinder the routine use of SSNMR in the analysis of drugs at the preformulation and formulation stages of drug development.

In Chapter 3, the first research project is presented, which increases the throughput and sensitivity of SSNMR. The design, construction, and proof of concept are demonstrated on a two-module multiple sample probe for SSNMR. SSNMR spectra are presented that show simultaneous data acquisition on identical samples of hexamethyl benzene. Additionally, spectra on two different pharmaceutically relevant samples with significantly different NMR relaxation times were collected simultaneously (aspirin and ibuprofen). The probe can be used to increase throughput by a factor of two or increase sensitivity by acquiring data on the same sample packed in two rotors.

1.4.4 Production of stable amorphous small molecules

In Chapters 4 and 5 the alternative of using ^{19}F SSNMR to quantitate crystalline and amorphous forms is shown. Very few techniques can measure low-level limits of amorphous material in a crystalline physical mixture, and no current techniques can be used to measure low-levels (>1%) of amorphous material in a formulation. ^{13}C SSNMR is partially limited because of the inherent insensitivity. ^{19}F SSNMR spectroscopy was employed to detect and quantitate low levels of amorphous material in a crystalline physical mixture. A process was designed to select the ideal model compound for the ^{19}F SSNMR studies. In Chapter 4, the

sample screening process is outlined for selecting a fluorinated drug for low-level amorphous quantitation. Approximately twenty drugs were examined as potential candidates. Many of the drugs were not approved for this proof-of-concept study due to issues such as physical or chemical stability, limited aqueous solubility for spray drying and lyophilization, chemical degradation at the melting point, inability to amorphize the compound, or there was limited chemical shift resolution from the crystalline peaks in the ^{19}F SSNMR spectra. Triamcinolone was selected as the model form for low-level amorphous quantitation using ^{19}F SSNMR. Once the model form was selected, the crystalline polymorphs were studied, and the amorphous generation technique was optimized.

1.4.5 Using ^{19}F SSNMR spectroscopy to quantitate low levels of amorphous drug

In Chapter 5, physical mixtures of the amorphous and crystalline forms of triamcinolone were prepared and examined with ^{19}F SSNMR. Two unsuccessful quantitation attempts are presented. In the first attempt, stability concerns of the amorphous state required low-temperature conditions during data acquisition. Straightforward quantitation from a single spectrum did not provide sufficient expression of the amorphous form. In the second quantitation attempt, the difference-NMR technique was used.[24] Two SSNMR spectra were collected with different pulse delays and spectrally subtracted to increase the suppression of the crystalline form. During this attempt, form conversion was observed, and the NMR relaxation times of the amorphous and crystalline components were unstable. Finally, physical

mixtures of stable amorphous and crystalline forms were prepared and analyzed with the difference-NMR technique. The technique exhibited great power in suppressing the crystalline form, and detected the amorphous form in the 0.5% physical mixture.

1.4.6 Effect of oxygen-induced relaxation phenomenon

When performing the difference-NMR technique, accurate determination of NMR relaxation times is extremely important. During the second quantitation attempt in Chapter 5, the relaxation time of amorphous triamcinolone increased 3-4 fold during an overnight experiment. After removing the sample from the spectrometer, the relaxation time returned to the initially measured value, and followed a similar relaxation time profile overnight. In Chapter 6, the relaxation change was studied and determined to arise from oxygen being purged from the sample rotor while spinning. The effect of oxygen was demonstrated on amorphous and crystalline material as well as both ^{19}F and ^{1}H nuclei. Aspirin was cryoground and cycled through oxygen-rich, nitrogen-rich, and oxygen rich environments. The NMR relaxation times were measured under each condition and compared to a bulk sample treated identically. The changes in relaxation time highlight the importance in accurate determination of NMR relaxation times, and the changes in relaxation time upon exposure to oxygen. The effect of oxygen on NMR relaxation gives us a potential probe to measure the presence of oxygen in solid-state pharmaceutical samples.

1.5 References

1. Hancock BC, Parks M 2000. What is the true solubility advantage for amorphous pharmaceuticals? Pharmaceutical Research 17(4):397-404.

2. Byrn SR, Pfeiffer RR, Stowell JG. 1999. Solid-State Chemistry of Drugs. Second ed., West Lafayette, IN: SSCI Inc. p 574.

3. Bauer J, Spanton S, Henry R, Quick J, Dziki W, Porter W, Morris J 2001. Ritonavir: an extraordinary example of conformational polymorphism. Pharmaceutical Research 18(6):859-866.

4. Hilfiker R. 2006. Polymorphism in the Pharmaceutical Industry. ed., Wienheim, Germany: WILEY-VCH Verlag GmbH & Co. KGaA. p 414.

5. Henck J-O, Griesser UJ, Burger A 1997. Polymorphie von Arzneisstoffen. Pharmaceutical Industry 59(2):165-169.

6. Storey R, Docherty R, Higginson P, Dallman C, Gilmore C, Barr G, Dong W 2004. Automation of solid form screening procedures in the pharmaceutical industry - How to avoid the bottlenecks. Crystallography Reviews 10(1):45-56.

7. Byrn SR, Pfeiffer RR, Stephenson G, Grant DJW, Gleason WB 1994. Solid-State Pharmaceutical Chemistry. Chemistry of Materials 6(8):1148-1158.

8. Pikal MJ 1999. Impact of polymorphism on the quality of lyophilized products. Drugs Pharm Sci 95(Polymorphism in Pharmaceutical Solids):395-419.

9. Karpinski PH 2006. Polymorphism of active pharmaceutical ingredients. Chemical Engineering & Technology 29(2):233-238.

10. Katrincic LM, Sun YT, Carlton RA, Diederich AM, Mueller RL, Vogt FG 2009. Characterization, selection, and development of an orally dosed drug polymorph from an enantiotropically related system. International Journal of Pharmaceutics 366(1-2):1-13.

11. Burger A, Ramberger R 1979. On the polymorphism of pharmaceuticals and other molecular crystals. I. Theory of thermodynamic rules. Mikrochimica Acta 2(3-4):259-271.

12. Burger A, Ramberger R 1979. On the polymorphism of pharmaceuticals and other molecular crystals. II. Applicability of thermodynamic rules. Mikrochimica Acta 2(3-4):273-316.

13. Byrn SR, Sutton PA, Tobias B, Frye J, Main P 1988. Crystal structure, solid-state NMR spectra, and oxygen reactivity of five crystal forms of prednisolone tert-butylacetate. Journal of the American Chemical Society 110(5):1609-1614.

14. Brittain HG 2007. Polymorphism and solvatomorphism 2005. Journal of Pharmaceutical Sciences 96(4):705-728.

15. Brittain HG 2005. Polymorphism and solvatomorphism 2004. Profiles of Drug Substances, Excipients, and Related Methodology 32:263-283.

16. Kumar L, Amin A, Bansal AK 2007. An overview of automated systems relevant in pharmaceutical salt screening. Drug Discovery Today 12(23&24):1046-1053.

17. Wermuth CG, Stahl PH. 2002. Introduction. In *Handbook* of Pharmaceutical Salts: Properties, Selection and Use. ed.: WILEY-VCH.

18. Vishweshwar P, McMahon Jennifer A, Bis Joanna A, Zaworotko Michael J 2006. Pharmaceutical co-crystals. Journal of Pharmaceutical Sciences 95(3):499-516.

19. Cheng YT, Johnson WL 1987. Disordered materials: a survey of amorphous solids. Science (Washington, DC, United States) 235(4792):997-1002.

20. Hancock BC, Zografi G 1997. Characteristics and Significance of the Amorphous State in Pharmaceutical Systems. Journal of Pharmaceutical Sciences 86(1):1-12.

21. Offerdahl TJ, Salsbury JS, Dong Z, Grant DJW, Schroeder SA, Prakash I, Gorman EM, Barich DH, Munson EJ 2005. Quantitation of crystalline and amorphous forms of anhydrous neotame using ^{13}C CPMAS NMR spectroscopy. Journal of Pharmaceutical Sciences 94(12):2591-2605.

22. Ahlneck C, Zografi G 1990. The molecular basis of moisture effects on the physical and chemical stability of drugs in the solid state. International Journal of Pharmaceutics 62(2-3):87-95.

23. Hancock BC, Zografi G 1997. Characteristics and significance of the amorphous state in pharmaceutical systems. Journal of Pharmaceutical Sciences 86(1):1-12.

24. Harris DJ, de Azevedo ER, Bonagamba TJ 2003. Difference-NMR techniques for selection of components on the basis of relaxation times. Journal of Magnetic Resonance 162(1):67-73.

Chapter 2

Pharmaceutical Analysis Using Solid-State NMR Spectroscopy

2.1 Introduction

In Chapter 1, the basics of the solid-state chemistry of pharmaceuticals were provided. The focus of this chapter is the application of nuclear magnetic resonance (NMR) spectroscopy for the analysis of pharmaceuticals in the solid state. Solid-state NMR (SSNMR) spectroscopy has developed into an extremely powerful analytical tool for pharmaceuticals in the solid state. SSNMR is a non-destructive, non-invasive technique that can obtain unique information about the structure and dynamics of drugs in pharmaceutical formulations. SSNMR can be used for a variety of applications from routine collection of NMR spectra of drug substance to multi-dimensional analyses of drug product. For pharmaceutical systems, ^{13}C spectra are typically collected. An understanding of some basics of NMR and the differences between collecting solution and solid-state data are necessary to fully understand the strengths and weaknesses of SSNMR and are reviewed below.

2.2 Basics of NMR

2.2.1 Spin and Resonance

All nuclei have a spin quantum number, typically referred to as "I". Certain nuclei have NMR 'active' spins. Nuclei that have a spin quantum number of zero (I = 0) do not produce an NMR signal. Nuclei with a non-zero spin quantum number in multiples of ½ (I = 1/2, 1, 3/2, 2, 5/2, etc.) have angular momentum, P, and charge.

The motion of charge generates a small magnetic moment, μ. Angular momentum and magnetic moment are related in Equation 2.1.

$$\mu = \gamma P \tag{2.1}$$

The term γ is the magnetogyric ratio and defined as the ratio of angular momentum to magnetic moment. The magnetogyric ratio is a constant for a given nucleus. Because the energy states are quantized, the magnetic moments exist in distinct numbers of spin states. The number of spin states are determined by the spin quantum number, *I*. There are 2I+1 potential spin states. For example, a spin I = 1/2 nucleus such as ^{13}C has two possible spin states. The spin states can be thought of as being antiparallel to each other. When an I $\neq$ 0 nucleus is exposed to a static, external magnetic field, the energy states become non-degenerate. For example, the spins that are aligned with the static magnetic field have a lower energy. One spin state is aligned with the external magnetic field and the other against.

A magnetic moment within an external field experiences torque, which causes the nucleus to precess around the axis of the field. The precession is commonly referred to as Larmor precession, and the frequency of precession is related to the magnetogyric ratio of each nucleus. The motion is defined by the angular velocity (ν) and is defined in Equation 2.2.

$$\nu = \frac{-\gamma B_0}{2\pi} \tag{2.2}$$

The direction of precession, clockwise or counter-clockwise, is determined by the sign of γ, but the direction is always the same for a given nuclide. In order for nuclear magnetic resonance to occur a nucleus must change its spin state by the absorption of quantized energy specific to the Larmor precession frequency. The appropriate energy can be determined from Equation 2.3.

$$\Delta E = h\nu = \frac{h\gamma B_0}{2\pi} \tag{2.3}$$

The Larmor frequency is proportional to the external magnetic field (B_0). NMR spectrometers are typically equipped with magnets between 2.35 and 21.15 T (tesla). Magnet field strengths are often referred to by their proton resonance frequency. Magnets with the field strengths described above would have a proton resonance range of 100-900 MHz in the radiofrequency portion of the electromagnetic spectrum.

As noted above, when a nucleus with spin I=1/2 is exposed to an external field, two spin states exist, +½ or α and -½ or β, that have different energy values. Because the α state is parallel to the magnetic field, it has a lower energy than does the β state. At magnetic equilibrium there will be an excess of nuclei in the α state. The population distribution of spins between the two states is defined by the Boltzmann distribution in Equation 2.4.

$$\Delta N_o = Ne^{\Delta E/k_b T} \tag{2.4}$$

N corresponds to the number of nuclei present, $\Delta E = \gamma \hbar B_o$ ($\hbar$ is Plank's constant divided by 2π), k_b is the Boltzmann constant, and T is absolute temperature. The difference in energy levels of spin states is extremely small. The small energy difference is the reason NMR is very insensitive compared to other techniques.

2.2.2 NMR relaxation

After the spins have been perturbed from their equilibrium values, they must return to their original state prior to the perturbation. This process is called relaxation, and there are three basic types of relaxation in NMR spectroscopy: spin-lattice (T_1), spin-spin relaxation (T_2), and spin-lattice relaxation in the rotating frame ($T_{1\rho}$).

An understanding of the spin-lattice relaxation (T_1), or longitudinal relaxation, is important when collecting a spectrum, quantitating components in a sample, or studying the dynamics of a system. T_1 relaxation occurs when the equilibrium spin states are repopulated after a 90° radiofrequency (RF) pulse. The magnetization follows an exponential behavior described by Equation 2.5.

$$M_z = M_0\left(1 - e^{-t/T_1}\right) \tag{2.5}$$

M_0 is the magnetization at thermal equilibrium and M_z is the magnetization along the +z axis at time t. T_1 is a first order time constant for the re-establishment of the original spin-state populations. In order for spins to fully relax after a pulse, a delay of times the T_1 value must be used (99.3% magnetization). In small-molecule pharmaceutical solids, spin-lattice relaxation times can vary from below one second to hundreds of seconds. The times are long because relaxation must occur through stimulated relaxation at the Larmor frequency. These frequencies can be generated by molecular motion such as the rotation of a methyl group or flipping of a phenyl ring. Due to the nature of the relaxation mechanisms of T_i, it is sensitive to molecular motion on the time scale of the resonance frequency. Spin-lattice relaxation times are measured with either a saturation recovery or inversion recovery pulse sequence.

After a 90° pulse, the individual magnetization vectors fan out in the x-y plane. After the magnetization fans out (ignoring longitudinal relaxation), there is no net magnetization in the transverse plane. Similar to T_1, spin-spin (T_2) or transverse relaxation occurs via exponential decay. Magnetic field differences can arise from two different sources: instrumental imperfection ($T_{2(\Delta B0)}$) that can be partially corrected for by shimming and intra- and intermolecular interactions in the sample (T_2). The two sources combine to define T_2^* as seen in Equation 2.6. Decay of the

$$\frac{1}{T_2^*} = \frac{1}{T_{2(\Delta B_0)}} + \frac{1}{T_2} \tag{2.6}$$

magnetization is observed in the free induction decay. T_2^* is proportional to NMR line widths. T_2^* can be calculated from the line width at half height of a peak in the NMR spectrum. T_2 relaxation occurs by a spin-spin exchange process. For example, a spin in the α-state will flip to the β-state and the reverse occurs simultaneously. Transverse relaxation occurs through a swapping of energy between spins. Because T_2 relaxation occurs prior to T_1 relaxation, T_2 relaxation will be finished prior to T_1 relaxation. Therefore, spin-spin relaxation can only be equal to or shorter than the spin-lattice relaxation.

A third relaxation rate is the spin-lattice relaxation time in the rotating frame ($T_{1\rho}$). After a 90° pulse the RF pulse is normally turned off. If the phase of the RF field is changed 90°, the field will be aligned with the magnetization in the transverse plane. When the applied RF field is along the same axis as the magnetization vector, the sample is spin locked. $T_{1\rho}$ is the time constant for the decay of magnetization along this axis. $T_{1\rho}$ is sensitive to molecular motions that correspond to the strength of the spin locking field. It is also sensitive to motions occurring at lower frequency (kHz) than those of which T_1 (MHz) times are sensitive.

All three relaxation time constants are related to correlation time (τ_c). Correlation time is the average time it takes a molecule to rotate through one radian (~60°). T_1 and $T_{1\rho}$ time constants are related to τ_c in Equations 2.7 and 2.8, respectively.

$$\frac{1}{T_1} = \frac{6}{20}\frac{\gamma^4\hbar^2}{r^6}\left\{\frac{\tau_c}{1+\omega_0{}^2\tau_c{}^2} + \frac{4\tau_c}{1+4\omega_0{}^2\tau_c{}^2}\right\} \tag{2.7}$$

$$\frac{1}{T_{1\rho}} = \frac{3}{20}\frac{\gamma^4\hbar^2}{r^6}\left\{\frac{3\tau_c}{1+4\omega_1{}^2\tau_c{}^2} + \frac{5\tau_c}{1+\omega_0{}^2\tau_c{}^2} + \frac{2\tau_c}{1+4\omega_0{}^2\tau_c{}^2}\right\} \tag{2.8}$$

In the two equations, the nuclear precession frequency is ω_0 and ω_1 is the frequency of the applied spin locking field. The correlation time can be obtained by plotting log of the relaxation time (T_1 or $T_{1\rho}$) versus inverse temperature. For both relaxation time constants, a V-shaped curve will be plotted. At the minimum in each plot, the following conditions are true: (T_1) $\omega_0\tau_c = 0.62$ and ($T_{1\rho}$) $\omega_1\tau_c = 0.52$. The V-curve is indicative of two distinct motional regimes. On the left-hand side or fast-motional regime, relaxation times (T_1, T_2, and $T_{1\rho}$) are approximately equal with all increasing with increasing temperature. On the other side of the curve, the relaxation time constants are markedly different. In the slow-motional regime, the relaxation time constants increase with decreasing temperature.

2.2.3 Sensitivity

A thorough understanding of NMR sensitivity is important when acquiring NMR data. Equation 2.9 shows the relationship between signal, S, magnetogyric ratio, γ, spectrometer field strength, B_o, number of nuclei present in the sample, N, a signal shape factor, $g(v)$, and temperature, T. From Equation 2.9, it is clear why

quantitation studies using NMR can be straightforward. The signal observed is directly proportional to the number of nuclei present in the sample.

$$S \propto \frac{\gamma^4 B_o^2 N B_1 g(v)}{T} \tag{2.9}$$

This relationship also illustrates the advantage of isotopic labeling to increase signal intensity. Due to the exponent on the γ term, nuclei with higher magnetogyric ratios have more intense signals than a nucleus with identical abundance at with a smaller γ value. Signal increases with higher magnetic field strengths, and at lower temperatures.

To compare the sensitivity of different nuclei both the magnetogyric ratio and the natural abundance must be considered. NMR receptivity is defined as $\left|\gamma^3 C\right|$ where C is the natural abundance. Often times a nucleus is compared to the receptivity of commonly observed ^{1}H or ^{13}C nuclei to more clearly illustrate the sensitivity differences. The ratio is called the relative receptivity.

2.3 Solid-State NMR Spectroscopy

2.3.1 NMR spectroscopy for pharmaceutical analysis

In the past half century, nuclear magnetic resonance spectroscopy has been primarily used as a solution-based technique. In solution NMR, lines are very sharp, because molecular tumbling that occurs in solution average most of the interactions

that lead to line broadening. Narrow NMR lines and the highly abundant (99.99%) ^{1}H nucleus have made solution ^{1}H NMR a walk-up machine for routine data collection that is an invaluable technique for all aspects of drug research. However, in the solid state, the molecules are in rigid and defined molecular orientations and conformations, which can lead to large dipolar couplings and chemical shift anisotropy. In addition, the ^{1}H nucleus is not easy to routinely observe. Lastly, the lack of extensive molecular motion in the solid state leads to longer spin-lattice relaxation times from a few seconds to minutes. This increases the time required to obtain a high-quality NMR spectrum from signal averaging. These factors have kept solid-state NMR spectroscopy from being incorporated into pharmaceutical development by because it is difficult and time intensive to perform SSNMR experiments. Three important advances have been made to acquire high-resolution NMR spectra of the solid state, which are high-power proton decoupling, magic-angle spinning, and cross polarization.

2.3.2 High-power proton decoupling

Due to the lack of molecular tumbling and limited molecular motion in the solid state, the $^{1}H/^{1}H$ homonuclear dipolar couplings are very strong. This causes extensive line broadening when trying to detect the ^{1}H nucleus. Therefore, the primary focus of SSNMR of pharmaceuticals has been on the ^{13}C nucleus. ^{13}C is also strongly coupled with the ^{1}H nucleus. The coupling can be eliminated by using a high-power ^{1}H decoupling sequence, such as continuous wave, two-pulse phase

modulated (TPPM), or Spinal-64. In general, high power ^{1}H decoupling is required for any system where there is an abundance of ^{1}H nuclei in the system.

Shown in Figure 2.1a is a ^{19}F SSNMR spectrum of triamcinolone applied with a single ^{19}F 90° pulse and high-power TPPM decoupling. A spectrum collected under typical solution conditions (not shown) would be fairly noisy with very weak or no signal. Using high-power proton decoupling produces the ^{19}F powder pattern of triamcinolone. When decoupling is employed, the peaks in the spectrum are broad and featureless providing limited information about the sample.

2.3.3 Magic-angle spinning

High-power proton decoupling eliminates a significant amount of line broadening. However, there is orientation dependence in the solid state that still exists due to the lack of molecular tumbling that occurs in solution. The narrow lines that are observed in solution NMR spectra are not present in the solid state even with high-power proton decoupling. Both dipole-dipole interactions and chemical shift anisotropy are orientation dependent. The orientation dependence gives rise to chemical shift anisotropy (CSA), an effect not typically observed in solution spectroscopy. CSA is a result of the different molecular orientations with respect to the magnetic field. For example, a single crystal placed in an external magnetic field would exhibit different chemical shifts depending upon its orientation with respect to the static magnetic field. Rapid molecular tumbling averages this effect to zero in solution, and only a single isotropic chemical shift is observed. The rigidity of

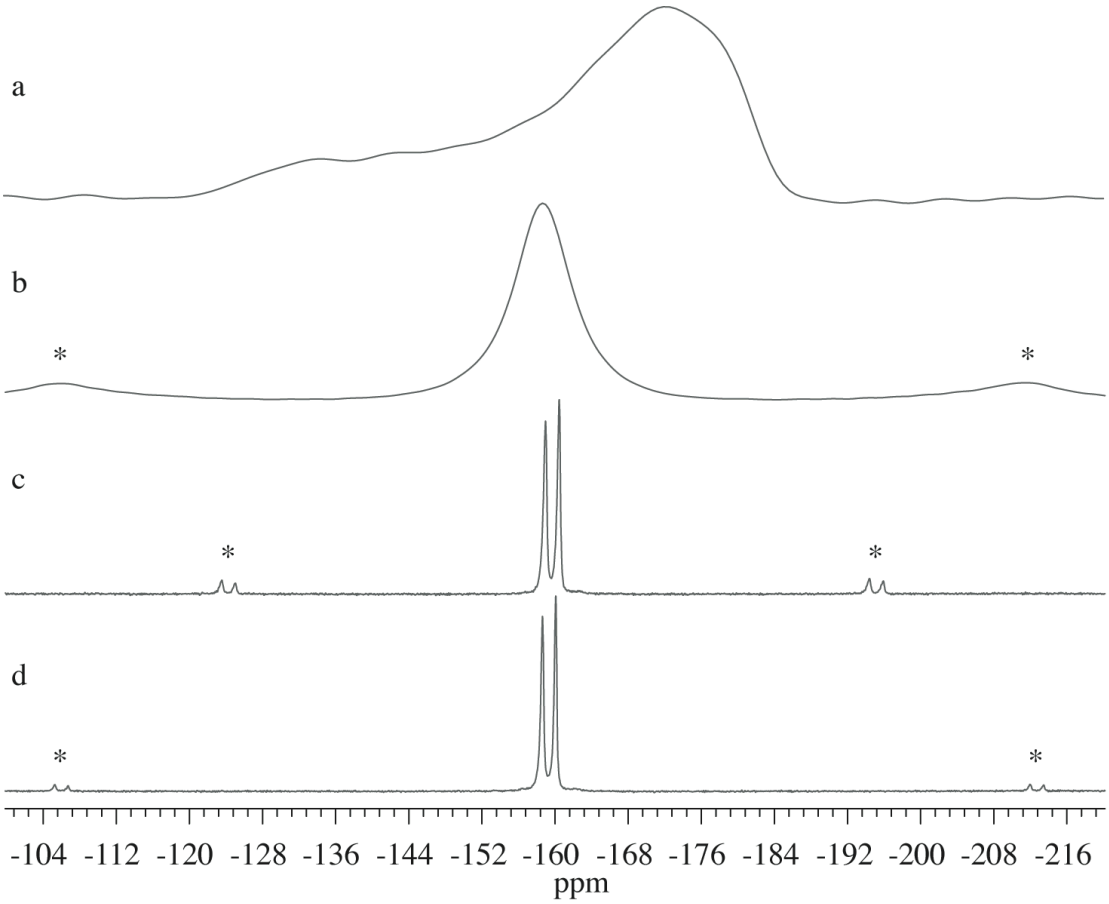

Figure 2.1. ^{19}F SSNMR spectra of triamcinolone a) single pulse experiment, static, TPPM proton decoupling, 100-s pulse delay, 512 scans, ~14 hour experiment time b) spinning at 15 kHz with no proton decoupling, 100-s delay, 256 scans, ~7 hour experiment time c) spinning at 10 kHz with TPPM proton decoupling, 100-s delay, 16 scans, ~26 minute experiment time and d) spinning at 15 kHz with TPPM decoupling and $^{1}H/^{19}F$ cross polarization 3-s delay, 16 scans, 48 seconds experiment time. Asterisks denote spinning sidebands.

molecules in the solid state compared to the external magnetic field give rise to a distribution of chemical shifts that is referred to as the powder pattern. The effect is due to a chemical shielding tensor, σ_{obs}, which can be separated into an anisotropic and an isotropic term as seen in Equation 2.10.

$$\sigma_{obs} = \sigma_{iso} + \left(3\cos^2\theta - 1\right)\sigma_{aniso} \tag{2.10}$$

The anisotropic shielding tensor can be eliminated when the sample is spun at an angle, θ, such that $(3\cos^2\theta\text{-}1) = 0$. The angle at which the term equals zero is 54.74°, and is termed the magic angle. The angle corresponds to the body diagonal of a cube. When spinning along that axis, commonly referred to as magic-angle spinning (MAS), the sample spends an equal amount of time on all three axes (x,y,z). The orientation dependence of the solid state is significantly reduced and the isotropic chemical shift is observed. If the sample-spinning rate is less than the width of the powder pattern, spinning sideband artifacts will appear at harmonics of the spinning speed. Dixon et al. developed a pulse sequence, which can be applied for total suppression of spinning sidebands (TOSS). A spectrum collected with TOSS will contain only the isotropic chemical shifts.

The line narrowing capability of MAS is shown in Figure 2.1b. A ^{19}F SSNMR spectrum of triamcinolone was collected with a single-pulse experiment with no proton decoupling with a 15 kHz MAS rate. The spectrum shows significant reduction in line broadening as compared to simply employing proton decoupling.

However, the peak is still extremely broad. Figure 2.1c shows the use of both proton decoupling and MAS in a single-pulse experiment. There are now two well-resolved peaks in the ^{19}F SSNMR spectrum of triamcinolone.

2.3.4 Cross polarization

Most of the solid-state NMR spectra of pharmaceutics are acquired for ^{13}C. However, the natural abundance of the ^{13}C nucleus is only 1.1% as compared to the 99.9% abundance of the ^{1}H nucleus. A technique that is often implemented to increase the sensitivity of a low-abundance nucleus, such as ^{13}C, is cross-polarization (CP). In the CP experiment, magnetization is transferred from an abundant spin (^{1}H) to a low abundance spin (e.g. ^{13}C and ^{15}N,).

CP is accomplished by applying a 90° radio-frequency (rf) pulse at the proton resonance frequency aligning the proton magnetization on the x-y plane. The phase of the pulse is immediately rotated by 90° and maintained for a short period of time, locking the spins in the x-y plane. Simultaneously, a second rf pulse is applied at the resonant frequency of the dilute spin (i.e. ^{13}C) for the duration of the contact time. With the appropriate rf field power levels and durations for each nucleus, the Hartmann-Hahn matching conditions are satisfied, and cross polarization is achieved.[1] The Hartmann-Hahn matching condition is displayed in Equation 2.11.

$$\gamma_H B_{1H} = \gamma_X B_{1X} \tag{2.11}$$

In Equation 2.10, γ_H is the magnetogyric ratio of the ^{1}H nucleus, B_{1H} is the magnetic field strength applied to the protons, γ_X is the magnetogyric ratio of the dilute spin (i.e. ^{13}C), and B_{1X} is the magnetic field strength applied to the X nuclei.

There are two valuable benefits that arise from using cross polarization. First, when executed at the Hartman-Hahn conditions, cross polarization results in a gain in sensitivity that corresponds to the ratio of the magnetogyric ratios of the abundant and dilute spins. For ^{1}H to ^{13}C cross polarization, the sensitivity per scan gain is approximately four-fold. Secondly, the relaxation times are now governed by the ^{1}H spin-lattice relaxation times rather than the ^{13}C T_1. ^{1}H relaxation times are typically much faster than ^{13}C times because of the increased atomic motion of the ^{1}H nucleus and spin diffusion. The faster relaxation times allow for more signal averaging in the same amount of time.

Figure 2.1d shows the ^{19}F spectrum of triamcinolone acquired with all three techniques: proton decoupling, magic-angle spinning, and ^{1}H/^{19}F cross polarization. Cross polarization does not appear to have a large effect on the resolution of the spectrum. This is due to the closeness in magnetogyric ratio between the ^{1}H and ^{19}F nucleus, so there is a minimal sensitivity enhancement expected (~1.05) compared to the four-fold enhancement for ^{1}H/^{13}C CP. The advantage to using CP is the time difference in relaxation of the proton nucleus. The pulse delay used for the single-pulse experiment is 100 s and 3 s for the CP experiment. A comparable ^{19}F CP spectrum can be acquired in a fraction of the time that it would take for the single-

pulse experiment. It should be noted that the benefits are based on the difference between relaxation times, and the difference is not always this extreme.

The use of high-power proton decoupling, magic-angle spinning, and cross polarization allow the collection of high-resolution NMR spectra in the solid state.

2.4 Characterization of Bulk Drugs Using SSNMR

2.4.1 Background on physical forms

As described in Chapter 1, drugs can exist in a multitude of physical forms in the solid state. Each state can have a variety of different physicochemical properties such as melting point, dissolution rate, hygroscopicity, solid-state reactivity, and processability. The changes in physicochemical properties can vastly affect the therapeutic efficacy of a drug product. Changes to the solid state can occur at any stage during processing, formulation, and/or storage of the drug product. Therefore, the formulated product must be monitored throughout all stages to ensure that the physical and chemical integrity of the drug substance is maintained.

Solid-state form changes are due to changes in the arrangement of molecules in the unit cell. The electronic environments of atoms will be different for each form of the drug. These changes in electronic environment are fairly easy to detect with ^{13}C CPMAS (cross polarization with magic-angle spinning) spectroscopy. Polymorphs, solvates, hydrates, and amorphous forms all give a unique SSNMR spectrum. The spectral difference allow for form identification and quantitation using

SSNMR spectroscopy. Chemical shift differences can vary up to 10 ppm between different solid forms in an NMR spectrum.

2.4.2 Identification of physical form

An early example of crystal form identification using SSNMR spectroscopy was performed by Byrn et al.[2] The crystal structures of five different solid forms (I (ethanol), II (2-propanol), III (DMF), IV (anhydrate), and V (hydrate)) of prednisolone tert-butylacetate were determined by single-crystal X-ray diffraction and SSNMR. The steroid rings were determined to be in similar configurations, yet the tert-butyl side chain conformation was the primary difference in conformation. The crystal packing was also shown to be very different between all forms, with the exception of Forms I and II. The ^{13}C CPMAS spectra of each of the forms showed significantly different chemical shifts, which were attributed to differences in the individual crystal packing of each form. The chemical shifts of the carbon atoms in the ester side chain are similar for each of the five crystal forms. The largest difference between forms was observed in the carbonyl carbon atoms and the unsaturated carbon atoms conjugated with them. Some of the chemical shift differences were as large as 8 ppm. The five forms were examined for reactivity with oxygen catalyzed by UV light. Oxygen reactivity only occurred with the monohydrate Form V. From the crystal structure it was hypothesized that oxygen traveled down a tunnel penetrating the crystal lattice. In this example, SSNMR

provided a knowledge of how the crystal packed, which helped explain the differences in chemical stability between various solid forms of a drug compound.

2.4.3 Quantitation of forms

Solid-state NMR spectroscopy is uniquely suited for the quantitation of solid forms and solid formulations. The technique is non-invasive, non-destructive, and inherently quantitative, so there is no need for a calibration curve with pure standards. The area of NMR peaks is proportional to the nuclei producing the NMR signal. In order to obtain quantitative data, several factors must be considered. First, the spectrum must be acquired with NMR parameters such that full relaxation of all compounds of interest is allowed. Saturation occurs when a sample is acquired with a pulse delay shorter than five times the longest spin-lattice relaxation time of the individual components. A pulse delay of five times the T_1 results in 99.33% of the magnetic equilibrium to recover. For single-pulse experiments using a sufficiently long pulse delay for all components in the sample, the relative peak areas can be compared to determine the percentage of each component in the sample.

During experiments where cross-polarization is used, the relaxation time is governed by the ^{1}H spin-lattice relaxation. The ^{1}H T_1 time is often shorter than ^{13}C or ^{19}F T_1 times, and the T_1 is uniform throughout the sample due to spin diffusion. Comparing relative peak areas, which is done in a single-pulse experiment, is not acceptable for CP experiments because the magnetization transfer in a CP experiment is not instantaneous, and the kinetics of the transfer must be accounted for during

quantitation. A review by Harris discusses the different aspects that must be considered during quantitative analysis using SSNMR spectroscopy.[3]

Offerdahl et al. demonstrated the utility of ^{13}C CPMAS SSNMR to quantitate crystalline and amorphous forms of anhydrous neotame.[4] The first thing to determine is which peaks are attributed to each solid form. Peaks in SSNMR can vary up to 10 ppm from their solution chemical shifts, and spectral interpretation can be difficult. Additionally, adequate peak resolution of each form present for ideal quantitation is necessary. Once the specific carbon was selected for quantitation of each form it was necessary to determine the relaxation time constants T_{CH}, ^{1}H T_1, and ^{1}H $T_{1\rho}$ associated with CP dynamics for each form. By measuring each of these time constants, one can determine the relative number of nuclei for each form. As noted before, the ^{1}H T_1 time is the amount of time it takes for the sample to return to magnetic equilibrium. The ^{1}H T_{CH} and $T_{1\rho}$ time constants associated with the rise and decay, respectively, of the ^{13}C magnetization upon cross polarization. Figure 2.2 displays the CP dynamics by plotting the natural log of relative peak area as a function of CP contact time for pure Forms A and G of anhydrous neotame. From the plot, it is clear that spectra acquired at different contact times would produce different relative intensities for the same carbon in each form. Because of this, spectra acquired with CP have traditionally been thought to be non-quantitative.

Figure 2.3 shows a ^{13}C CPMAS spectrum of a 50/50 mixture of Forms A and G acquired with a 2-ms contact time. The same aromatic peak in each form was deconvoluted. The deconvoluted peak areas have different values because of the CP

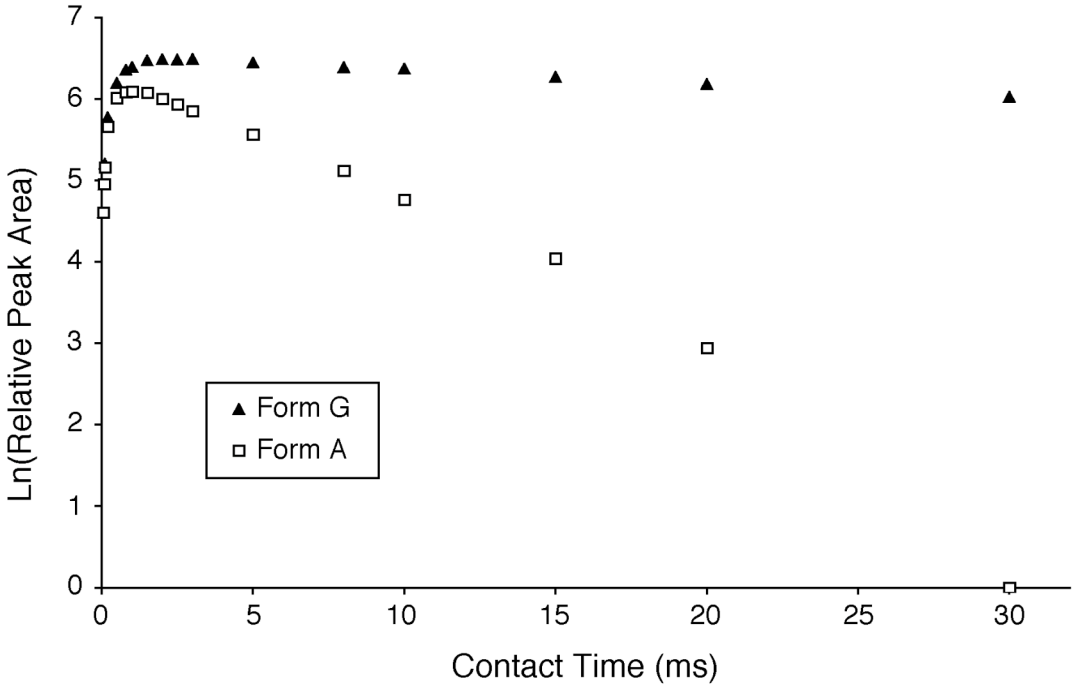

Figure 2.2. ^{13}C CPMAS SSNMR contact time profiles for neotame Form A and Form G. Adapted from reference 4.

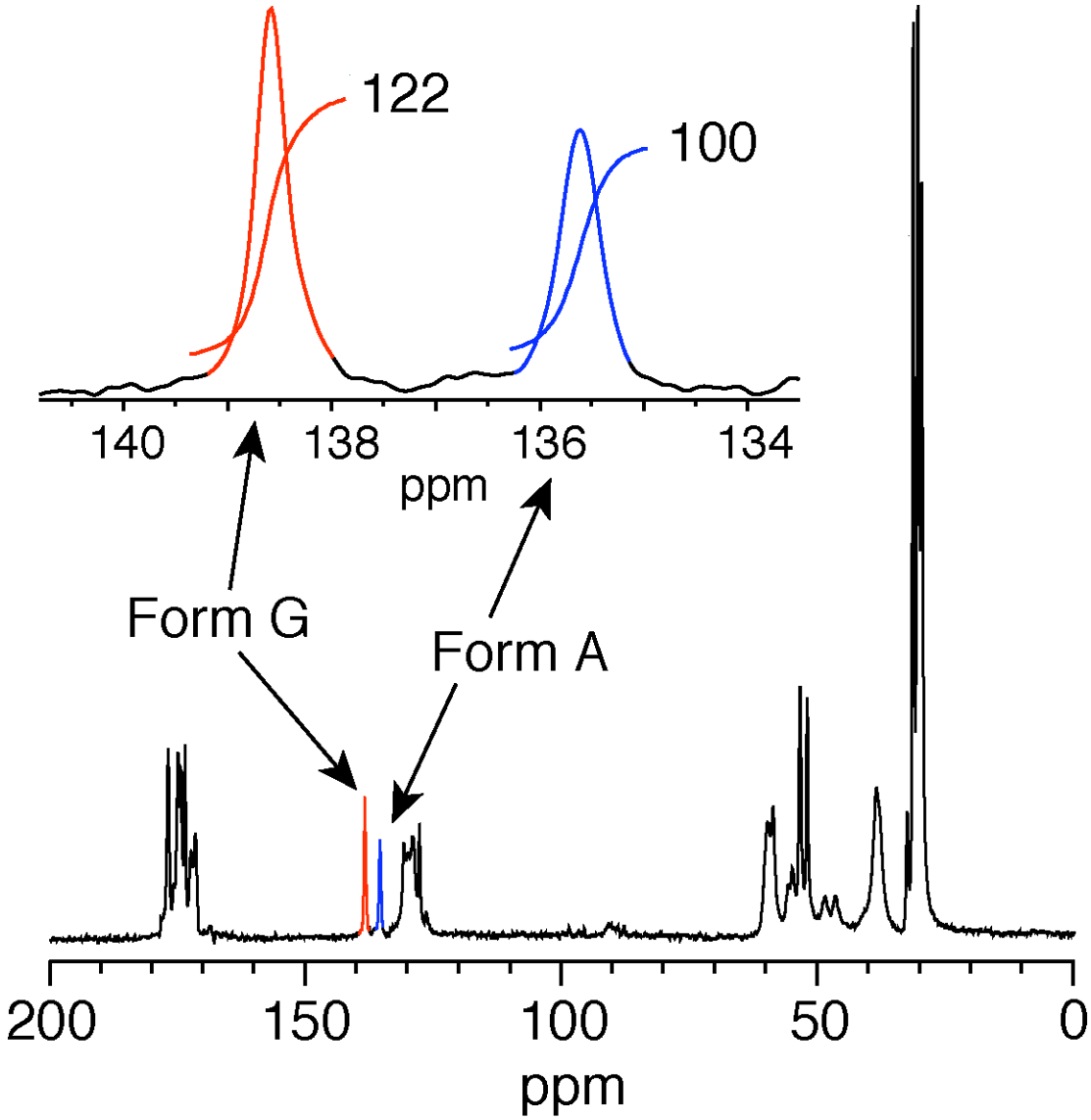

Figure 2.3. ^{13}C CPMAS NMR spectra of a 50/50 (w/w) physical mixture of anhydrous Forms A and G of neotame. The inset depicts the integrated peak areas for the aromatic carbon used for quantitation. Adapted from reference 4.

dynamics in the system. In order to determine the quantitative peak area, a plot of log of relative peak area versus contact time (> 5 T_{CH}) was extrapolated back to the y-intercept for each form. This simulates the absence of ^{1}H $T_{1\rho}$ relaxation and simultaneous magnetization transfer from ^{1}H to ^{13}C nuclei. From the y-intercepts, the absolute peak area for each form can be determined.

Table 2.1 displays the calculated weight percent by mass and the percentage determined from ^{13}C CPMAS experiments (NMR%) for the series of physical mixtures. The SSNMR data agrees well for all of the mixtures in the series.

Quantitation was also performed on physical mixtures of the amorphous form and crystal Form G. Figure 2.4 shows the ^{13}C CPMAS spectrum of a 50/50 physical mixture of Form G and amorphous neotame. Deconvolution peaks and peak areas are highlighted for the aromatic carbon used for quantitation. The same method of CP correction, which was applied for quantitation of crystals Forms A and G, was used to quantitate the physical mixtures of amorphous neotame and crystal Form G. Table 2.1 displays the quantitation data for the physical mixtures of amorphous and crystalline neotame. At first glance, the quantitation data does not agree between the calculated weight percent by mass and the calculated weight percent by SSNMR. When weight percent by mass and weight percent by SSNMR were plotted against each other, the slope was not one and a non-zero y-intercept was present. The y-intercept determined there to be a 13.5% amorphous impurity in the Form G standard. The data in Table 2.2 were recalculated to take into account the amorphous impurity

Table 2.1. Quantitation data for various physical mixtures of Form A and Form G of neotame. Adapted from reference 4.

%A	Form	Mass (g)	Wt. %	Intercept	Rel. Area	R^2	NMR %	Diff (abs)
10%	A	0.0478	12.62	7.2984	1478	0.9998	13.7	1.0
	G	0.3309	87.38	9.1421	9340	0.9899	86.3	
20%	A	0.0759	21.20	4.9549	141.9	0.9992	22.0	0.8
	G	0.2822	78.80	6.2208	503.1	0.9906	78.0	
30%	A	0.1034	29.71	4.8991	134.2	0.9928	29.4	0.4
	G	0.2446	70.29	5.7772	322.9	0.9682	70.6	
40%	A	0.1273	39.12	5.0380	154.2	0.9779	37.9	1.3
	G	0.1981	60.88	5.5337	253.1	0.9956	62.1	
50%	A	0.1961	49.73	4.8556	128.5	0.9994	50.3	0.5
	G	0.1982	50.27	4.8449	127.1	0.9954	49.7	
60%	A	0.1954	61.56	4.8684	130.1	0.9995	62.3	0.7
	G	0.1220	38.44	4.3667	78.8	0.9996	37.7	
70%	A	0.2413	70.29	4.8870	132.6	0.9981	71.4	1.1
	G	0.1020	29.71	3.9714	53.1	0.9476	28.6	
80%	A	0.2966	80.88	4.8781	131.4	0.9991	81.8	1.0
	G	0.0701	19.12	3.3723	29.1	0.9995	18.2	
90%	A	0.2961	88.41	7.1853	1320	0.9995	89.0	0.5
	G	0.0388	11.59	5.0989	164	0.9166	11.0	

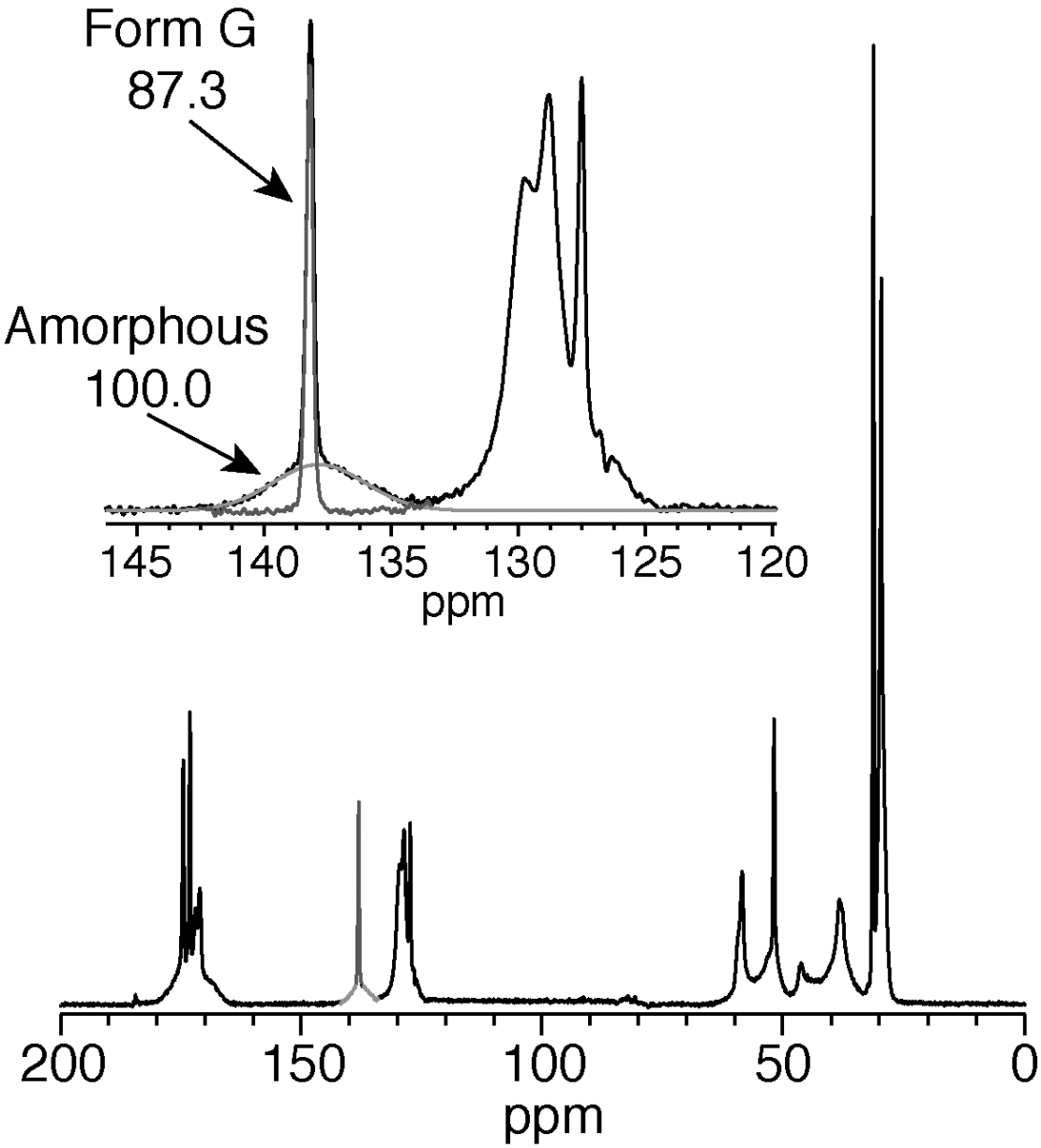

Figure 2.4. ^{13}C CPMAS spectrum of a 50/50 (w/w) physical mixture of amorphous Neotame and crystal Form G. The inset shows the aromatic region of the spectrum and the deconvolution peaks and areas for each form. Adapted from reference 4.

Table 2.2. Quantitation data for various physical mixtures of the amorphous form and Form G of neotame. Adapted from reference 4.

% Amorphous	Form	Mass (g)	Wt. %	Rel. Area	NMR %	Diff (abs)
20%	Amorphous	0.0966	20.07	119.3	32.1	12.0
	G	0.3847	79.93	252.8	67.9	
30%	Amorphous	0.1381	26.93	137.2	36.2	9.2
	G	0.3748	73.07	242.2	63.8	
40%	Amorphous	0.1845	41.08	124.5	47.7	6.6
	G	0.2646	58.92	136.6	52.3	
50%	Amorphous	0.2701	51.08	121.4	56.3	5.3
	G	0.2587	48.92	94.1	43.7	
70%	Amorphous	0.3220	67.10	121.5	69.8	2.7
	G	0.1579	32.90	52.5	30.2	
90%	Amorphous	0.3788	47.48	131.5	91.5	1.5
	G	0.4190	52.52	12.2	8.5	

in the crystal Form G. The new quantitation data agreed very well for each physical mixture

^{13}C CPMAS SSNMR spectroscopy is able to quantitate both mixtures of crystalline forms and physical mixture of crystalline and amorphous form. However, Offerdahl et al. were not able to easily observe the 13% amorphous impurity in the crystalline standard. Additional NMR experiments confirmed the presence of the amorphous impurity. Because NMR peaks of the amorphous form can be up to 10 times broader than the crystalline form, a sample containing 10% amorphous material could give a peak with ~1% of the crystalline peak intensity. To increase the sensitivity of similar experiments, other relevant nuclei are considered ^{15}N, ^{17}O, and ^{19}F.

2.5 Pharmaceutically Relevant NMR-Observable Nuclei

The employment of high-power decoupling, magic-angle spinning, and cross polarization have transformed SSNMR into a powerful technique for pharmaceutical analysis. As previously noted, it is difficult to obtain high-resolution NMR spectra for the ^{1}H nucleus due to the large homonuclear coupling that exists in the solid state. ^{13}C CPMAS NMR is the primary experiment used on pharmaceutically relevant samples. The low abundance, 1.1%, of the ^{13}C isotope leads to long experiment times. In some cases other nuclei should be considered. The two most obvious choices with pharmaceutical relevance are ^{15}N and ^{17}O. The ^{17}O nucleus has a low

natural abundance (0.037%) and relative receptivity (0.0611) as compared to the ^{13}C nucleus. It is also a quadrupolar nucleus with a spin of 5/2. The ^{15}N nucleus also has a low abundance (0.37%) and relative receptivity (0.0219) as compared to the ^{13}C nucleus.

^{31}P and ^{19}F are two other nuclei to be considered from an NMR perspective. Both nuclei are 100% abundant and have respective relative receptivities of 377 and 4730. When appropriate, ^{31}P is an attractive nucleus to observe. However, there are few pharmaceutical compounds that contain ^{31}P.

Over the past several decades, ^{19}F has been designed into drug molecules to increase certain drug properties such as inductive effects, enhanced binding interactions, and metabolic stability by lowering the susceptibility of cytochrome P450 enzymatic oxidation.[5-7] Current estimates have fluorine atoms in ~20% of all pharmaceuticals.[5] The combination of high relative receptivity and growing presence in pharmaceuticals make ^{19}F an attractive nucleus to utilize for analysis of pharmaceutical solids.

2.6 ^{19}F SSNMR spectroscopy

2.6.1 Comparison to ^{13}C SSNMR spectroscopy

When applicable, the ^{19}F nucleus is a good complement to observing the ^{13}C nucleus. Depending on the sample, ^{13}C SSNMR spectra typically take several hours to days to collect. Due to the high relative receptivity of ^{19}F, a SSNMR spectrum can

be collected in a fraction of the time with a fraction of the sample mass. The ^{13}C spectrum often has many peaks that can overlap with each other and make spectral interpretation difficult. Additionally, the excipients will be observed in the spectrum that could complicate interpretation further. ^{19}F SSNMR spectra typically have just a few peaks due to the fewer number of ^{19}F atoms in the molecule. There is no spectral interference from excipients, because no commonly used excipients contain fluorine. The chemical shift range is also much larger for ^{19}F NMR. Typically, ^{13}C SSNMR is acquired with a spectral width of 30 kHz and ^{19}F SSNMR is collected with a spectral width of 100 kHz.

There are several drawbacks to observing the ^{19}F nucleus. First, fluorine is not present in every pharmaceutical. Second, the strong homonuclear coupling and large CSA in fluorine-containing samples may require fast MAS speeds (>10 kHz). To spin faster than 10 kHz rotors with smaller sample volumes must be used to reach these speeds. The fast MAS speeds also cause significant sample heating[8], which could induce physical transformations in a sample. Next, the linewidths in ^{19}F SSNMR spectra are broader than in ^{13}C spectra. Finally, there are generally fewer ^{19}F peaks in the NMR spectrum. When quantitating solid forms, it can be beneficial to have several different peaks to compare. Different atoms can have varying degrees of resolution. If corresponding peaks from multiple forms overlap in a ^{13}C NMR spectrum, the user might be able to select a different pair.

2.6.2 Pharmaceutical applications

The homonuclear interaction of fluorine atoms can produce NMR linewidths in excess of 30 kHz in the solid state, if fluorine atoms are present at high levels.[9] In order to overcome such large dipolar couplings it is necessary to spin at a higher rate than the dipolar interactions present in a sample, or approximately 10 kHz. Prior to these probe developments, several multiple-pulse sequences were employed to reduce homonuclear dipolar interactions such as the WAHUHA-4, MREV-, and BR-24 sequences. All of them operate under the same principle: suppression of the dipolar interaction while the shielding anisotropy information is retained. The multiple-pulse sequences were troublesome when there were multiple fluorine types in a sample. The uses of these sequences were limited to mobile polymers and inorganic fluorides spinning at slow speeds. Commercially available probes that spin samples at fast spinning speeds (>15 kHz) have been developed over the last 20 years. These probes opened the door to more fast-spinning applications such as the study of fluorocarbon polymers. Isbester et al. used ^{19}F SSNMR spectroscopy and combined high MAS rates (>25 kHz) with elevated temperatures (>150 °C) to dramatically improve the resolution of the NMR spectra of Kel-F, a fluorocarbon polymer composed of vinylidene fluoride and chlorotrifluoroethylene.[10] The research was extended to six other vinylidene fluoride based polymers where elevated temperatures (250 °C) and fast MAS rates (>25 kHz) produced solution-like spectra of the polymers.[11] The increased resolution from these conditions allowed assignment of monomer peaks based on solution NMR data. The monomer composition of each of the six polymers

was quantitated and agreed with monomer composition data from solution spectroscopy.

Fast spinning speeds help eliminate the ^{19}F homonuclear dipolar coupling, but the samples analyzed have had few to no ^{1}H nuclei in the molecular structure. There is little heteronuclear line broadening that exists. However this is far from the case for pharmaceutical samples. Prior to 1996, solids containing abundant protons received very little attention with ^{19}F SSNMR spectroscopy.[12] For other common pharmaceutically relevant NMR nuclei (^{13}C, ^{15}N), high-power proton decoupling can be applied with relative ease, and the dipolar interactions with ^{1}H nuclei can be suppressed. However, due to the proximity of the ^{19}F and ^{1}H resonant frequencies (284 vs 300 MHz at 7 T), high-power proton decoupling represents a significant challenge for ^{19}F NMR of proton-containing solids. High-specification filters that can efficiently discriminate between two nearby frequencies became available in the past 15 years.[12] Carss et al. demonstrated the use of high-power proton decoupling, fast MAS, and cross polarization on three fluorinated steroids.[12] The researchers were able to detect polymorphism in one of the steroid samples. The improvement in resolution from the employment of these techniques also allowed the researchers to study several other phenomena: dipolar dephasing, rotational resonance, and spin diffusion.

The production of probes equipped to spin at fast speeds coupled with high-specification filters, the increased development of fluorine-containing

pharmaceuticals and the advent of SSNMR spectroscopy, have made ^{19}F SSNMR a promising tool for analysis of solid-state drug substances and drug products.

2.6.3 *Pharmaceutical applications of ^{19}F SSNMR spectroscopy*

^{19}F SSNMR has been applied to a variety of pharmaceutical systems. Wenslow used ^{19}F SSNMR spectroscopy with fast MAS (15 kHz) to characterize low-dose (2%) tablets of multiple solid forms, including two anhydrous (forms I and II), one sesquihydrate, and one amorphous form, of a Muscarinic M3 receptor antagonist.[13] ^{19}F SSNMR was successful in distinguishing between each of the four pure solid forms. The ^{19}F NMR spectrum of a low-dose placebo of 2% form I was compared to a tablet dosed with 2% form I. The spectra of the tablet showed that the desired form I had converted to another crystalline form or the amorphous form. High-temperature (110 °C) ^{19}F MAS conditions were used in an attempt to produce higher resolution spectra. The spectra of the sesquihydrate and amorphous forms were collected immediately upon reaching the elevated temperature. Line narrowing was observed for both forms, which was attributed to increased molecular motion due to solvent escape. Multiple solid forms were identified and analyzed with ^{19}F SSNMR spectroscopy. Additionally, it was shown that changes in the solid form of the API could be monitored in low-dose formulations.[13]

Farrer et al. used $^{1}H/^{19}F$ CPMAS SSNMR to quantitate crystalline material within a liquid vehicle.[14] Crystalline sodium (2R)-7-{3-[2-chloro-4-(2,2,2-trifluoroethoxy)phenoxy]propoxy}-2-methyl-3,4-dihydro-2H-chromane-2-

carboxylate (**I**) was detected at low levels (0.2mg/g) within a solid mixture and a slurry with a liquid vehicle. The area of the NMR peaks in the $^{1}H/^{19}F$ CPMAS spectra of the solid mixture and the slurry were both linearly dependent upon the mass of **I** in the rotor as determined by HPLC with a least square fit below 2%. The limit of detection was 2% crystallization within a 100mg/g formulation of **I**. Increased signal-averaging could improve the signal-to-noise ratio and lower the limit of detection.

Aso et al. demonstrated that ^{19}F SSNMR spectroscopy could be used to assess the molecular mobility of amorphous flufenamic acid in a melt quenched solid dispersion[15] Amorphous solid dispersions were prepared by melt-quenching flufenamic acid (FLF) in various ratios with poly(vinylpyrrolidone) (PVP) or hydroxypropylmethylcellulose (HPMC). The spin-lattice relaxation times (T_1 and $T_{1\rho}$) were measured for each dispersion across a range of temperatures (-20 to 150 °C). A minimum in the relaxation times was exhibited across the temperature range. The minimum relaxation time and the observed relaxation value were used to calculate the correlation time (τ_c) or rotational molecular mobility of the sample. The τ_c value for the 20% PVP dispersion was 2-3 times longer than the 20% HPMC dispersion. This indicated that the molecular mobility of FLF in the 20% PVP solid dispersion was significantly lower than the 20% HPMC dispersion. When the solid dispersions were stored at 60 °C, the crystallization of the amorphous FLF was monitored by analyzing the solid echo signals of the fluorine atoms in FLF, and the amorphous FLF remaining was successfully estimated.[15]

2.7 Conclusions

The incorporation of magic-angle spinning, high-power proton decoupling, and cross polarization have transformed ^{13}C SSNMR spectroscopy into a powerful tool for analysis of solid-state pharmaceuticals. It has been demonstrated to be particularly useful in distinguishing different crystalline and amorphous solid forms, quantitation of different forms, and observing the API in a formulation. However, the low natural abundance of the ^{13}C nucleus and long relaxation times in the solid state can lead to prohibitively long analysis times, especially in low-dose formulations and low-level detection of the amorphous state. ^{19}F NMR is a relatively new technique to be used for the analysis of solid-state pharmaceuticals. ^{19}F SSNMR can distinguish between different physical forms, quantitate crystalline material in a formulation, and be used to monitor differences in molecular mobility of amorphous solid dispersion that correlate with the relative physical stability of the drug in dispersion.

The objective of the research presented in this thesis was designed to reduce the analysis time of SSNMR by increasing the sensitivity of this technique using two approaches. First, the design, development, and testing of a multiple-sample solids probe for solid-state NMR spectroscopy was accomplished and is presented in Chapter 3. A prototype probe was constructed that shuffled two samples through the bore of the superconducting magnet for simultaneous data collection. Data for identical samples could be acquired in both modules to increase sensitivity, or data

for different samples could be acquired simultaneously in each module to increase throughput.

In Chapters 4 and 5, a second method for increasing sensitivity is presented. This approach takes advantage of the relative NMR receptivity of the ^{19}F nucleus as compared to the ^{13}C nucleus. It is then possible to quantitate low-level amorphous impurities in a crystalline physical mixture with ^{19}F SSNMR.

2.8 References

1. Hartmann SR, Hahn EL 1962. Nuclear double resonance in the rotating frame. Physical Review 128:2042-2053.

2. Byrn SR, Sutton PA, Tobias B, Frye J, Main P 1988. Crystal structure, solid-state NMR spectra, and oxygen reactivity of five crystal forms of prednisolone tert-butylacetate. Journal of the American Chemical Society 110(5):1609-1614.

3. Harris RK 1985. Quantitative aspects of high-resolution solid-state nuclear magnetic resonance spectroscopy. Analyst (Cambridge, United Kingdom) 110(6):649-655.

4. Offerdahl TJ, Salsbury JS, Dong Z, Grant DJW, Schroeder SA, Prakash I, Gorman EM, Barich DH, Munson EJ 2005. Quantitation of crystalline and amorphous forms of anhydrous neotame using 13C CPMAS NMR spectroscopy. Journal of Pharmaceutical Sciences 94(12):2591-2605.

5. Muller K, Faeh C, Diederich F 2007. Fluorine in pharmaceuticals: looking beyond intuition. Science 317(5846):1881-1886.

6. Hagmann WK 2008. The Many Roles for Fluorine in Medicinal Chemistry. J Med Chem 51(15):4359-4369.

7. Park BK, Kitteringham NR, O'Neill PM 2001. Metabolism of fluorine-containing drugs. Annual Review of Pharmacology and Toxicology 41:443-470.

8. Isbester PK. 1999. Development of an Isolated Flow Variable-Temperature Magic-Angle Spinning (MAS) Nuclear Magnetic Resonance (NMR) Probe for Heterogeneous Catalysis Studies and High-Temperature High-Speed ^{19}F MAS NMR Techniques Applied to Fluoropolymers. Department of Chemistry, ed., Minneapolis: The University of Minnesota. p 179.

9. Harris RK, Jackson P 1991. High-resolution fluorine-19 magnetic resonance of solids. Chemical Reviews (Washington, DC, United States) 91(7):1427-1440.

10. Isbester PK, Kestner TA, Munson EJ 1997. High-resolution variable-temperature MAS 19F NMR spectroscopy of fluorocarbon polymers. Macromolecules 30(9):2800-2801.

11. Isbester PK, Brandt JL, Kestner TA, Munson EJ 1998. High-Resolution Variable-Temperature 19F MAS NMR Spectroscopy of Vinylidene Fluoride Based Fluoropolymers. Macromolecules 31(23):8192-8200.

12. Carss SA, Scheler U, Harris RK, Holstein P, Fletton RA 1996. 19F NMR of proton-containing solids. Magnetic Resonance in Chemistry 34(1):63-70.

13. Wenslow RM 2002. ^{19}F solid-state NMR spectroscopic investigation of crystalline and amorphous forms of a selective muscarinic M3 receptor antagonist, in both bulk and pharmaceutical dosage form samples. Drug Development and Industrial Pharmacy 28(5):555-561.

14. Farrer BT, Peresypkin A, Wenslow RM 2006. Quantitation of crystalline material within a liquid vehicle using $^{1}H/^{19}F$ CP/MAS NMR. Journal of Pharmaceutical Sciences 96(2):264-267.

15. Aso Y, Yoshioka S, Miyazaki T, Kawanishi T 2009. Feasibility of 19F-NMR for assessing the molecular mobility of flufenamic acid in solid dispersions. Chemical & pharmaceutical bulletin 57(1):61-64.

Chapter 3

Multiple-Sample Probe for Solid-State NMR Spectroscopy

3.1 Introduction

Solid-state NMR spectroscopy (SSNMR) is a very powerful technique for the analysis of pharmaceuticals and pharmaceutical formulations, because of the vast quantity of information obtained about the structure and dynamics of compounds in a formulation.[1-3] SSNMR has the capability to determine the state of a drug either in the bulk state or within a formulated product *without* having to extract the drug from the formulation. It is selective, in that the drug usually has a different chemical shift than that of the excipients, making it easy to identify the drug in the formulation. SSNMR is quantitative, and can be used to determine the relative amounts of different crystalline forms and amorphous content. Drug–excipient interactions can also be studied. Determination of mobilities can help identify why a drug may have failed (or will fail) stability tests. Controlled-release devices are complex systems which could be much better formulated if the state of the drug could be determined directly, which is possible using SSNMR.

New drug compounds are often poorly crystalline or even amorphous, have long relaxation times, and are present at low levels in a formulation. This creates a significant problem for analyzing these compounds with SSNMR. Analysis times can range from a few minutes to a few days, depending upon the state of the sample (i.e. bulk drug or formulated product; crystalline or amorphous), relative sensitivity (i.e. choice and number of different nuclei in molecule), and relaxation parameters. For example, quantitation of a mixture of two forms of a compound can take a few hours

(for a sample with short relaxation times) to a few days. Analyzing a series of formulated products may take a month or more of spectrometer time. This leads to low throughput, high cost per sample analysis, and has relegated SSNMR in many cases to be a prohibitively expensive problem-solving technique compared to other analytical techniques such as powder X-ray diffraction (PXRD), infrared and Raman spectroscopy, and differential scanning calorimetry (DSC).

Increasing the signal to noise ratio (SNR) by signal averaging (in samples containing nuclei with low magnetogyric ratios, low natural abundance, and low sample concentration) is a problem if the sample has spin-lattice relaxation times (T_1) of minutes, hours, or even days, because the number of transients acquired is limited to one to several dozen. Table 3.1 shows the relaxation times for many pharmaceutical solids reported in the literature.[4-10] For example using aspirin as a representative pharmaceutical solid, it has a ^{1}H T_1 relaxation time of approximately 30 s at 300 MHz. In a ^{13}C cross polarization magic-angle spinning (CPMAS) experiment the delay between acquisitions must be > 90 s to avoid saturation. Note that some of the compounds listed in Table 3.1 may have been chosen for study by researchers because they have relatively short relaxation times and could produce high-quality spectra in a short period of time.

The SNR in an NMR experiment is proportional to the signal divided by the noise.[11] The two most common approaches to improve SNR are to increase signal or decrease noise (or both). This assumes that the sample and coil are at the same temperature, and does not take into consideration fixed parameters such as line width,

Table 3.1. Pulse delays for various pharmaceutical compounds.

Compound	^{1}H Frequency	Pulse Delay (s) used	Pulse Delay at 9.4 T (s)	Ref,
R.O.Y.*	300	40-70	70-125	4
Cimetidine	360	15	18	5
LY297802	400	5-10	5-10	6
Ephedrine	200	1.5	6	7
Aspirin	300	90	160	†
Salicylic Acid	300	1000	1780	†
Prednisolone t-Butylacetate	200	3	12	8
Acetaminophen	200	2	8	9
Carbamazepine	200	3	12	10
Enalapril Maleate	200	2	8	9
Ibuprofen	200	2	8	9

*5-methyl-2-[(2-nitropheny)amino]-3-thiophenecarbonitrile (R.O.Y.), †from our laboratory

magnetogyric ratios, spin quantum numbers, etc. A further discussion of optimizing sensitivity can be found in Freeman.[11] One potential solution to increasing signal is higher magnetic field strengths, but that also has several disadvantages for solid pharmaceuticals. First, resolution often will not increase dramatically at higher fields if the sample line width is limited by bulk magnetic susceptibility or a range of conformations (as in amorphous materials). Second, higher fields require faster spinning speeds to obtain the same separation in parts per million (ppm) between isotropic peaks and spinning sidebands. This implies smaller sample volumes or masses and therefore less signal per scan. Third, for crystalline solids, especially those without methyl groups, the relaxation rate is often inversely proportional to the square of the magnetic field strength.[12,13] Going from 7.05 T to 18.8 T could potentially increase relaxation delays by about a factor of seven, significantly mitigating any sensitivity gains obtained by going to higher field strengths.

Another method to increase signal intensity is to increase the sample volume. However, there are several significant limitations to the development of a large MAS probe capable of CP and high-power ^{1}H decoupling. These include producing a high-power ^{1}H RF field capable of minimal decoupling for a moderately rigid proton environment, the ability to spin a large sample at the magic angle with minimal sidebands, and producing a homogeneous magnetic field over the entire sample. In fact, the directions of research in MAS has been to decrease sample size. Finally, lowering the temperature of the coil and other electronics can reduce noise, and is the approach taken in the cryoprobe.[14,15] The sensitivity gains arise from lower noise

figures for both the coil and the preamplifier, and a higher Q (quality factor).[14] Some sacrifice is made in filling factor, which limits the gains in sensitivity. In the solid state, especially for MAS systems, cooling the coil without cooling the sample would be extraordinarily difficult, although there are current research efforts in this area.[16] Even cooling the entire MAS system is technically challenging.

Oldfield recognized more than a decade ago that throughput was a significant issue with high-field NMR spectrometers.[17] He designed a probe that contained three different samples simultaneously located in the homogeneous region of the magnetic field. Although in his design all of the samples were static, he proposed that at least one could incorporate sample spinning. The resolution of this system was quoted as ~1 ppm. This concept has been extended to solution NMR spectroscopy.[18-25] Raftery and coworkers have shown that up to four different samples could be located simultaneously in the homogeneous region of the magnetic field.[18] However, the increase in the number of samples simultaneously present in this region of the magnetic field comes at a cost of smaller sample volumes. This design does not easily allow for incorporation of MAS for multiple samples at typical (0.5 cm^3) solid sample sizes.

In a typical 1-dimensional NMR experiment, an RF pulse is applied and a single scan or transient is acquired and collected on the order of the spin-spin relaxation (T_2) time. In signal averaging, a pulse delay, on the order of the spin-lattice relaxation (T_1) time, is necessary before a subsequent pulse can be applied. This means that the preparation and acquisition time, rather the time the spectrometer

is actively collecting data is typically tens of milliseconds (typical T_2 times). Before the sample can be pulsed again, the spins must relax for several seconds to several hours (representative T_1 times) as the bulk magnetization returns to its equilibrium value. During this time the sample must remain in a large static magnetic field while the spectrometer hardware is idle. During relaxation the external magnetic field is not required to be homogeneous. The spin-lattice relaxation time, T_1, is usually several orders of magnitude longer than T_2 in the solid state.[12] Because of this, the spectrometer is idle for a very large percentage of the time a sample occupies the magnet. Our approach to increasing sensitivity and throughput uses the fact that in SSNMR, the spin-spin relaxation time, T_2, is usually several orders of magnitude shorter than T_1. We exploit this fact by shuttling multiple MAS systems through the magnet bore, pulsing another sample while the original sample is undergoing T_1 relaxation.

3.2 Probe Concept and Design Considerations

3.2.1 Probe concept

The basic probe design consists of multiple MAS systems that are located in the bore of the superconducting magnet dewar. One possible design of this probe is shown in Figure 3.1. The MAS modules can be moved into the homogeneous region of the magnet for signal acquisition. When the signal is not being acquired, the spinning systems may be moved into a non-homogeneous magnetic field. The MAS

modules are moved in the bore of the magnet using an electric, hydraulic, or other mechanism that can change the location of the MAS modules in the magnet bore. In Figure 3.1, the concept of using a stepping motor assembly to move the probe in the magnetic field is shown. Ideally, each spinning system would feature its own air supply lines, radio-frequency (RF) connections, and magic-angle adjustment mechanism, although some or all of these features may be combined. In the design shown in Figure 1, there is a remote RF tuning and switching box that serves two purposes. First, each MAS module/circuit can be selected independently for signal acquisition. Second, it allows each circuit to be tuned independently outside the bore of the magnet dewar. Each module may have variable-temperature capability, independent spinning speed control, and independent shimming parameters.

There are several advantages of this probe design. First, it has the capability of increasing throughput by a factor of 2–10, depending upon the number of spinning modules/samples that could be analyzed. This number could be significantly higher, if the analysis time for one sample was several days. During that time, the samples in the other spinning modules could be changed several times without disturbing the sample with the long analysis time. Moreover, this system has the capability of being automated, because the probe would be designed so that all of the MAS modules could be accessed from below the magnet. The throughput advantage could be increased to 10–50 compared to a probe with no autosampler, if the samples were changed five times during an overnight run or over a weekend. If the choice were

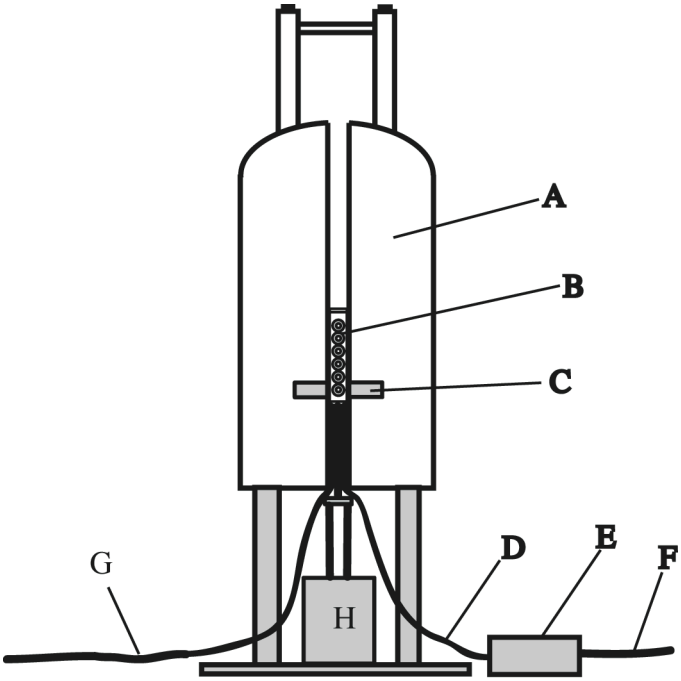

Figure 3.1. Schematic of experimental design. (A) superconducting magnet dewar; (B) MAS modules in magnet bore; (C) homogeneous region of magnet; (D) coaxial cables supplying each module; (E) RF switching and external tuning device; (F) connection to X and H high-power RF amplifiers; (G) air supply lines; (H) micro-stepping probe positioning motor.

made to run the same sample nine times, then the SNR would be tripled. It would take nine times as long to triple the SNR by signal averaging using just one spinning module. Moreover, there should be little or no loss in field homogeneity, sensitivity, MAS speed, or ^{1}H decoupling field strength compared to conventional NMR probes, nor is there a need to develop specialized spinning modules, pulse sequences, or RF technology. While this approach can be used at any magnetic field strength, it would work better at higher field strengths, where T_1 relaxation times are several times longer than at lower field strengths.[13] Higher fields also imply faster spinning systems and therefore smaller sample volumes and MAS modules. This would mean that more spinning systems could be placed in the static magnetic field, enabling more samples to be run.

There are also some limitations to this probe design. For example, this probe design is not as useful for studying nuclei in samples that have short relaxation times, such as many quadrupolar nuclei. Also, additional sample is needed if an increased SNR is desired. The modules would be self-contained, which could limit the experiments to fixed angle, double resonance, and room temperature. The constant moving of the probe may make it more prone to mechanical breakdown, and the multiple spinning modules/circuits will increase maintenance problems. Finally, having multiple spinning modules will require significantly more compressed air. All of these limitations are relatively minor compared to the gains in throughput/sensitivity that would be achieved with this probe.

3.2.2 Magnetic field strength along the magnet bore

The ideal superconducting magnet for the multiple-sample probe would have a magnetic field strength that remained approximately constant for as long as possible along the axis of the solenoid. A diagram of the field strength for an Oxford (Oxford, UK) 9.4 Tesla, 89 mm bore magnet is shown in Figure 3.2. The effective field, defined as the point at which the field remains >80%, is ~18 cm from the center of the solenoid. If all samples were confined to an 18 cm range, then only the two outer samples would feel a magnetic field of <95%, and then only while one of the outer samples was being analyzed.

3.2.3 Objectives

The goal of Chapter 3 is to demonstrate that current probe technology can be used to develop a two-module SSNMR probe. The following sections will exhibit the construction, spectrometer integration, proof of concept, and pharmaceutical application of a prototype two-module SSNMR probe.

3.3 Experimental

3.3.1 Samples

The hexamethyl benzene (HMB) used to demonstrate proof of concept was a sample from our laboratory. It was used to measure the SNR of the NMR spectrometer.

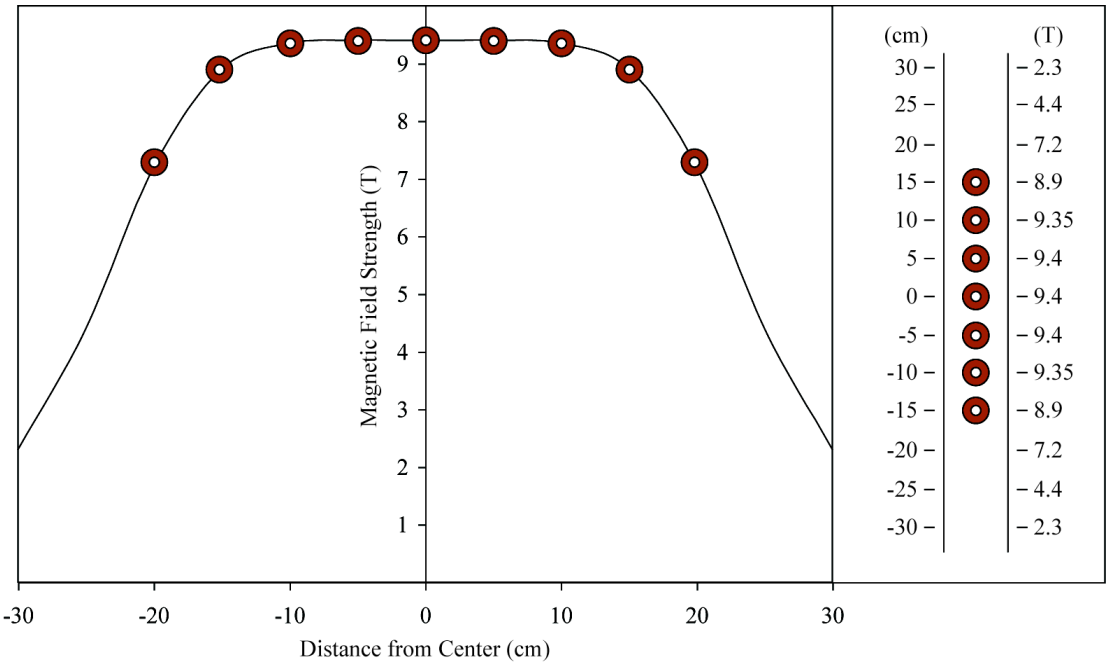

Figure 3.2. Schematic of the magnetic field strength gradient experienced by modules positioned 5 cm apart (center to center) in a 9.4 T Oxford superconducting magnet.

operation. Aspirin and ibuprofen were purchased from Sigma (St. Louis, MO) and used as-received without further processing.

3.3.2 Solid-state NMR spectroscopy

All spectra were acquired using a Chemagnetics (Fort Collins, CO) CMX-II SSNMR spectrometer operating at 75.6 MHz for ^{13}C. Samples were packed in a 7.5 mm O.D. zirconia rotor with a Kel-F endcaps and drive tip. Samples were spun at the magic angle at a rate of ~3.0 kHz. Variable-amplitude cross polarization (VACP)[26,27] was used to acquire all spectra. Proton decoupling powers of 40-80 kHz were used to acquire all spectra. Acquisition parameters for hexamethylbenzene (HMB) were: 512 data points, 30 kHz spectral width, and 17 ms acquisition time. All spectra were zero-filled to 4096 points prior to Fourier transform. No apodization was used. SNR measurements of HMB spectra were made by using a macro feature of the Spinsight software (Chemagnetics; Fort Collins, CO). Noise was sampled over a 30 ppm chemical shift range. Signal intensity was determined from the methyl peak of HMB. SNR was reproducible within 5% on consecutive acquisitions.

3.4 Results

The results section of Chapter 3 is divided into two parts. In the first part the design and testing of a two-module prototype probe are described. The second

describes the design and testing of a single-module probe that can be scaled up to seven modules.

A two-sample probe based upon a lumped element (Hester-Waugh)[28] tuning circuit was developed to test the feasibility of multiple-sample probe technology. A picture of the probe is shown in Figure 3.3. The probe was designed and built in our laboratory with a rotational axis of symmetry which facilitated construction. There were four main components to the probe: MAS modules (Figure 3.3 b and d), air lines, tuning circuits, and RF transmission lines. Standard Varian (Palo Alto, CA) 7.5 mm spinning modules were used. The modules were approximately 1.5" in diameter and have the capability to spin 7.5 mm zirconia rotors to speeds of 7 kHz. Flexible plastic tubing, 1/8" i.d., supplied compressed air to Delrin plastic supports. The Delrin supports held the spinning module in place and delivered the drive and bearing gas for the spinning systems.

The tuning circuit was comprised of several elements based on the Hester-Waugh[28] design. The coil was made from four turns of 16-gauge (0.0508" diameter) solid copper wire. American Technical Ceramics (Huntington Station, NY) fixed capacitors, and variable capacitors from Polyflon (Norwalk, CT) were used to match and tune the circuit. A quarter wavelength isolation element was made by using 1/2" o.d, copper pipe and 3/16" diameter solid copper wire to complete the tuning circuit. Tuning wands made of mixed plastic and brass parts were used to adjust the variable

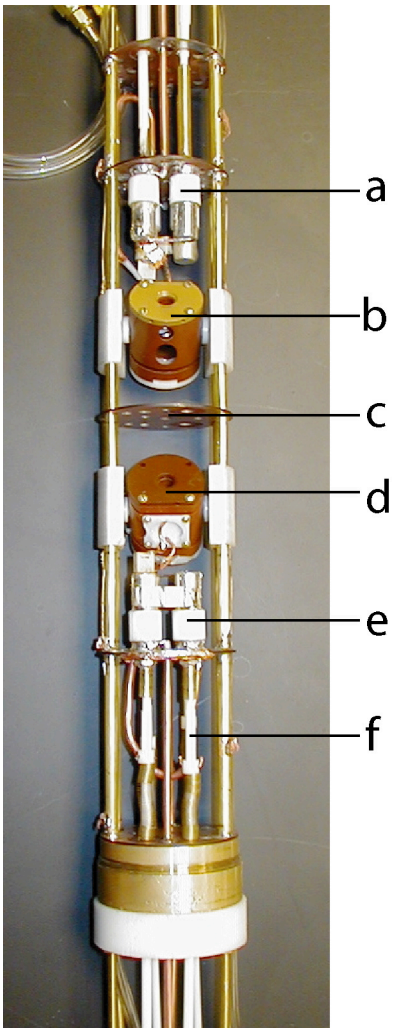

Figure 3.3. Picture of multiple-sample probe with lumped element (Hester-Waugh) tuning circuits: (a) top tuning circuit, (b) top MAS module, (c) RF isolation plane, (d) bottom MAS module, (e) bottom tuning circuit, (f) tuning wands.

capacitors from outside the magnet. RF power was supplied to the tuning circuit via 1/8" o.d., semi-rigid copper coaxial cable.

Figure 3.4 shows a photograph of the two-module probe in the bore of the superconducting magnet dewar. A PVC probe guide was used to avoid having the probe body rub against the magnet bore while moving. An Emerson Electric Co. (St. Louis, MO) model DXM-138 stepper motor, controlled via model MO35138 controller, was attached via pulley to a worm screw. The worm screw could adjust the assembly (shown in Figure 4b) approximately 20 cm. Operation of the stepper motor under the magnet had no noticeable effect on the spectra.

The samples in the MAS modules were located approximately 12 cm apart in the probe. When the top module was located in the homogeneous region of the magnet, it took roughly 1 s to move the bottom module into the homogeneous region of the magnet. For an unidentified reason, possibly related to the controller software, it took approximately 2 s to lower the two-module probe. A computer running a Microsoft Excel macro was used to control movement height and speed. Although it was possible to interface the movement control to the spectrometer hardware, the difficulty in synchronizing the two programs prompted us to delay direct spectrometer interfacing.

The spectra of HMB acquired in both the top and bottom spinning modules are shown in Figure 3.5. The SNR for the top module was ~320, which was comparable to the SNR observed using our conventional probes. The SNR of the bottom module was ~250. The reduced SNR probably reflects poor RF shielding.

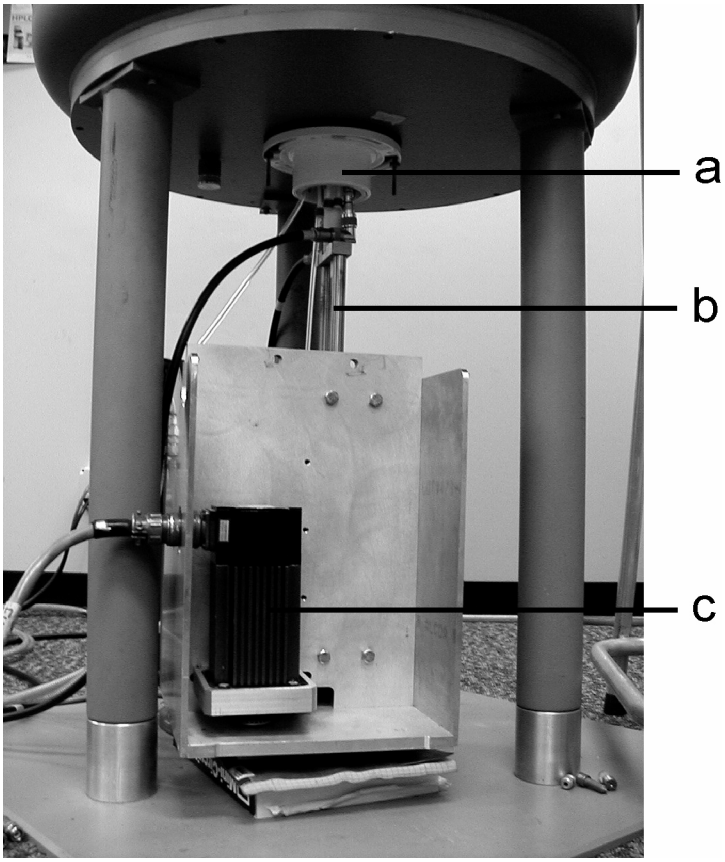

Figure 3.4. Photograph of probe in magnet. The probe is moved using a stepper motor assembly: (a) probe guide in magnet, (b) probe movement assembly, (c) stepper motor.

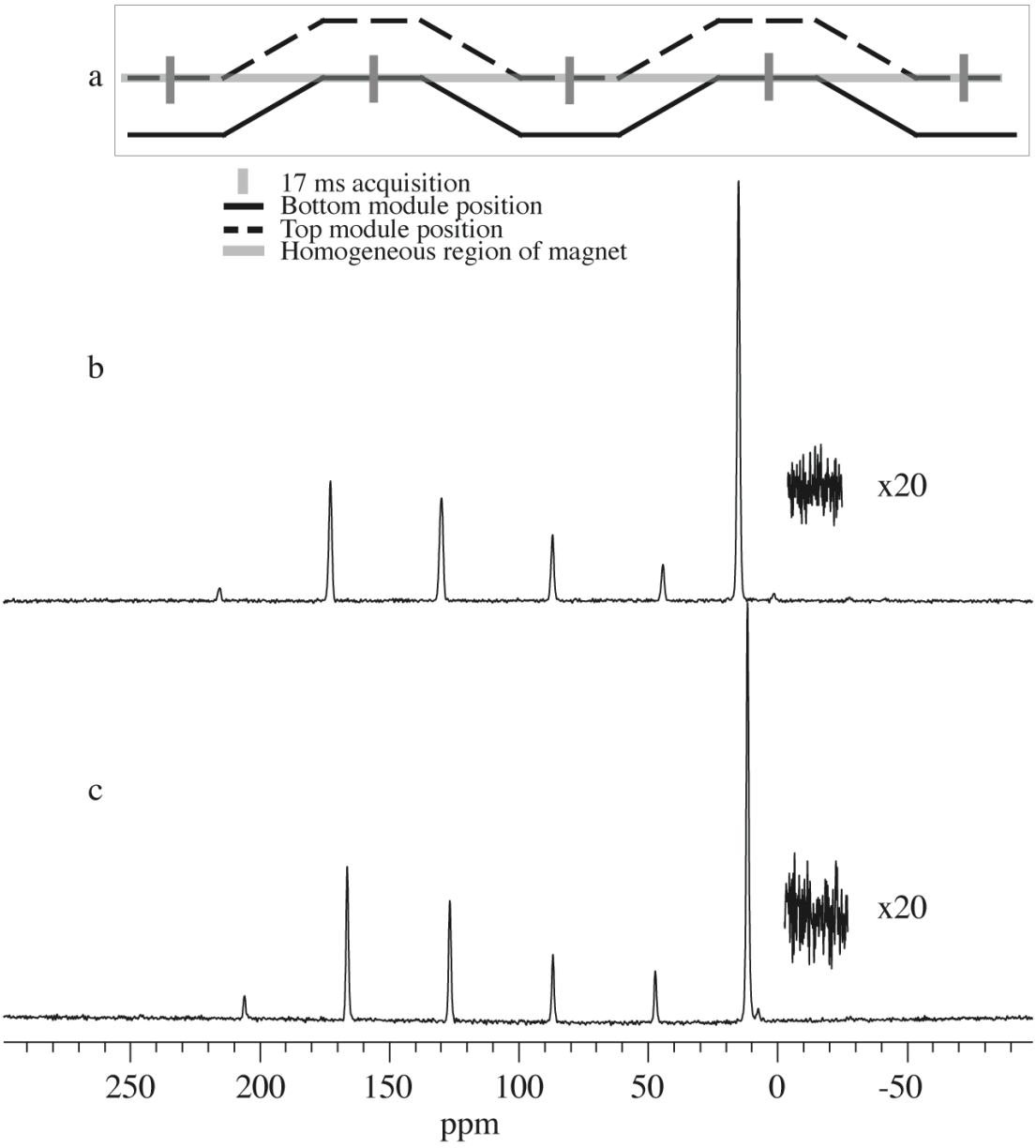

Figure 3.5. HMB spectra acquired from top and bottom module. Each spectrum was 12 acquisitions and each acquisition was alternated between the modules: (a) schematic of module position in magnet and pulse timing, (b) spectrum acquired in top module, (c) spectrum acquired in bottom module.

The ^{1}H 90° pulse widths for both modules were ~4.0 μs. The spectra in Figure 3.5 were acquired by alternating each acquisition between the top and bottom module, showing that it was possible to return each module in the probe to the homogeneous region of the magnet.

Figure 3.6 shows a spectrum of HMB acquired with motion using a single module. The purpose of this experiment was to synchronize data acquisition with probe/sample movement and to demonstrate robustness of the NMR acquisition. The schematic in Figure 3.6a shows the timing sequence of the probe movement in the bore of the magnet. Figure 3.6b is the NMR spectrum of HMB acquired while moving the probe as if spectra from two modules were being collected. The following cycle took 5 s, where the order refers to which sample is in the homogeneous region of the magnet: top module (1 s), move to bottom (1 s), bottom module (1 s), move to top module (2 s). The cycle of probe position was very reproducible, and a spectral acquisition with a 4.8 s pulse delay was used, starting with the top module in the homogeneous region of the magnet. The HMB spectrum obtained was comparable to those acquired without movement in Figure 3.5.

Aspirin and ibuprofen were used to demonstrate the pharmaceutical applicability of the two-module prototype. A spectrum of aspirin was collected in one module while ibuprofen was collected in the other. The sample of crystalline aspirin had a ^{1}H T_1 time of ~60 s at 7.05 T. For optimal SNR per time, pulse delays of ~1.25 times the T_1 value are used. The sample of aspirin was collected with a 90-s pulse delay, and 64 transients were acquired. Ibuprofen has a ^{1}H T_1 time of ~2 s, and

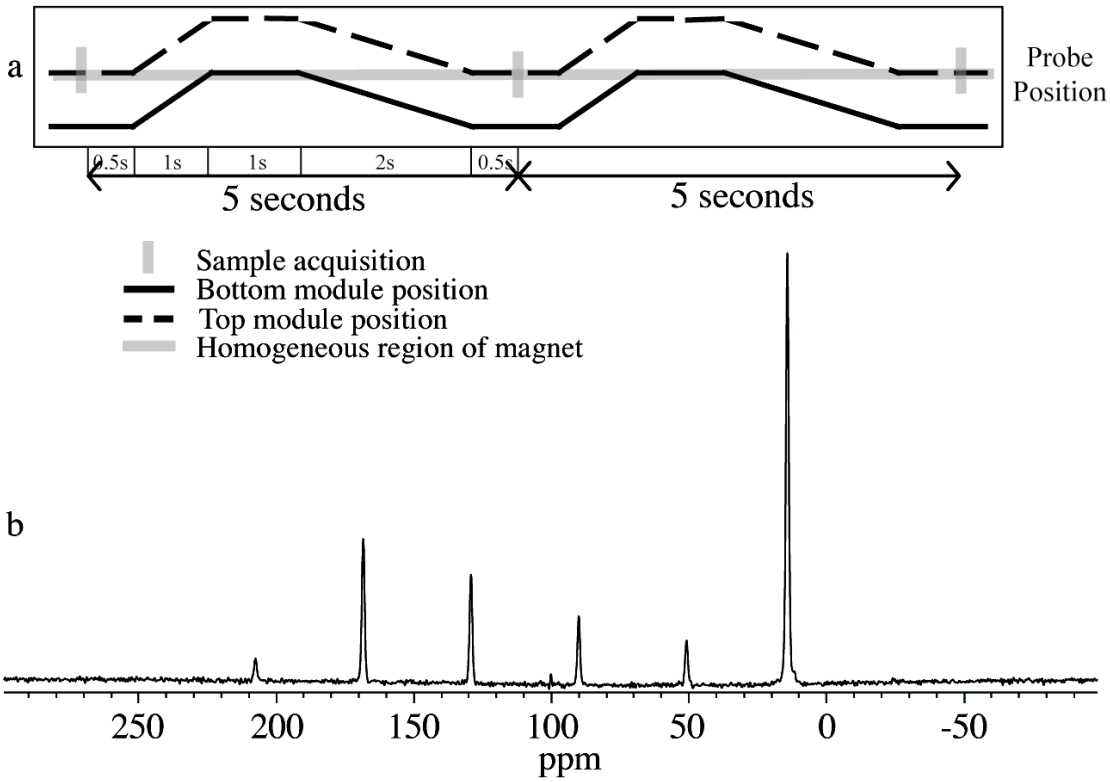

Figure 3.6. Spectrum of HMB acquired using the bottom module with the pulse sequence timing chosen to coincide with probe movement: (a) schematic of timing of probe movement and spectral acquisition, (b) HMB spectrum.

a 3-s pulse delay was used. The probe pulsed the ibuprofen sample in the bottom module 30 times while the aspirin magnetization was allowed to equilibrate. Then the stepper motor lowered the probe height until the top module was in the homogeneous region of the magnet. At this point, one transient of aspirin was collected. The probe was raised, and this cycle was completed 64 times. In the end, 64 transients of aspirin were collected along with 1920 transients of ibuprofen. The 13C CPMAS NMR spectra of aspirin and ibuprofen are shown in Figure 3.7. The spectrum of aspirin acquired simultaneously with ibuprofen is shown in Figure 3.7b. The spectrum of ibuprofen is displayed in Figure 3.7c. A spectrum of aspirin was acquired with 64 transients without motion to compare the spectral quality with and without motion.

Several interesting features can be observed from the spectra in Figure 3.7. First, the spectra of aspirin acquired with and without movement are nearly indistinguishable. There may be slight differences in peak resolution, which could be attributed to intermittent arcing, changes in tuning, and/or the overall efficiency of probe operation. Second, the field at which the aspirin was located while the spectrum of ibuprofen was acquired must have been very close to 7 T in order for the Boltzmann population difference to return to the same value as in the spectrum acquired without movement. Finally, the concept of sample shuttling has been demonstrated as a method of simultaneous acquisition in a superconducting magnet.

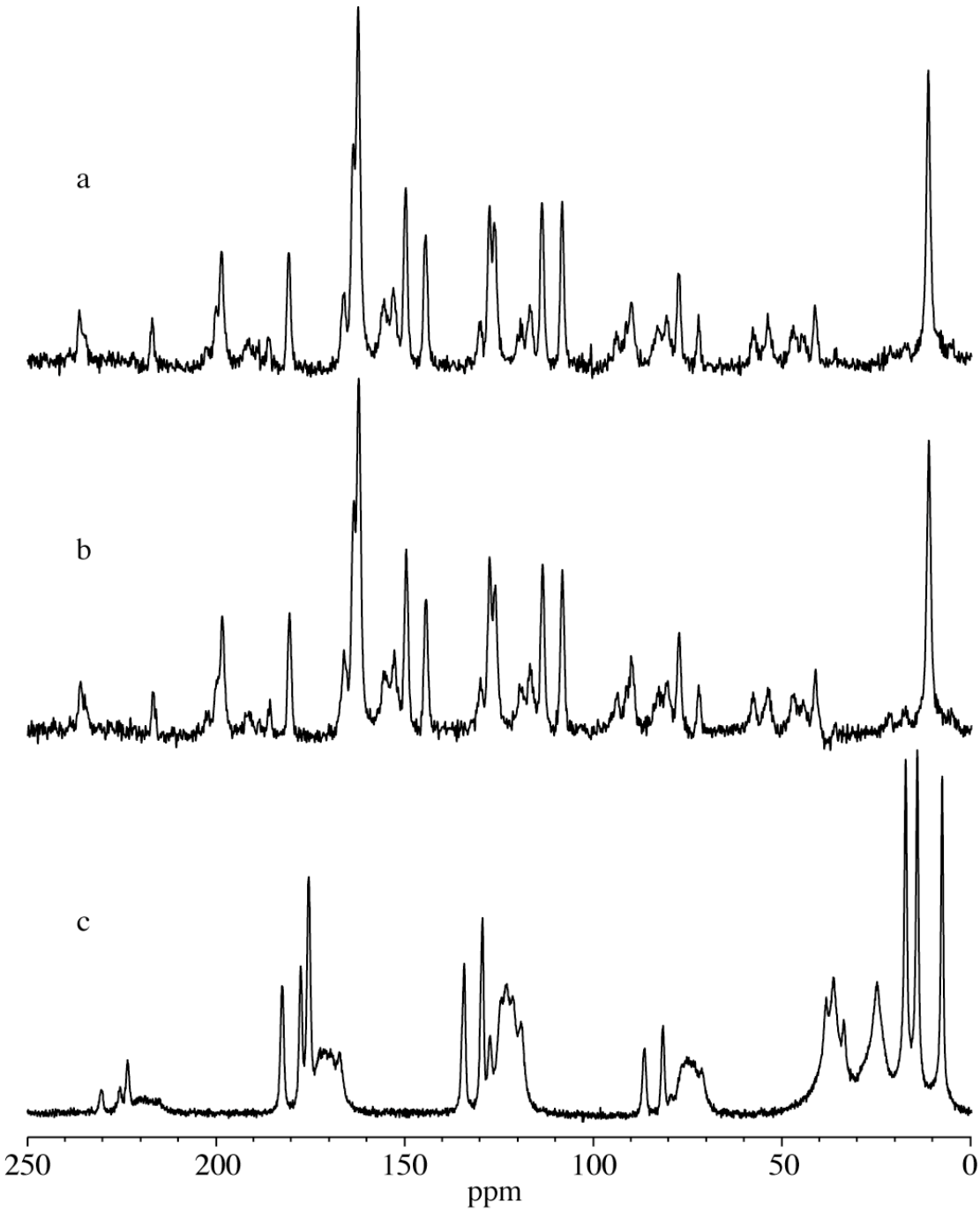

Figure 3.7. ^{13}C CPMAS Spectra of aspirin and ibuprofen: (a) aspirin acquired without motion, (b) aspirin acquired with motion and switching, (c) ibuprofen acquired with motion and switching.

3.5 Conclusions

In this chapter, a two-module prototype probe was constructed using current probe technologies. Spectra were collected on each module that had comparable SNR of those manufactured by Chemagnetics. A stepper motor was attached and the motion of the probe was synchronized with data acquisition. Lastly, the ^{13}C CPMAS spectra of two pharmaceutical samples were acquired simultaneously. To fully incorporate this probe, it is necessary to further investigate many areas, specifically RF isolation between modules and magnetic field gradient effects on relaxation. First, the proximity of each module in relation to the other might allow "cross talk" between modules. The RF pulse on one module could potentially affect the signal in the other module. Proper RF isolation will eliminate this possibility. There were not issues with RF isolation on the two-module protype; however, the modules in the two-module prototype were ~12 cm apart. The incorporation of additional modules would cause the distance between modules to be reduced to a few centimeters. Second, spin-lattice relaxation times are a function of magnetic field strength. When a sample is relaxing outside the homogeneous region, the magnetic field gradient causes it to experience a slightly slower magnetic field. The amount of time a sample spends at lower field strengths could affect its T_1 time. Before the probe is used for quantitation studies, this effect should be carefully studied.

3.6 References

1. Bugay DE 1993. Solid-State Nuclear Magnetic Resonance Spectroscopy: Theory and Pharmaceutical Applications. Pharmaceutical Research 10:317-327.

2. Bugay DE. 1995. Magnetic Resonance Spectrometry. In Brittain HG, editor Physical Characterization of Pharmaceutical Solids, ed., New York: Marcel Dekker, Inc. p 93-125.

3. Offerdahl TJ, Munson EJ 2004. Solid-State NMR Spectroscopy of Pharmaceutical Materials. American Pharmaceutical Review 7:109-112.

4. Smith J, MacNamara E, Raftery D, Borchardt T, Byrn SR 1998. Application of Two-Dimensional ^{13}C Solid-State NMR to the Study of Conformational Polymorphism. Journal of the American Chemical Society 120:11710-11713.

5. Middleton DA, Le Duff CS, Berst F, Reid DG 1997. A Cross-Polarization Magic-Angle Spinning ^{13}C NMR Characterization of the Stable Solid-State Forms of Cimetidine. Journal of Pharmaceutical Sciences 86:1400-1402.

6. Reutzel SM, Russell VA 1998. Origins of the Unusual Hygroscopicity Observed in LY297802 Tartrate. Journal of Pharmaceutical Sciences 87:1568.

7. Schmidt WF, Honigberg IL 1991. Nuclear Magnetic Resonance (NMR) Spectroscopic Investigation of Interaction Energies of Ephedrine Steroisomers in Non Crystalline Solids and its Correlation with Thermodynamic Data. Pharmaceutical Research 8:1128-1136.

8. Byrn SR, Sutton PA, Tobias B 1988. The Crystal Structure, Solid-State NMR Spectra and Oxygen Reactivity of Five Crystal Forms of Prednisolone tert-butylacetate. Journal of the American Chemical Society 110:1609-1614.

9. Saindon PJ, Cauchon NS, Sutton PA, Chang C-j, Peck GE, Byrn SR 1993. Solid-State Nuclear Magnetic Resonance (NMR) Spectra of Pharmaceutical Dosage Forms. Pharmaceutical Research 10:197-203.

10. Suranarayanan R, Wiedmann TS 1990. Quantitation of the Relative Amounts of Anhydrous Carbamazepine and Carbamazepine Dihydrate in a Mixture by Solid-State Nuclear Magnetic Resonance. Pharmaceutical Research 7:184-187.

11. Freeman R. 1988. A Handbook of Nuclear Magnetic Resonance. ed., New York: John Wiley and Sons Inc,. p 312.

12. Fyfe CA. 1983. Solid State NMR for Chemists. ed., Guelph, Ontario, Canada: C.F.C. Press. p 593.

13. Harris RK. 1989. Nuclear Magnetic Resonance A Physicochemical View. ed., New York: John Wiley and Sons, Inc. p 260.

14. Styles P, Soffe NF, Scott CA, Cragg DA, Row F, White DJ, White PCJ 1984. A High-Resolution NMR Probe in Which the Coil and Preamplifier are Cooled with Liquid Helium. Journal of Magnetic Resonance 60:397-404.

15. Serber Z, Richter C, Moskau D, Boehlen J-M, Gerfin T, Marek D, Haeberli M, Baselgia L, Laukien F, Stern AS, Hoch JC, Doetsch V 2000. New Carbon-Detected Protein NMR Experiments Using CryoProbes. Journal of the American Chemical Society 122(14):3554-3555.

16. Shevgoor S, Spitzmesser JB, Kulkarni J, Staab JP, Entzminger G, Doty DF. Experimental NMR Conference, Providence, Rhode Island, 2005.

17. Oldfield E 1994. A Multiple-Probe Strategy for Ultra-High-Field Nuclear Magnetic Resonance Spectroscopy. Journal of Magnetic Resonance, Series A 107:255-257.

18. MacNamara E, Hou T, Fisher G, Williams S, Raftery D 1999. Multiplex sample NMR: an approach to high-throughput NMR using a parallel coil probe. Analytica Chimica Acta 397(1-3):9-16.

19. Hou T, MacNamara E, Raftery D 1999. NMR Analysis of Multiple Samples Using Parallel Coils: Improved Performance Using Reference Deconvolution and Multidimensional Methods. Analytica Chimica Acta 400:297-305.

20. Fisher G, Petucci C, MacNamara E, Raftery D 1999. NMR Probe for the Simultaneous Acquisition of Multiple Samples. Journal of Magnetic Resonance 138(1):160-163.

21. Hou T, Smith J, MacNamara E, Macnaughtan M, Raftery D 2001. Analysis of Multiple Samples Using Multiplex Sample NMR: Selective Excitation and Chemical Shift Imaging Approaches. Analytical Chemistry 73:2541-2546.

22. Zhang X, Sweedler JV, Webb AG 2001. A Probe Design for the Acquisition of Homonuclear, Heteronuclear, and Inverse Detected NMR Spectra from Multiple Samples. Journal of Magnetic Resonance 153(2):254-258.

23. Raftery D, Fisher GG, Petucci CJ, McNamara E. 2002. Nuclear Magnetic Resonance of Multiple Samples. US Patent and Trademark Office, ed., USA. p 26.

24. MacNaughtan MA, Hou T, Xu J, Raftery D 2003. High-Throughput Nuclear Magnetic Resonance Analysis Using a Multiple Coil Flow Probe. Analytical Chemistry 75(19):5116-5123.

25. Ike, Okada T, Suematsu H, Yamakoshi Y. 2003. NMR probe for multiplex resonance [Machine Translation]. Jpn Kokai Tokkyo Koho, ed., Jp: (Jeol Ltd., Japan). p 7 pp.

26. Peersen OB, Wu XL, Kustanovich I, Smith SO 1993. Variable-Amplitude Cross-Polarization MAS NMR. Journal of Magnetic Resonance Series A 104(3):334–339.

27. Pines A, Gibby MG, Waugh JS 1973. Proton-enhanced NMR of Dilute Spins in Solids. Journal of Chemical Physics 59(2):569–590.

Chapter 4

Model Compound Selection

4.1 Introduction

4.1.1 Background

There is a significant interest in being able to quantitate the solid forms present in a formulated product, as these forms can significantly contribute to the overall chemical and physical stability, dissolution rate, bioavailability, and overall therapeutic efficacy of the drug product.[1-4] In particular, detecting and quantitating mixtures of crystalline and amorphous forms of an API is a challenging problem.[1,2] Traditional analytical methods such as DSC and PXRD have difficulty in detecting and monitoring amorphous drug content when it is below 5%.

Solid-state NMR spectroscopy has great potential to quantitate crystalline and amorphous content in pharmaceutical formulations. The objective of this research is to determine the limits of detection and quantitation crystalline and amorphous forms of API in formulations using ^{19}F SSNMR.[5,6] ^{19}F SSNMR provides several advantages over the more traditionally observed ^{13}C nucleus such as improved sensitivity and no background from excipients. However, a major concern with ^{19}F SSNMR for quantitation purposes is the ability to discriminate between the crystalline and amorphous components. In order for us to determine the ability of ^{19}F SSNMR to quantitate API forms, it was determined that it was necessary to generate pure standards of fluorine-containing API. Having pure standards of each form can greatly aid in quantitation, because NMR properties such as relaxation times and line widths

can be measured for the pure material. In addition, pure standards allow for the technique to be validated for the system under study.

In this chapter the process of selecting an appropriate compound for study will be described. We identified the following characteristics that a standard should have: physical and chemical stability; reproducible generation of crystalline/amorphous forms using standard techniques such as recrystallization, desolvation, cryogrinding, milling, lyophilization, or spray drying; compatibility of forms such that one form will not induce changes in another form; and ^{19}F SSNMR chemical shift separation between amorphous and crystalline forms.

4.1.2 Generating stable amorphous compounds

Although macromolecular excipients, large peptides and proteins are usually amorphous, small molecule organic molecules, such as many of the current API on the market, are usually crystalline. There are several common methods that are used to make these small-molecule compounds amorphous. Some of these include: supercooling a melt, milling, vapor condensation, and precipitation. These techniques are briefly described in the following paragraphs.

Melting a solid forms a liquid in which the molecules are randomly distributed with a high degree of molecular motion. If this liquid can be cooled below its melting temperature (T_m) without solidification, the disorder of the liquid can be kinetically frozen, and is referred to as supercooled melt.

Milling crystals can destroy the long-range order of the crystalline material. Cryomilling or cryogrinding consists of grinding a sample in a bath of liquid nitrogen. An advantage of cryogrinding rather than milling is the reduced likelihood of thermal degradation.

Spray drying and lyophilization are examples of precipitation from solution, and can be used to generate the amorphous form. In the case of lyophilization, the drug solution is frozen and the solvent slowly sublimes. As the solvent is removed, a high degree of disorder of the drug can be retained. Lyophilization requires that a solvent exhibits a triple point and does not transition through the liquid phase prior to reaching the gas phase. A liquid phase could allow the material to crystallize. Spray drying consists of spraying drug solution through a heated nozzle and exposing the droplets to heated gas. The solvent rapidly evaporates, and/or the material condenses quickly from the solution. In many cases, the compound will retain the molecular disorder it possessed in the solution.

4.2 Selecting a Model Amorphous Compound as a Quantitation Standard

An acceptable fluorine-containing model compound for these studies has to contain fluorine and be pharmaceutically relevant. The intent of the project was to demonstrate the ability of ^{19}F SSNMR spectroscopy to quantitate low levels of amorphous material in drug substance and drug product, so only compounds that are currently marketed or were previously marketed were considered.

The amorphous form of the model compound should have two important characteristics. First, the form should be physically stable. A common rule of thumb to ensure physical stability is to be 50 °C below the glass transition, so an ideal T_g is greater than 50 °C above ambient temperature.[7] When possible, the experiments were performed at ambient temperature. If the T_g is too low, the amorphous form could crystallize during the experiment. Second, the crystalline and amorphous forms of interest should have significantly different chemical shifts in the ^{19}F SSNMR spectrum. Chemical shift resolution of several ppm is necessary because amorphous materials typically have very broad peaks. If adequate resolution cannot be achieved, then the amorphous and crystalline peaks must be deconvoluted. Many solid forms of the same drug have different SSNMR properties. Amorphous forms of drugs typically have NMR line widths that are much broader (5-10 times) than their crystalline counterparts. The breadth of the lines is due to the increase in distribution of molecular environments. It is common for different solid forms to have different chemical shifts and NMR relaxation times.

A search was performed to locate pharmaceutical substances to consider as potential model compounds for quantitation using ^{19}F SSNMR spectroscopy. Presented in Table 4.1 is a list of potential candidates. The compounds in the list are used in many different therapeutic areas, and the vast majority of these compounds contained a single mono-fluoro (-F) or trifluoromethyl (-CF_3) group. Each compound was examined to determine the suitability for quantitation of

Table 4.1. Physicochemical and cost data for some of the potential model compounds for ^{19}F NMR quantitation. The data help determine which amorphous generation process is best suited for each compound. Sample mass is determined based on the cost of one gram of material ($50 > (H), $50 < (M) < $200, $200 < (L)).

Compound	Fluorine Group	Sample Mass	T_m (°C)	Estimated T_g (°C)
Bendroflumethiazide	CF3	H	224.5-225.5	76-150
Ciprofloxacin	F	H	318-320	141-230
Dexamethasone	F	H	262-264	102-183
Flecainide	2(CF3)	L	145-147	20-83
Florfenicol	F	M	153-154	26-90
Fludrocortisone acetate	F	H	233-234	82-158
Flufenamic acid	CF3	H	125	6-65
Flumequine	F	H	253-255	96-175
Flumethasone acetate	2(F)	L	260-264	102-182
Flunarizine 2(HCl)	2(F)	H	251.5	94-173
Flunisolide	F	L	?	?
Fluocinolone acetonide	2(F)	M	265-266	104-185
5-Fluorouracil	F	H	282-283	116-199
Flurbiprofen	F	H	110-111	-5-53
Flutamide	CF3	H	111.5-112.5	-4-54
Fluvastatin Na	F	L	194-197	55-125
Hydroflumethiazide	CF3	H	272-273	109-191
Levofloxacin	F	H	218	71-144
Triamcinolone	F	M	269-271	107-189
Triamcinolone acetonide	F	H	186-188	49-118
Triamcinolone diacetate	F	H	292-294	123-208
Trifluoperazine 2(HCl)	CF3	H	242-243	88-165

amorphous content by ^{19}F SSNMR. Table 4.1 contains a list of common fluorine drug compounds, sample mass availability based on cost, the melting temperature (T_m) (the T_m could change based on solid form or processing), and the estimated glass transition (T_g) temperature. Several examples were chosen to highlight the difficulties in selecting an ideal model compound. It should be noted that many of these compounds were potentially chosen for development because of their relative physical and chemical stability and may not be representative of many of the compounds currently in the pipelines of many pharmaceutical companies.

4.3 Experimental

4.3.1 Materials

Bendroflumethiazide, ciprofloxacin, 5-fluorouracil, levofloxacin, and triamcinolone were purchased from Sigma (St. Louis, MO). Dexamethasone was purchased from Alfa Aesar (Ward Hill, MA).

4.3.2 Sample preparation

Multiple sample preparation methods were used to create amorphous materials. The cryogrinding and spray drying methods are described below.

4.3.2.1 Cryogrinding

Cryogrinding was performed with a SPEX CertiPrep 6750 Freezer/Mill (SPEX CertiPrep, Inc., Metuchen, NJ). Approximately 500 mg of as-received material was loaded into the cryovial for each process. Samples were pre-cooled for 15 minutes, followed by 30 cycles. Each cycle consisted of two minutes of impaction and two minutes of cooling time. The impaction rate was 10 impacts/s. After grinding, the cryovial was allowed to return to ambient temperature while umder vacuum prior to removal of the powdered sample in order to prevent the formation of condensate on the powder.

4.3.2.2 Spray drying

Bendroflumethiazide and 5-fluorouracil were spray dried with a Buchi Mini 190 (New Castle, DE). The spray dryer was set up with an injection rate of 2-3 mL/min, an airflow rate of 600 Nl/h, and an aspirator rate of 100%. The solution for bendroflumethiazide consisted of 2-3% (wt/wt) of drug and 75% (v/v) ethanol:water. The inlet temperature was 75-80 °C. Nitrogen gas was used to eliminate oxygen in the spray-drying chamber. Two grams of 5-fluorouracil were dissolved in 500 ml of water. The inlet temperature of the spray dryer was set to 165 °C.

Levofloxacin and triamcinolone were spray dried with a custom-built spray dryer (Bend Research, Inc., Bend, Oregon). Approximately 200 mg of drug was dissolved in 10 g of warmed methanol, producing approximately a 2 wt% solution. The solution was injected into the spray dryer at a rate of 1.3 mL/min with an inlet

temperature of 70 °C. The material was collected on a piece of 110-mm Whatman filter paper, and an anti-static gun was used to discharge any electrostatic charge. The spray-dried material was exposed to a vacuum for one hour at ambient temperature to remove any residual methanol.

4.3.3 Sample analysis

Multiple complementary techniques were used to characterize the materials produced by the various preparation methods. Each analytical technique provides complementary information. Each of the techniques is described below.

4.3.3.1 Differential scanning calorimetry (DSC)

Differential scanning calorimetry (DSC) was performed on a TA Instruments (New Castle, DE) Q100 with a refrigerated cooling system. The DSC was calibrated with Indium. Aluminum pans were filled with 5-15 mg of sample and hermetically sealed. An empty hermetically-sealed aluminum pan was used as a reference. Samples were equilibrated at -50 °C and then ramped at a rate of 10 °C/min to 240-300 °C. Data analysis was performed on Universal Analysis 2000 software version 4.3, provided by TA instruments.

4.3.3.2 Solid-state NMR spectroscopy

^{19}F SSNMR spectra on all solid forms of ciprofloxacin, levofloxacin, dexamethasone, and the solid forms of triamcinolone as shown in Figure 4.8 were

performed on a Bruker (Bruker, Billerica, MA) Avance 500 three-channel spectrometer outfitted with an $^{1}H/^{19}F/X$ triple-resonance probe and operating at 469.8 MHz for ^{19}F and 499.3 MHz for ^{1}H. Samples were packed in 4-mm zirconia rotors , sealed with Vespel drive trips, and spun at a rate of 15 kHz.[8,9] A 2.7-μs ^{19}F 90° pulse-width was used in direct polarization of the ^{19}F nucleus with two-pulse phase modulated (TPPM) proton decoupling. The spectral width was 100 kHz (212.9 ppm), 3072 points were collected in all cases, and acquisition times were between 10 and 16 ms. All samples acquired on the Bruker Avance 500 were referenced to a 1:1 solution of trifluoroacetic acid (TFA) and water at -76.54 ppm. ^{19}F and ^{13}C SSNMR spectra of bendroflumethiazide, dexamethasone, and triamcinolone (Figures 4.6, 4.11, and 4.12) were collected on a Tecmag (Houston, TX) Apollo three-channel spectrometer operating at 284.1 MHz for ^{19}F, 301.9 MHz for ^{1}H, and 75.9 for ^{13}C. A Chemagnetics (Varian, Inc., Fort Collins, CO) double-resonance $^{1}H/^{19}F$ probe was used to collect the data. The samples were packed in 3.2-mm o.d. zirconia rotors with torlon endcaps and a Vespel drive tip. Samples were spun at a rate of 10-20 kHz. ^{1}H to ^{19}F cross polarization (CP)[10,11] was employed along with two-pulse phase modulated (TPPM) proton decoupling. A ^{1}H 90° pulse of 2.9 μs and a contact time of 2 ms were used. A spectral sweep width of 100 kHz was used. All spectra were referenced to Teflon at -121.1 ppm. The temperature of triamcinolone samples was adjusted using a variable-temperature accessory that delivered liquid-nitrogen cooled air directly to the spin module housing. The temperature was calibrated with methanol.

4.3.3.3 Polarized-light microscopy

Light microscopy was performed on an Olympus BX51 (McCrone, Westmont, IL) equipped with a digital camera.

4.4 Results

4.4.1 Introduction to sample selection

There is not one sample preparation method that consistently and reproducibly generates a stable amorphous material for all compounds. The solubility (aqueous and organic), melting temperature, and sample mass are important to consider when selecting a process to generate an amorphous solid. Ideally, several hundred milligrams of amorphous material should be relatively easy to generate. Table 4.1 contains a list of compounds, their aqueous solubility, melting temperature, and available sample mass (based on cost).

Spray drying and cryogrinding both require several hundred milligrams of bulk crystalline material. If necessary, lyophilization and melt quenching can be performed with significantly less. Spex Certiprep manufactures a low sample mass cryovial, but low-sample mass (<100 mg) grinding was largely unsuccessful. The second caveat is aqueous solubility; the solubility of a chemical is extremely important for spray drying and lyophilization to be applicable. For samples with poor aqueous solubility, quench cooling a melt and cryogrinding are better options. When using the Buchi spray dryer, larger samples masses were necessary because the

collected spray-dried product yield was approximately 25%. The Buchi spray dryer was not designed to routinely spray dry from organic solvents. Because of these two considerations, very few compounds could be spray dried with the Buchi Mini 190. The custom-built spray dryer from Bend Research could spray-dry from organic solvents safely and easily, and produced yields of approximately 75-80%.

4.4.2 Initial compound selection

Several candidates were excluded based on available sample mass (Table 4.1), which was determined by the cost of the drug. High (H) sample mass corresponded to a compound that was available for a cost of less than $50/gram. A medium (M) tag was applied when the price was less than $200/gram, and a chemical was tagged low (L) when the drug exceeded $200/gram. All drugs with a low sample mass were eliminated: flecainide, flumethasone acetate, flunisolide, and the fluvastatin sodium salt.

Other candidates were excluded because it was estimated that the glass transition would be too low for adequate physical stability. Byrn et al. derived a relationship between T_g and T_m for a list of amorphous pharmaceuticals.[12] They found that the T_g/T_m ratio was typically between 0.7 and 0.85.[12] A model compound for this study should have a glass transition 50 °C above room temperature (75 °C).[13] According to this estimation method, a T_g above 75 °C would correspond to a T_m range of 136-224 °C. Flufenamic acid, flurbiprofen, and flutamide were attractive

candidates for melt quenching and cryogrinding, but the estimated glass transitions were too low.

The final criterion for excluding several of the compounds was that an amorphous form of the compound could not be generated. The model compound search was structured to focus on previously or currently marketed fluorinated drugs. As noted before, many of these drug substances were likely selected for the thermodynamic stability of the crystalline form and low susceptibility to physical transformations. 5-fluorouracil was cryoground and spray dried. In the ^{19}F SSNMR spectra (not shown) there were no discernible changes in line width, line shape, or chemical shift between the processed material and the bulk materials. It was not uncommon for the processes to generate only crystalline forms and not amorphous material. Melt-quenching the compounds was not a viable method for the substances in this study because many organic compounds thermally degrade at or below their melting point.

Hence, the list of potential model compounds was reduced to five: bendroflumethiazide, ciprofloxacin, levofloxacin, dexamethasone, and triamcinolone. An amorphous form was generated for each of these substances, and the drug that best met the criteria of a good model compound was selected. In Figure 4.1, the structures of the five compounds are shown. In the next section an evaluation of each compound is described which highlights the suitability of that substance as model for ^{19}F SSNMR quantitation.

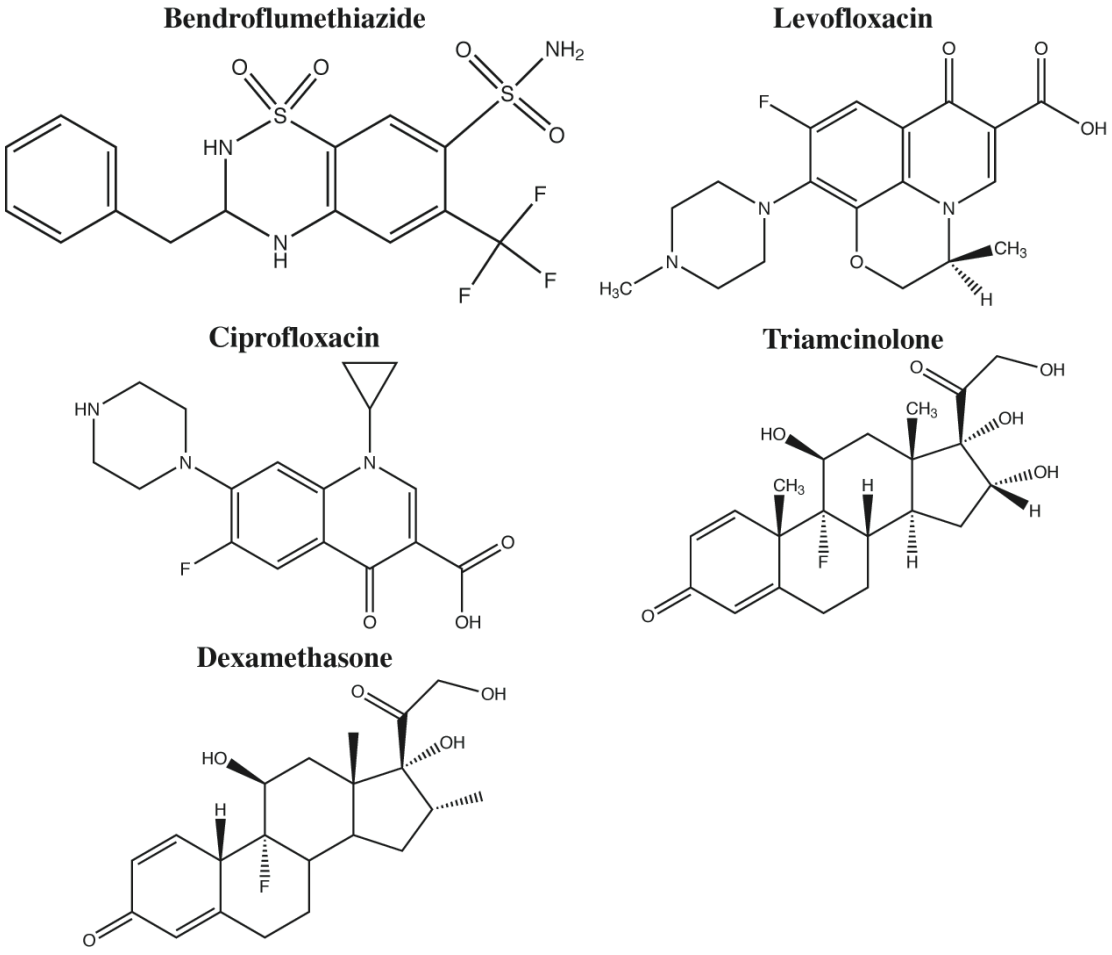

Figure 4.1. Potential model compounds and their structures.

4.4.3 Partial amorphous generation

The ^{19}F SSNMR spectra of the bulk as-received material and cryoground ciprofloxacin are shown in Figure 4.2. The isotropic crystalline NMR peak of the as-received material shown in Figure 4.2a had a chemical shift of -119.5 ppm and a line width of ~500 Hz. After cryogrinding for 60 minutes, a broad peak was observed at the base of the crystalline peak. The broad peak at the base was interpreted as the presence of the amorphous form of ciprofloxacin. The ^{19}F SSNMR spectrum of the cryoground ciprofloxacin was deconvoluted with two peaks: one peak each for the crystalline and amorphous forms.

The crystalline form had a chemical shift of -119.5 ppm and a line width of ~500 Hz. The other peak, due to the presence of amorphous ciprofloxacin, had a chemical shift of -119.6 ppm and a line width of ~2700 Hz. The amorphous peak was 5-6 times broader than the crystalline peak. The presence of the crystalline peak in Figure 4.2b indicated that cryogrinding ciprofloxacin for 60 minutes was not sufficient to fully generate the amorphous form. The grinding process could potentially be lengthened to generate a pure amorphous form, but even if a stable amorphous form were generated for ciprofloxacin, the lack of resolution between the crystalline and amorphous peaks makes it an unattractive model compound. Different polymorphic forms can have different chemical shifts.[14] If a stable amorphous form could be produced for ciprofloxacin, it may be possible to use a different crystalline polymorph standard in the physical mixtures. Ciprofloxacin was not spray dried because it is insoluble in methanol, acetone, and water.

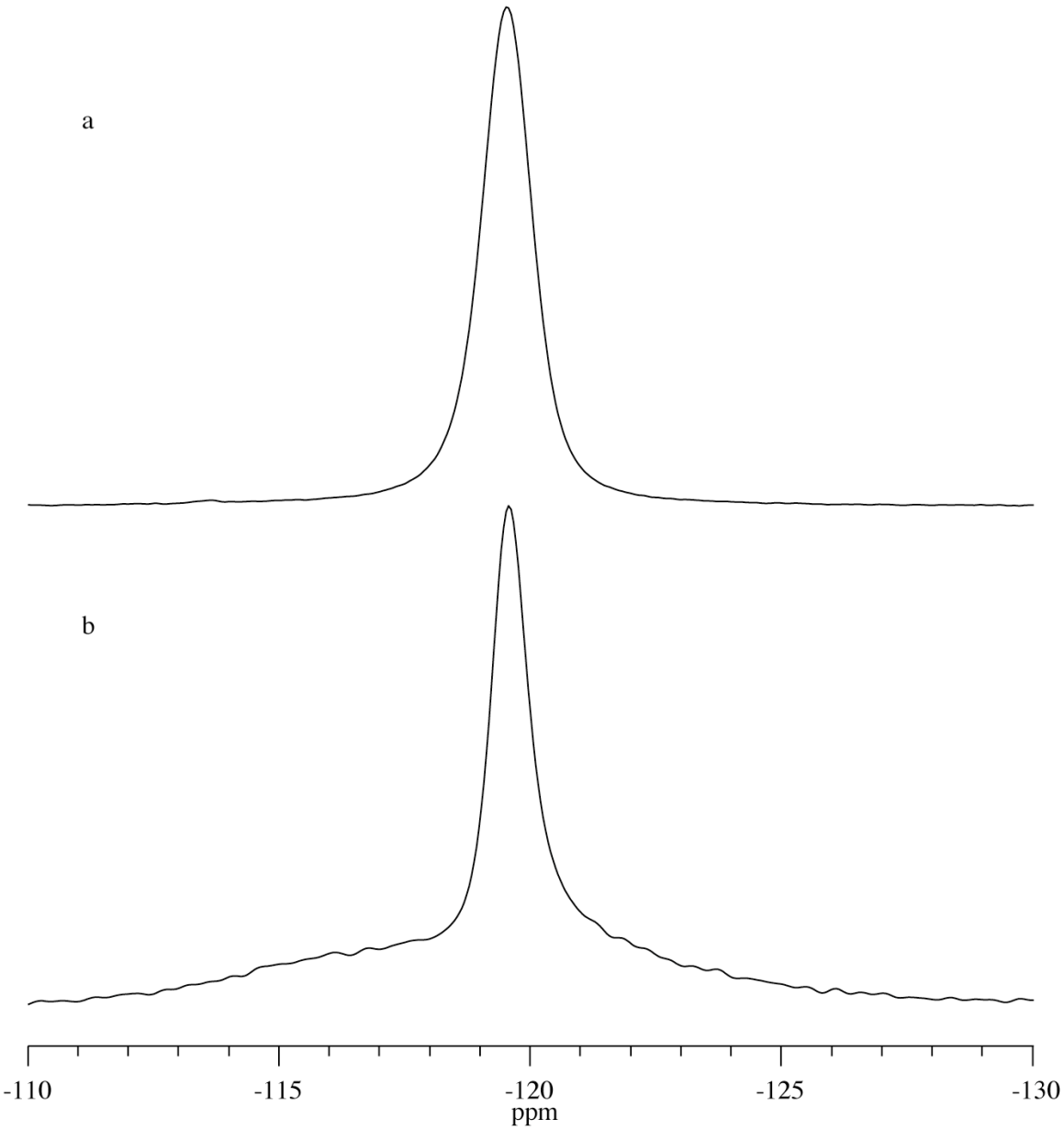

Figure 4.2. ^{19}F SSNMR spectra of a) ciprofloxacin as-received from Fluka and b) ciprofloxacin cryoground for 60 minutes.

4.4.4 Lack of chemical shift resolution

The lack of significant chemical shift resolution between the crystalline and amorphous forms eliminated several compounds, even though pure amorphous forms could be generated. For example, amorphous bendroflumethiazide was prepared by spray drying from an ethanol and water solution previously demonstrated by Corrigan et al.[14] The generation of amorphous material was confirmed by ^{13}C and ^{19}F SSNMR spectra, as shown in Figure 4.3. Figure 4.3a shows the ^{13}C CPMAS spectrum of as-received bendroflumethiazide.

When compared to the spectrum of the spray-dried material in Figure 4.3b, the lines became significantly broader after spray drying. The aromatic peaks (120-140 ppm) broadened until they were no longer distinguishable. The ^{19}F SSNMR spectrum of the as-received material is shown in Figure 4.3c. There were two peaks located at -55.8 and -56.8 ppm with line widths of 380 Hz and 350 Hz, respectively. The ^{19}F SSNMR spectrum of the spray-dried material had two peaks with chemical shifts of -54.8 ppm and -56.8 ppm and line widths of 560 Hz and 1015 Hz. The broader line width in the spray-dried sample suggests the presence of the amorphous form. However, bendroflumethiazide has a single trifluoromethyl group and a single peak was anticipated in the ^{19}F SSNMR spectrum of the amorphous form.

It is unclear why there were two peaks in the ^{19}F SSNMR spectrum. The solid crystalline form of bendroflumethiazide has two asymmetric sites per unit cell, meaning that there are two unique sites for each molecule. The two sites have different electronic environments and appear as separate and distinct NMR peaks.

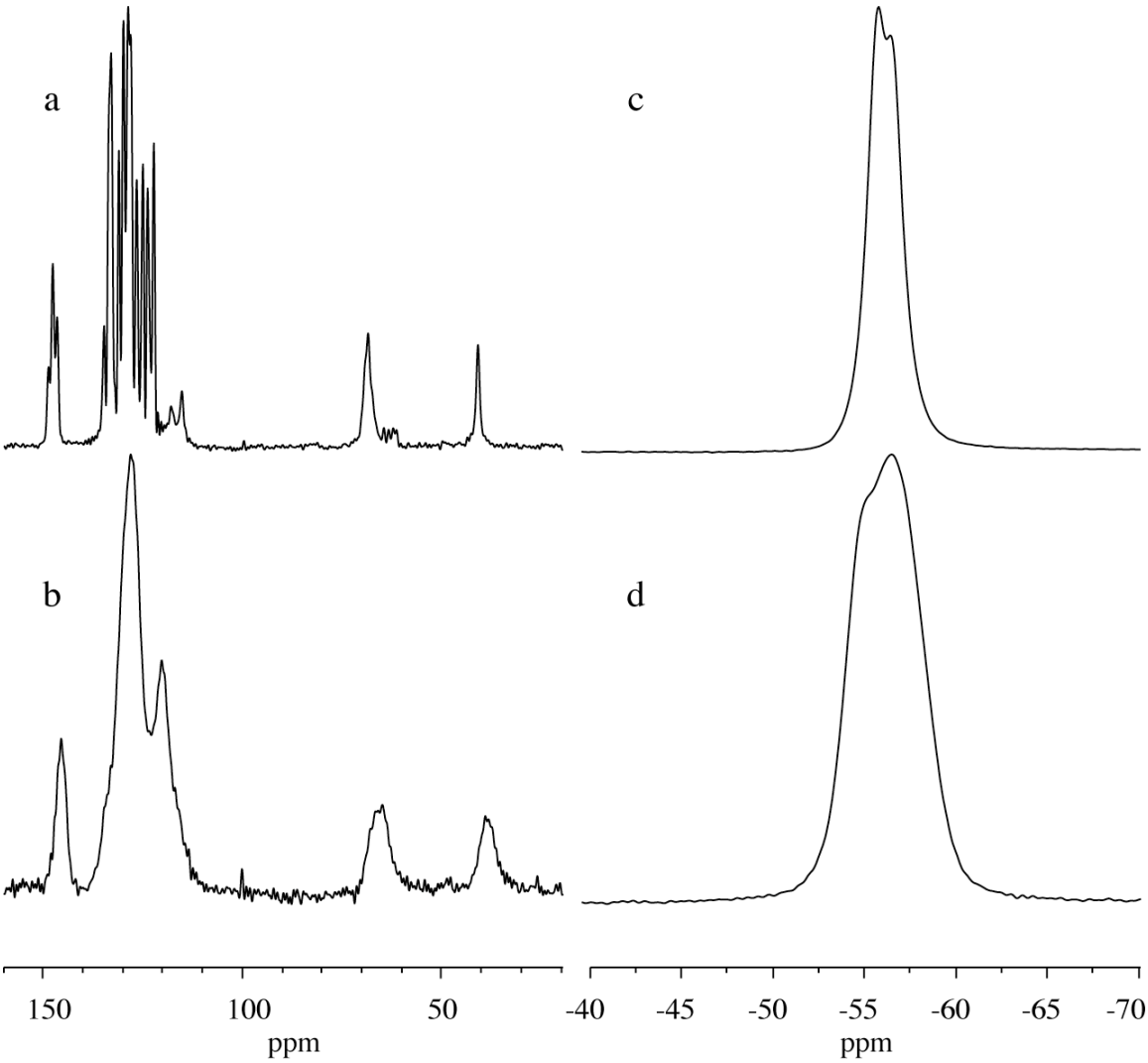

Figure 4.3. ^{13}C CPMAS spectra of a) bulk bendroflumethiazide and b) bendroflumethiazide spray dried from ethanol. ^{19}F SSNMR spectra of c) bulk bendroflumethiazide and d) spray dried bendroflumethiazide.

The asymmetry explains the presence of two peaks in the crystalline ^{19}F SSNMR spectrum. However, this asymmetry should not be present in a true amorphous compound. Multiple peaks in the ^{19}F SSNMR spectrum suggest that the material was crystallizing in the rotor or that there is an unexplained peak in the spectrum. The complications due to multiple peaks in the spectrum of the spray-dried bendroflumethiazide and the lack of significant chemical shift resolution with the peaks of the crystalline material were reasons to eliminate bendroflumethiazide as a model candidate.

The amorphous form of dexamethasone was produced by cryogrinding. The ^{19}F SSNMR spectra of as-received dexamethasone and cryoground amorphous dexamethasone are shown in Figure 4.4. In Figure 4.4a, the ^{19}F spectrum of the as-received material had a single peak with a chemical shift of -165.8 ppm and a line width of 260 Hz. As seen in Figure 4.4b, the spectrum of the cryoground amorphous form also had a single peak. The peak exhibited a chemical shift of -164.8 ppm and a line width of ~2200 Hz. The peak of the amorphous form was noticeably asymmetric. NMR peaks are typically symmetric, so the asymmetry of this peak is notable. The chemical shift difference between the amorphous and crystalline forms was not large enough to pursue dexamethasone as a model compound for these studies. However, another polymorphic form of dexamethasone could possibly be crystallized that has a larger chemical shift difference with the amorphous form. Before pursuing this option further, two other candidates were considered.

4.4.5 Crystallization of the amorphous material

The next candidate that was examined was levofloxacin. The ^{19}F SSNMR spectrum of as-received levofloxacin is shown in Figure 4.5a. This particular crystal form of levofloxacin had two asymmetric sites per unit cell. The two unique sites in the crystal correspond to two unique peaks in the NMR spectrum. The chemical shifts of the peaks were at -114.8 and -116.6 ppm with line widths of 370 and 380 Hz, respectively. Amorphous levofloxacin was prepared by spray drying from methanol. Figure 4.5b shows the ^{19}F SSNMR spectrum of the spray-dried amorphous form. There was a single peak located at -119.7 ppm with a line width of ~2300 Hz. The line width of the amorphous form was 6-7 times broader than the peaks of the crystalline form. The chemical shift resolution between the crystalline and amorphous forms was 3 ppm.

The ^{19}F NMR peak resolution between forms was large enough to consider quantitation, yet closer examination of the spectrum of the amorphous form reveals the presence of a slight shoulder on the downfield side of the amorphous peak. The shoulder corresponded to the chemical shifts of the crystalline form, indicating an impure amorphous form with a minor crystalline component. A second ^{19}F SSNMR spectrum was acquired less than 10 minutes after the first. As one can see in Figure 4.5c, the amorphous levofloxacin partially crystallized in the rotor while spinning at 15 kHz.

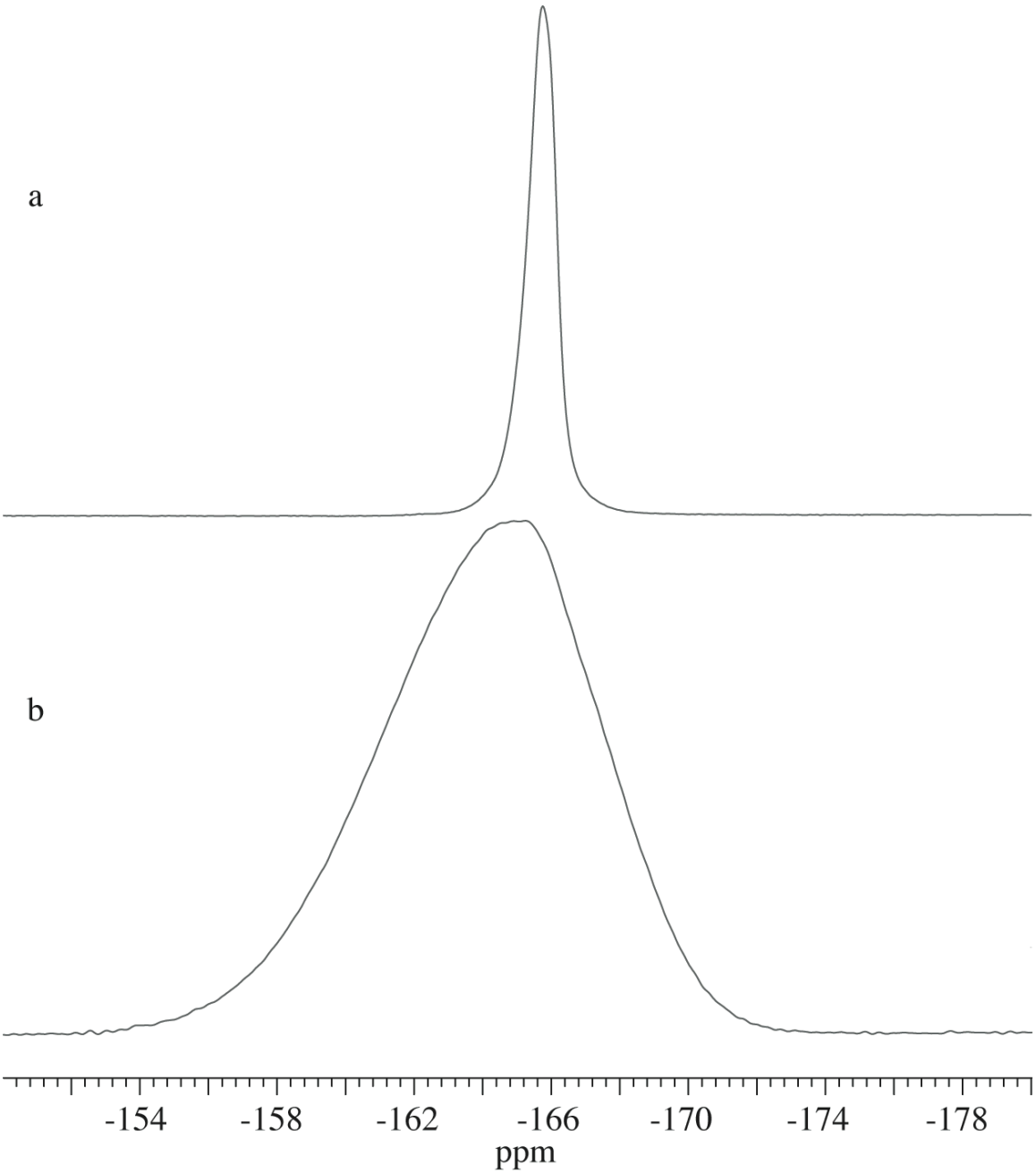

Figure 4.4. ^{19}F SSNMR spectra of a) as-received dexamethasone and b) cryoground amorphous dexamethasone.

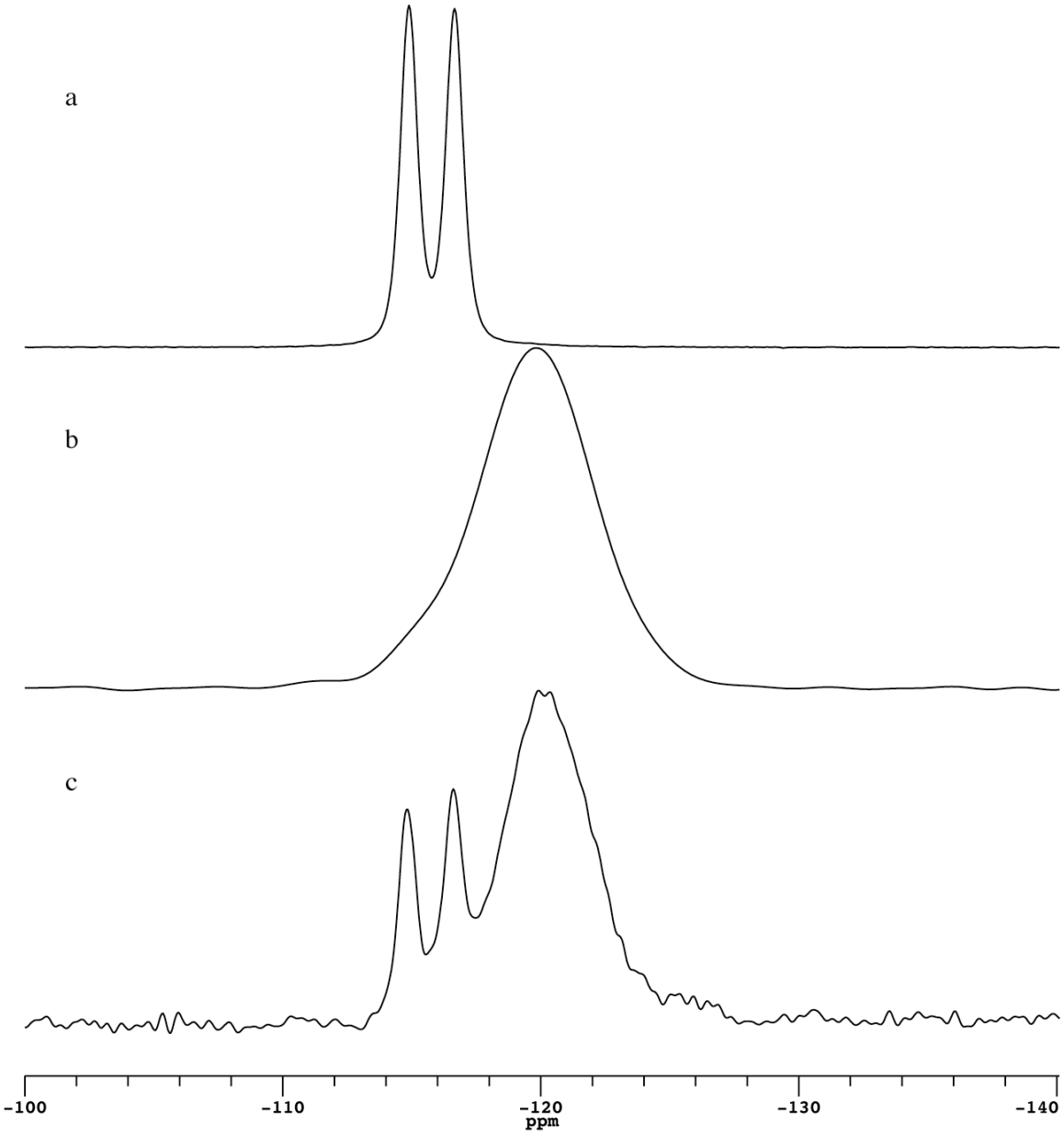

Figure 4.5. ^{19}F SSNMR spectra of a) as-received levofloxacin, b) spray-dried levofloxacin, and c) sample **b)** collected 10 minutes after the initial acquisition.

Quantitation could be attempted at lower temperatures, which could reduce or eliminate the crystallization of the amorphous material. Spinning speeds could also be lowered to 8-10 kHz to lessen spin-induced sample heating. However, a compound with a high propensity to crystallize is not ideal as a model compound for quantitation.

4.4.6 Model compound - triamcinolone

The next, and final, compound that was studied was triamcinolone. Triamcinolone ((11β,16α)-9-fluoro-11,16,17,21-tetrahydroxypregna-1,4-diene-3,20-dione) is a glucocorticoid steroid that has a fluorine atom at the 9-position in the steroid structure.[15]

Initially, amorphous triamcinolone was generated by cryogrinding. The ^{19}F SSNMR spectra of the crystalline (as-received material) and the amorphous form are shown in Figure 4.6. Figure 4.6a is the ^{19}F spectrum of the as-received crystalline material. The crystalline form has two peaks corresponding to two asymmetric sites per unit cell. The peaks had chemical shifts of -159.1 and -160.5 ppm. Figure 4.6b shows the ^{19}F SSNMR spectrum of cryoground amorphous triamcinolone. The ^{19}F SSNMR spectrum of the amorphous form has a single peak. The line shape of the amorphous peak is asymmetric, similar to that noted for amorphous dexamethasone. The asymmetric line shape of the amorphous form of triamcinolone was observed on different spectrometers operating at different magnetic field strengths. The cause of

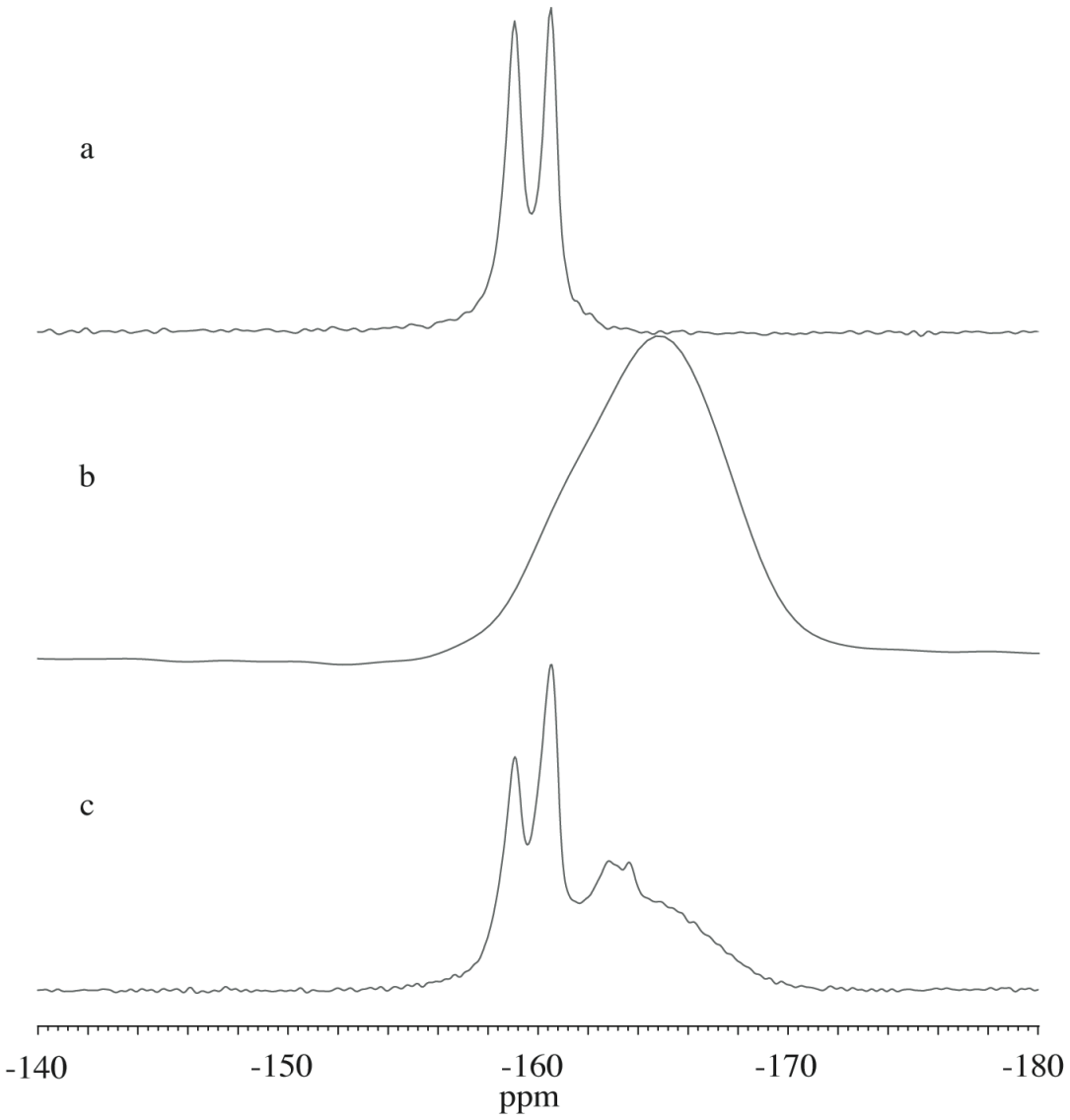

Figure 4.6. The ^{19}F SSNMR spectra of a) crystalline (polymorph B) standard, b) amorphous (cryoground) standard, and the c) physical mixture of 50% amorphous triamcinolone and 50% polymorph B.

the asymmetry is unknown but could indicate a non-Gaussian distribution of molecular arrangements within the amorphous form of triamcinolone.

The peak of the amorphous form had a chemical shift of -164.9 ppm and a linewidth of 3300 Hz. The ^{19}F SSNMR spectrum of a 50:50 physical mixture of the two forms is shown in Figure 4.6c. Peaks corresponding to the original crystalline and amorphous forms are both visible in the spectrum; however, there were two additional peaks that appeared at -163.2 and -164.0 ppm. The new peaks were attributed to a second polymorph of triamcinolone. The material physically transformed during storage, mixing, and/or acquisition of the NMR data. A closer look at the spectrum of the cryoground amorphous form shows a slight hump on the downfield side of the peak. The slight shoulder indicated the cryoground material was not a pure amorphous form and contained a minor component of polymorph B.

Cryoground triamcinolone was analyzed by DSC and ^{19}F SSNMR to determine its suitability as an amorphous form. The DSC of triamcinolone is shown in Figure 4.7. The glass transition was not visible in the thermogram, but there was a crystallization exotherm at 80-105 °C. An endotherm was also present at 220 °C, which was attributed to the melting temperature of polymorph A. The temperature of the crystallization exotherm was relatively close to the temperatures that the sample may have been exposed to during SSNMR analysis due to friction generated at high spin speeds. To assess reproducibility in the generation of the amorphous material, several cryoground samples were analyzed by DSC (not shown) . There was great

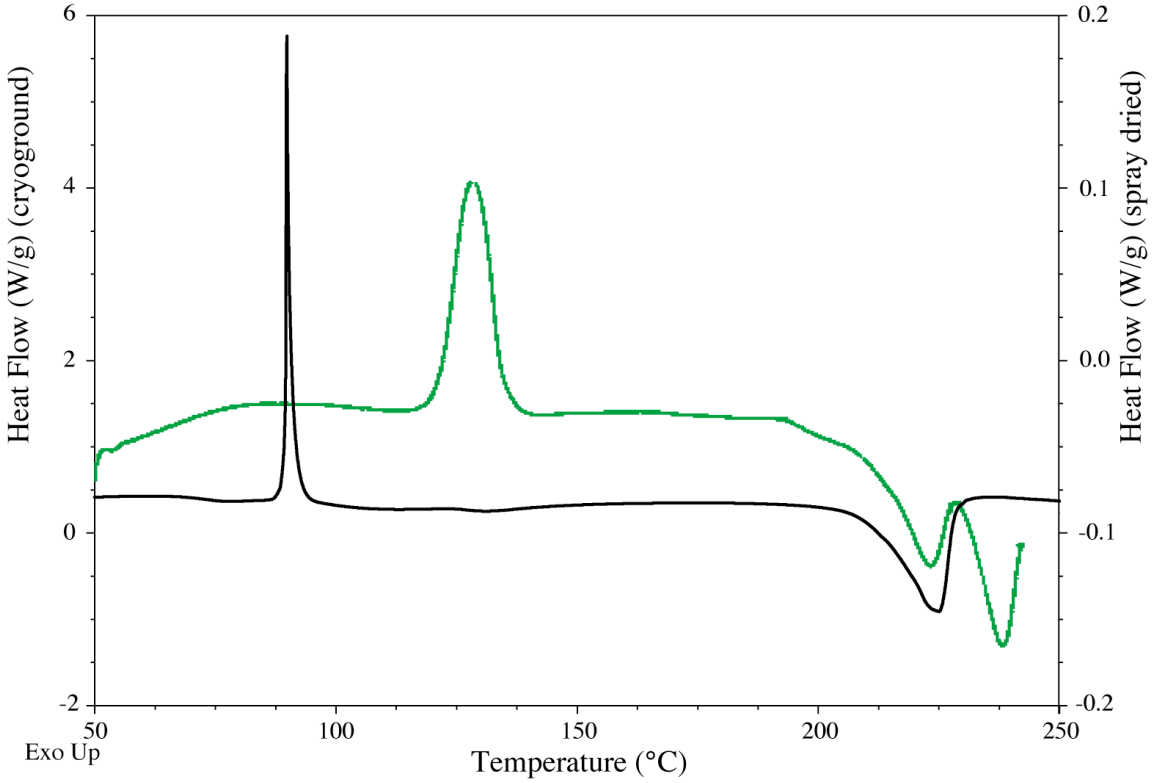

Figure 4.7. DSC thermograms of a) cryoground and b) spray-dried amorphous triamcinolone.

variability in the number of transitions that appeared as well as the relative temperatures at which they appeared. From the DSC analysis it was clear that the amorphous form was difficult to reproduce by cryogrinding. In addition, when cryoground triamcinolone samples were analyzed with ^{19}F SSNMR, the material commonly recrystallized into polymorph A. Triamcinolone was a promising candidate, but the production methods used to make the amorphous and crystalline standards required refinement.

The amorphous generation method was changed from cryogrinding to spray drying from methanol to make a stable amorphous form of triamcinolone. The spray-dried material was uniformly white, whereas the cryoground material had a brown tinge to it. An anti-static gun was used to remove residual electrostatic charge after spray drying, and the material was exposed to a vacuum for one hour to remove any residual solvent. The DSC thermogram of the amorphous material generated by cryogrinding is shown in Figure 4.7a. A glass transition was not visible.

The thermogram had a recrystallization exotherm at 92°C and a melting endotherm at 225 °C, attributed to the melting of polymorph A.[15] The thermogram of the spray-dried amorphous material is shown in Figure 4.7b. The crystallization of polymorph A exotherm shifted to a higher temperature (~120°C). Two endotherms were also observed. The endotherm at 218°C was the melting of polymorph A; whereas, the endotherm at at 241 °C was attributed to the melting of polymorph B.[15] The crystallization exotherm was approximately 25 °C higher for the spray-dried material than for the cryoground. The increase in temperature of the crystallization

exotherm is indicative of the increased physical stability of the spray-dried amorphous form as compared to the cryoground amorphous form. Spray drying triamcinolone generated a reproducible stable amorphous form. When analyzed with ^{19}F SSNMR at spinning speeds of 15 kHz, no crystallization was detected.

After amorphous triamcinolone was generated, the crystalline form of triamcinolone had to be selected. The three known crystalline forms of triamcinolone (polymorph A, polymorph B, and the monohydrate) have been well characterized with PXRD by Suitchmezian et al.[15] No reference to the amorphous form of triamcinolone was made in their research. Polymorph A was not crystallized for this research: however, it appeared in many of the lots that were purchased. In Figure 4.8, the ^{19}F SSNMR spectra of an as-received lot from Sigma (containing polymorph A), polymorph B, the monohydrate, and the spray-dried amorphous form are shown. Figure 4.8a shows the spectrum of the as-received material. The as-received material is a mixture of polymorphs A and B. Polymorph A had chemical shifts of -163.2 and -164.0 ppm, and the presence of two peaks in the SSNMR spectrum for a single fluorine indicated that there are two asymmetric sites in the unit cell. Polymorph B was crystallized from methanol due to the presence of multiple polymorphs in the as-received material. The ^{19}F spectrum of the recrystallized material is displayed in Figure 4.8b. The peaks of polymorph B were located at chemical shifts of -159.7 and -161.2 ppm with line widths of 145 and 122 Hz, respectively. The spectrum of the monohydrate is shown in Figure 4.8c. The monohydrate has a single peak in the spectrum at -160.9 ppm with a line width of 223 Hz. Lastly, the ^{19}F SSNMR

spectrum of spray-dried amorphous triamcinolone is displayed in Figure 4.8d. The spray-dried amorphous NMR peak had a chemical shift of -164.9 ppm and a line width at half height of 3300 Hz.

A vertical line highlights the chemical shift differences between the amorphous form, the monohydrate, and polymorph B. The chemical shift resolution is 3.7 ppm between the amorphous peak and the downfield peak of polymorph B. Coincidentally, the upfield peak of polymorph B and the peak from the monohydrate overlapped. The chemical shift resolution between the amorphous form and the crystalline forms were large enough to proceed with triamcinolone as the model compound. Both the monohydrate and polymorph B were used as model crystalline forms for quantitation in Chapter 5.

4.4.7 Uniform mixing of standards

When preparing physical mixtures, homogeneous mixing is crucial to the integrity of the experiment. Homogeneous mixing could be affected by differences in electrostatic charge of the mixture components. After spray drying, the amorphous material was charged and quite mobile. To reduce the presence of static effects, an anti-static gun was used on spray-dried samples prior to mixing. Homogeneous mixing could also be affected by the particle sizes of the components.

Polarized-light microscopy was performed on both a cryoground sample and polymorph B recrystallized from methanol. The images are displayed in Figure 4.9. Polymorph B has long needle-shaped colorful crystals. In the image of polymorph B

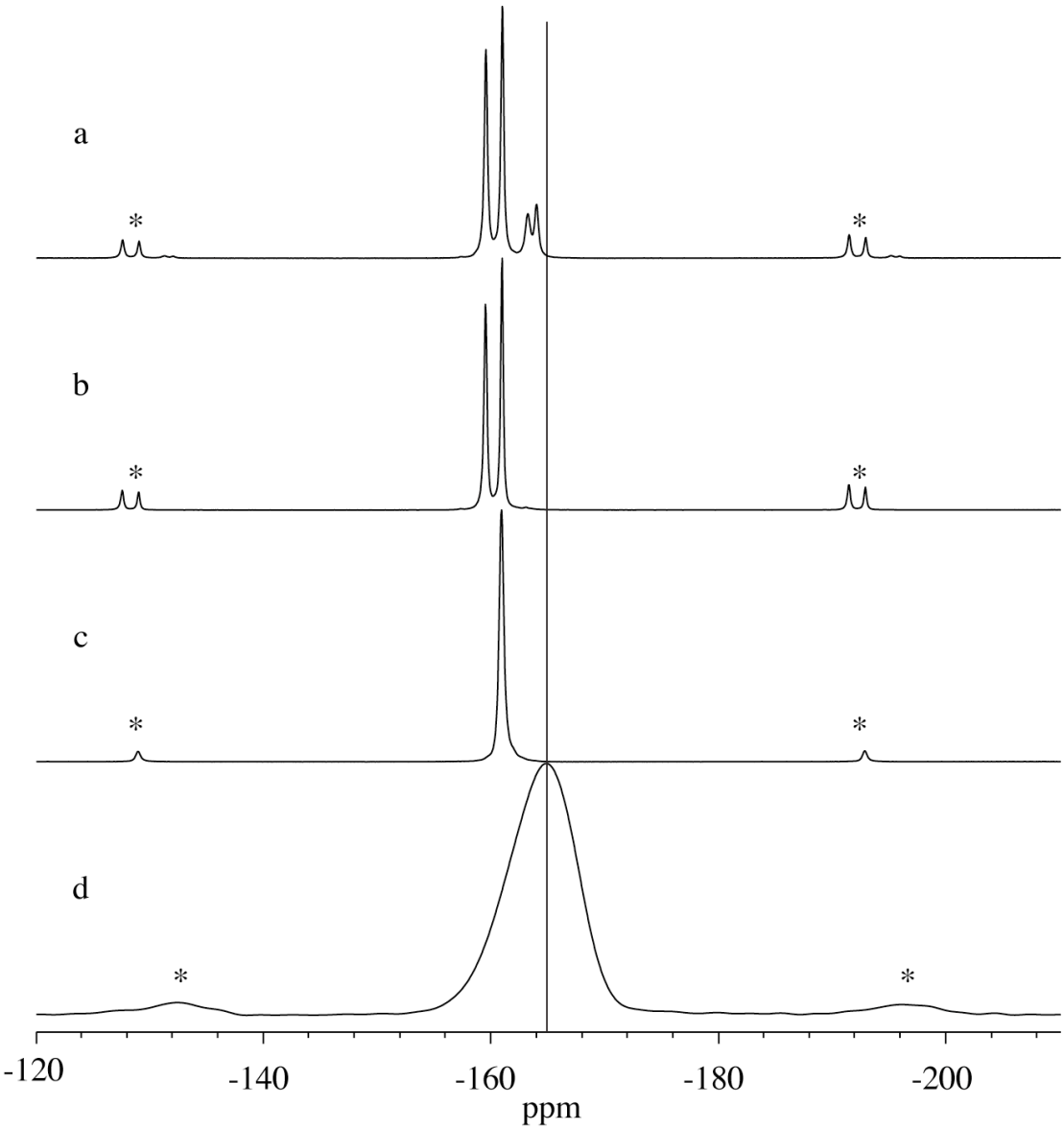

Figure 4.8. ^{19}F SSNMR spectra of the four forms of triamcinolone: a) polymorphs A and B (as-received from Sigma), b) polymorph B, c) the monohydrate, and d) the amorphous form. The vertical line highlights the spectral resolution between the amorphous form and the crystalline forms. Asterisks denote spinning sideband

(Figure 4.9b), there is a bar that indicates a 1000-micron distance. Some of the crystals were on that order in length. In the image of the amorphous form, the particles were small and gray with no distinctive features. The bar in the image of the amorphous form depicts a 100-micron distance. In this case, the particles of the amorphous form were 1-2 orders of magnitude smaller. The vast size differences between amorphous and crystalline forms could result in inhomogeneous mixing. The spray-dried amorphous form was not observed under the microscope but initial particle size analyses of the two amorphous generation methods suggested that spray drying produced particles that were more uniform in size.

Manually grinding and sieving the crystals of polymorph B could effectively reduce the crystalline particle size. Polymorph B was manually ground for a few minutes with a mortar and pestle. The sample was not sieved and analysis was performed with ^{19}F SSNMR. The spectra of polymorph B before and after manually grinding are shown in Figure 4.11. The peaks of the material before grinding were sharp and distinct with line widths of 125 and 100 Hz. After grinding, the lines were broader (240 and 210 Hz but the chemical shifts of the two peaks did not change. Peak resolution was reduced in the ground sample due to broader lines. The decreased intensity of the downfield peak can be explained by one of three possibilities. First, the site was subjected to more internal disorder, leading to a broader distribution of molecular fluctuation at that particular site. The line would be broader, therein decreasing its intensity as compared to the other site.[16] Second, a small amount of amorphous material was generated during

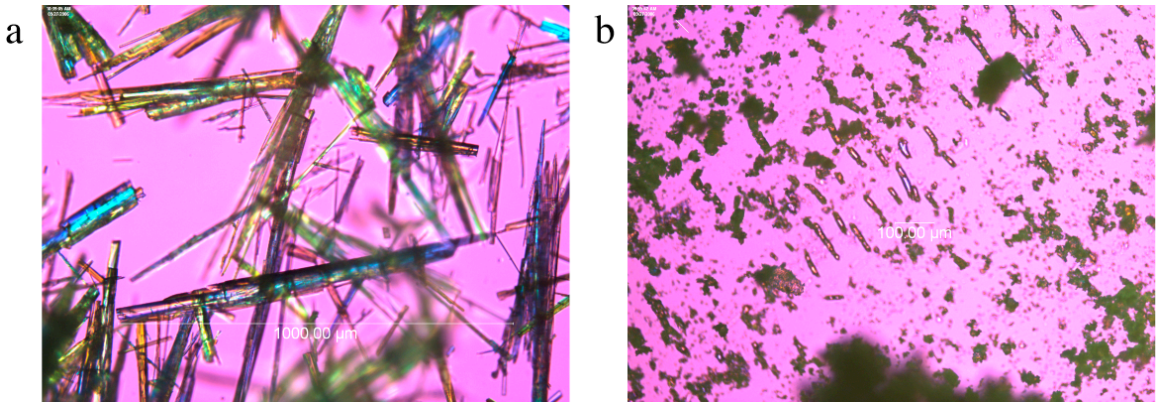

Figure 4.10. Polarized-light microscopy (20X) images of triamcinolone a) polymorph B and b) the cryoground amorphous form.

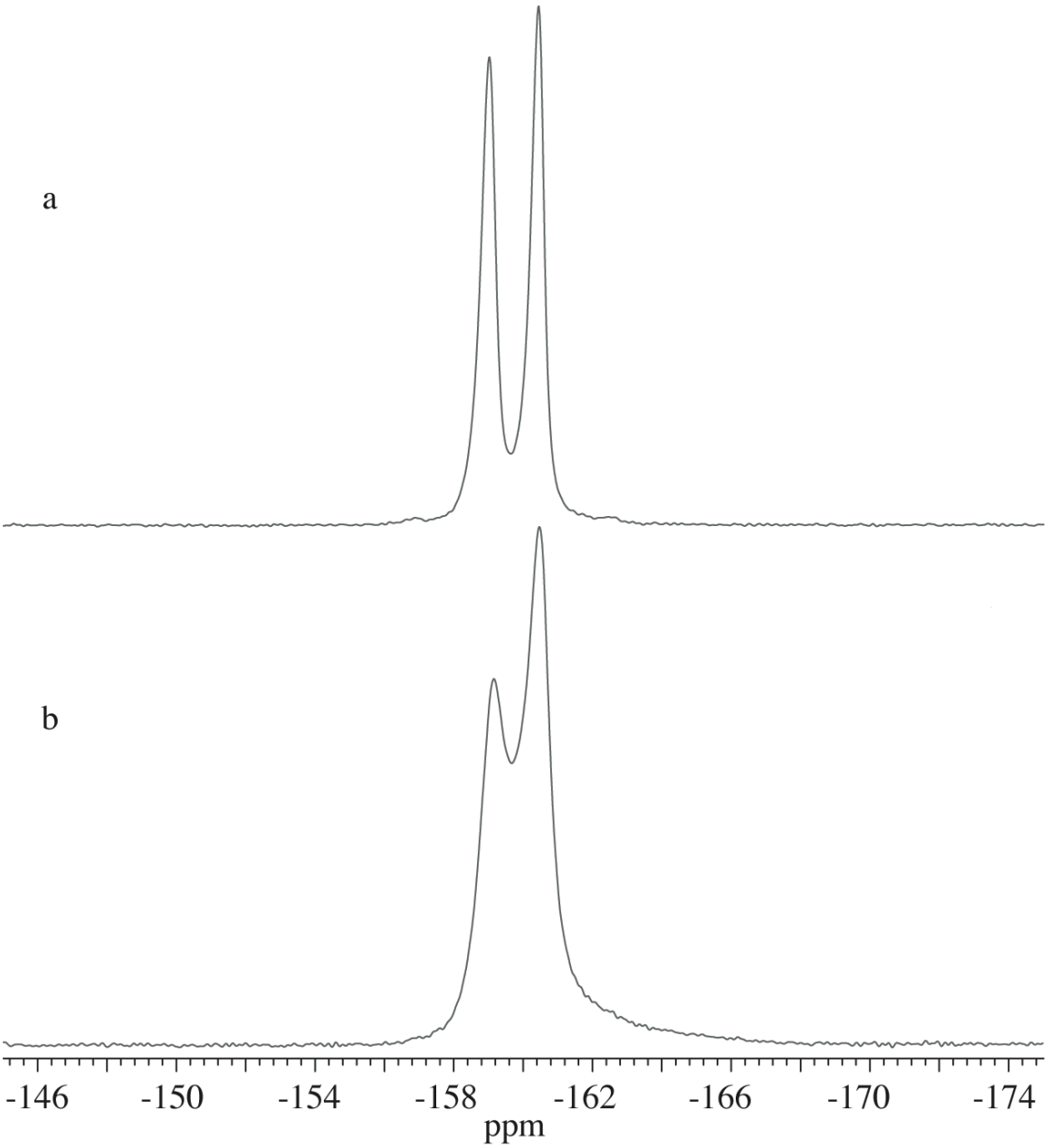

Figure 4.11. ^{19}F SSNMR of polymorph B of triamcinolone a) recrystallized from methanol and b) after manually grinding for one minute.

grinding. Finally, grinding could induce a transformation to the monohydrate. As noted before, the peak of the monohydrate overlapped with the upfield peak of polymorph B. Conversion to the monohydrate would enhance the intensity of the upfield peak of polymorph B. The conclusion is that triamcinolone is a fragile crystal that will need to be physically mixed with no grinding.

4.4.8 Temperature effects on chemical shifts of triamcinolone

Lowering the temperature of the probe and sample in the magnet was necessary to maintain physical stability of the cryoground amorphous form. No significant temperature dependent changes in chemical shift or line width were observed for the amorphous form (-164.6 ppm). However, a series of spectra of polymorph B were collected at different temperatures, and the chemical shifts of both peaks moved upfield while lowering the temperature. Initially, polymorph B of triamcinolone was collected with no VT gas while spinning at 20 kHz. The thermocouple read 23 °C without spinning and 35 °C while spinning. Spinning-induced temperature changes have been observed previously by Isbester et al.[17] The thermocouple was a few inches above the sample, so there is a difference in sample temperature versus thermocouple reading. The thermocouple temperature was slowly lowered to -70 °C. The ^{19}F SSNMR spectra of polymorph B at different temperatures are shown in Figure 4.12. The chemical shifts of polymorph B range from -159.1 and -160.5 ppm at 35 °C to -160.2 and -161.7 ppm at -70 °C. The chemical shifts are plotted against the thermocouple temperature reading in Figure 4.13.

The spectra acquired at 35 and 36 °C were collected with no control of sample temperature. The chemical shift changes of the two peaks exhibit similar slopes when changing temperature. Spinning at 20 kHz produced a thermocouple reading approximately 12-13 °C above ambient temperature inside the magnet bore. The chemical shift changes of the two peaks exhibit similar slopes when changing temperature.

As noted before, sample spinning induces sample heating, and changes in spin speed produced changes in sample temperature. At low spinning speeds (4 kHz) the chemical shifts were -159.4 and -161.1 ppm, and at high spinning speeds (20 kHz) the chemical shift was -159.1 and -160.5 ppm. According to the equation from the plot, the sample temperature changed approximately 23 °C for the downfield peak and 52 °C for the upfield peak. If each peak were affected similarly, the calculated change should be the same for both peaks, so more points would need to be defined to fully characterize the relationship.

The changes in chemical shifts are not readily explainable. Some compounds exhibit a chemical shift change with changes in crystal density.[18] If it is true that the peak of amorphous triamcinolone does not change, and the chemical shifts of polymorph B do change, then the temperature could be manipulated to provide a larger chemical shift difference for quantitation. For these studies, the temperature was kept constant (through constant spinning), so it was presumed that the chemical shifts did not change between samples. Additionally, polymorph B could be developed as a quicker and safer alternative to lead nitrate to monitor temperature changes in SSNMR spectroscopy.[18]

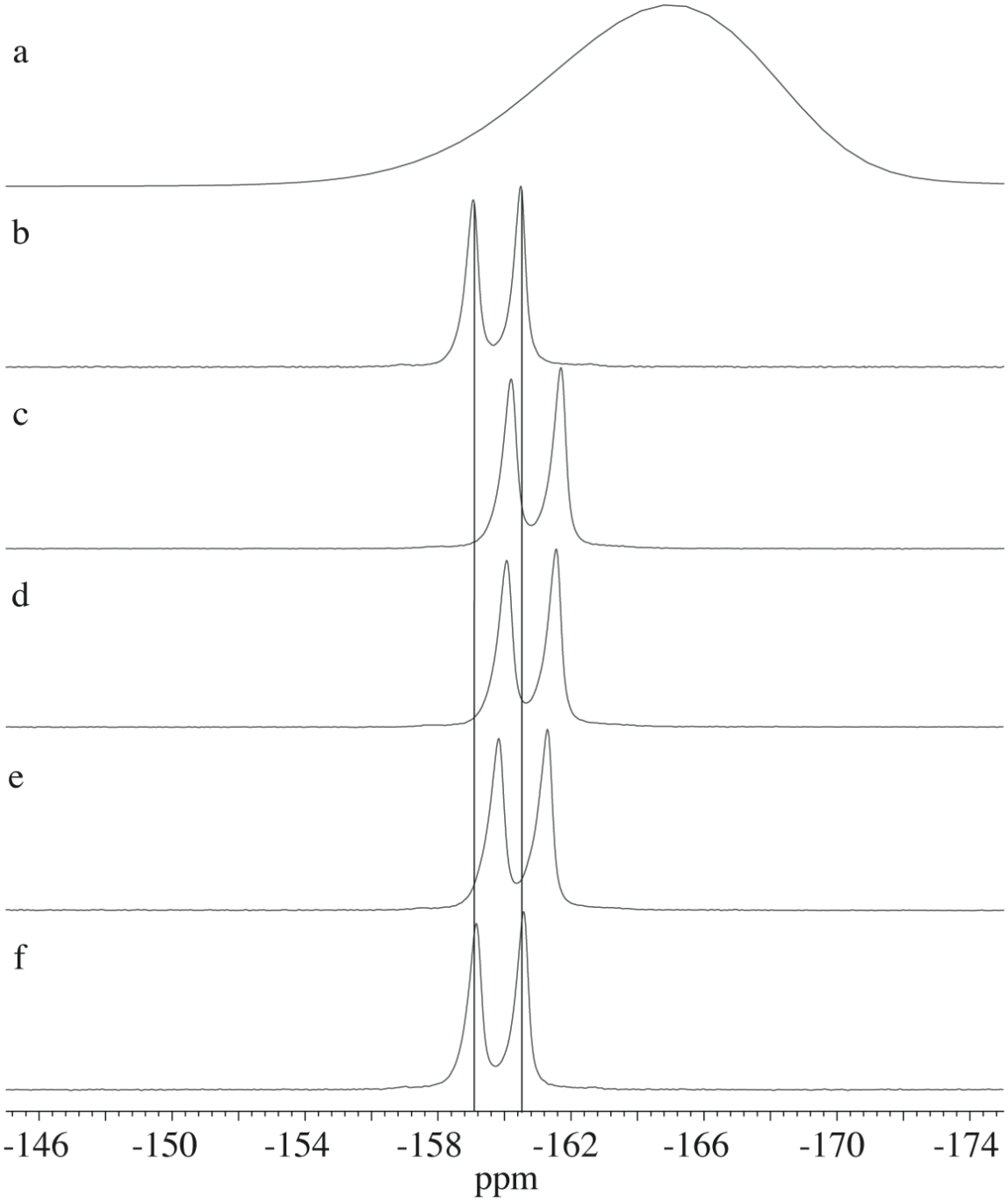

Figure 4.12. ^{19}F SSNMR spectra of a) amorphous triamcinolone at -70 °C and polymorph B at b) 35 °C, c) -70 °C, d) -50 °C, e) -10 °C, and f) 36 °C. The lines help discern the chemical shift changes with changes in temperature.

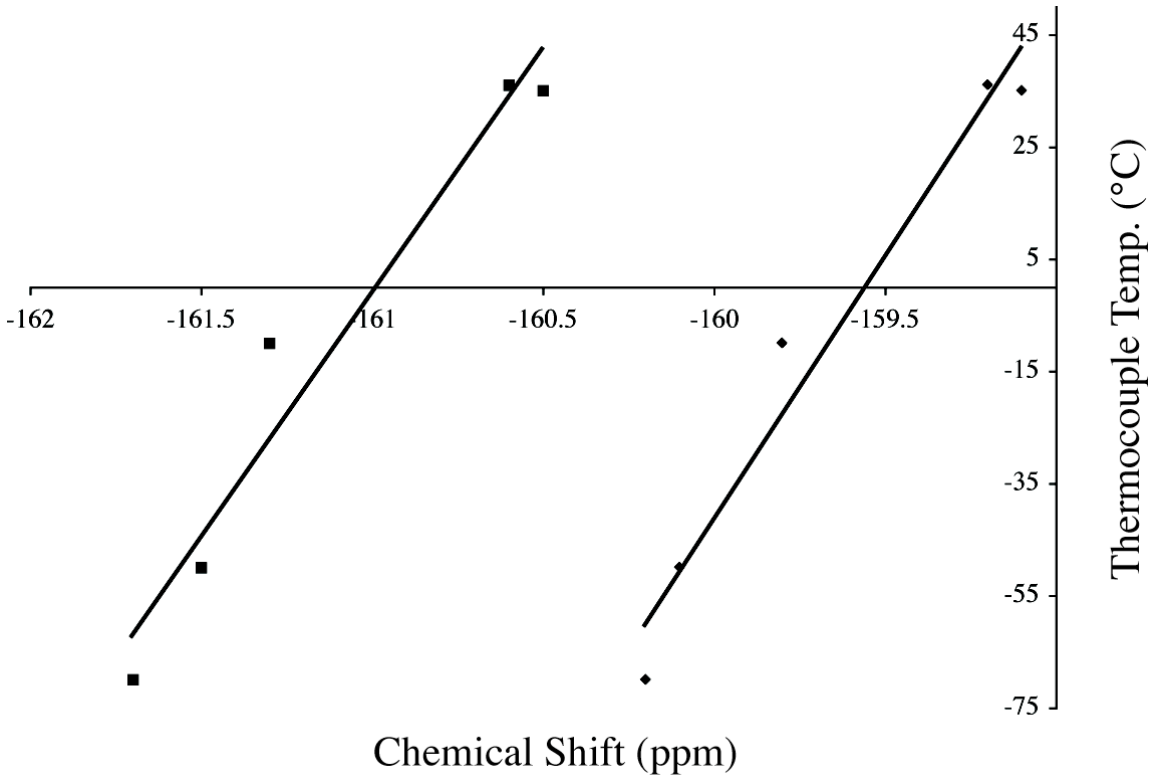

Figure 4.13. Chemical shift of the two ^{19}F SSNMR chemical shifts of polymorph B of triamcinolone plotted at different temperatures (35 °C to -70 °C).

4.5 Conclusions

Many fluorine-containing compounds were analyzed for consideration as candidates for low-level amorphous quantitation using ^{19}F SSNMR. The reasons that most compounds were eliminated as potential candidate were due to high cost, low glass transition temperatures, the inability to generate a fully-amorphous solid, lack of chemical shift resolution between forms, and amorphous crystallization. No single technique was able to produce amorphous material for all compounds. In the case of small, organic, fluorine-containing molecules, cryogrinding and spray drying (from organic solvents) were the best options to generate amorphous compounds. When possible, spray drying from methanol and acetone was the most effective and reproducible method that produced the most stable amorphous form.

The steroid triamcinolone was selected as the model compound for ^{19}F SSNMR quantitation studies. Polymorph B and the monohydrate were used as the model crystal forms, and both the cryoground and spray-dried amorphous forms were used during quantitation studies described in Chapter 5.

4.6 References

1. Shah B, Kakumanu VK, Bansal AK 2006. Analytical techniques for quantification of amorphous/crystalline phases in pharmaceutical solids. Journal of Pharmaceutical Sciences 95(8):1641-1665.

2. Offerdahl TJ, Salsbury JS, Dong Z, Grant DJW, Schroeder SA, Prakash I, Gorman EM, Barich DH, Munson EJ 2005. Quantitation of crystalline and amorphous forms of anhydrous neotame using 13C CPMAS NMR spectroscopy. Journal of Pharmaceutical Sciences 94(12):2591-2605.

3. Lefort R, De Gusseme A, Willart JF, Danede F, Descamps M 2004. Solid state NMR and DSC methods for quantifying the amorphous content in solid dosage forms: an application to ball-milling of trehalose. International Journal of Pharmaceutics 280(1-2):209-219.

4. Bruni G, Milanese C, Bellazzi G, Berbenni V, Cofrancesco P, Marini A, Villa M 2007. Quantification of drug amorphous fraction by DSC. Journal of Thermal Analysis and Calorimetry 89(3):761-766.

5. Farrer BT, Peresypkin A, Wenslow RM 2006. Quantitation of crystalline material within a liquid vehicle using 1H/19F CP/MAS NMR. Journal of Pharmaceutical Sciences 96(2):264-267.

6. Carss SA, Scheler U, Harris RK, Holstein P, Fletton RA 1996. 19F NMR of proton-containing solids. Magnetic Resonance in Chemistry 34(1):63-70.

7. Stephen R. Byrn RRP, Joseph G. Stowell. 1999. Solid-State Chemistry of Drugs. 2nd ed., West Lafayette, IN: SSCI Inc. p 574.

8. Andrew ER 1971. Narrowing of NMR spectra of solids by high-speed specimen rotation and the resolution of chemical shift and spin multiplet structures for solids. Progress in Nuclear Magnetic Resonance Spectroscopy 8(Pt. 1):1-39.

9. Andrew ER, Bradbury A, Eades RG 1959. Removal of dipolar broadening of nuclear magnetic resonance spectra of solids by specimen rotation. Nature (London, United Kingdom) 183:1802-1803.

10. Pines A, Gibby MG, Waugh JS 1972. Proton-enhanced nuclear induction spectroscopy. Method for high-resolution NMR of dilute spins in solids. Journal of Chemical Physics 56(4):1776-1777.

11. Pines A, Gibby MG, Waugh JS 1973. Proton-enhanced NMR of dilute spins in solids. Journal of Chemical Physics 59(2):569-590.

12. Stephen R. Byrn RRP, and Joseph G. Stowell. 1999. Solid-State Chemistry of Drugs. Second ed., West Lafayette: SSCI, Inc.

13. Hancock BC, Zografi G 1997. Characteristics and significance of the amorphous state in pharmaceutical systems. J Pharm Sci 86(1):1-12.

14. Corrigan OI, Holohan EM, Sabra K 1984. Amorphous forms of thiazide diuretics prepared by spray-drying. International Journal of Pharmaceutics 1 8(1-2):195- 200.

15. Suitchmezian V, Jess I, Naether C 2007. Investigations on the Polymorphism and Pseudopolymorphism of the Glucocorticoid Triamcinolone: New Findings for a Well-Known Drug. Crystal Growth & Design 7(1):69-74.

16. Barich DH, Davis JM, Schieber LJ, Zell MT, Munson EJ 2006. Investigation of solid-state NMR line widths of ibuprofen in drug formulations. Journal of Pharmaceutical Sciences 95(7):1586-1594.

17. Isbester PK. 1999. Development of an Isolated Flow Variable-Temperature Magic-Angle Spinning (MAS) Nuclear Magnetic Resonance (NMR) Probe for Heterogeneous Catalysis Studies and High-Temperature High-Speed 19F MAS NMR Techniques Applied to Fluoropolymers. Department of Chemistry, ed., Minneapolis: The University of Minnesota. p 179.

18. Neue G, Dybowski C 1997. Determining temperature in a magic-angle spinning probe using the temperature dependence of the isotropic chemical shift of lead nitrate. Solid State Nuclear Magnetic Resonance 7(4):333-336.

Chapter 5

Quantitation of a Low-Level Amorphous Impurity

5.1 Introduction

5.1.1 Presence of amorphous materials in formulation

Amorphous drug substances can be produced at low levels during the processing and manufacturing of pharmaceuticals and can have a large influence on the chemical and physical stability of a drug. For example, the high-energy amorphous state has the potential for undesired physical transformations, such as polymorphic conversions, that can lead to changes in physicochemical properties of a drug. These changes can affect the drug's therapeutic efficacy. Additionally, the increased dynamics associated with the amorphous state could lead to increased chemical reactivity of the drug. From a regulatory standpoint, quantitating low levels of amorphous drug is important to ensure safety and efficacy of a formulated drug product. In the past, much of the research on amorphous solids has been focused on understanding the relationship between molecular mobility and drug stability. Recently, research efforts have included attempts to quantitate the amorphous state or percent crystallinity.[1-4] In many of these studies, the primary objective is quantitation of low levels of amorphous content in a physical mixture of crystalline and amorphous forms. Some of the techniques described in the next section can quantitate amorphous drug levels to less than one percent; however, few techniques are capable of studying low levels of amorphous drug in a formulated product. In this chapter we describe the capability of ^{19}F solid-state NMR (SSNMR) spectroscopy to

study low levels (<1%) of an amorphous drug while also monitoring chemical and physical changes of that form.

5.1.2 Analytical methods for quantitation of amorphous solids

Many techniques are available for the quantitation of amorphous pharmaceuticals.[1] These techniques include powder X-ray diffraction (PXRD), differential scanning calorimetry (DSC), isothermal micro-calorimetry (IMC), solution calorimetry (SC), dynamic vapor sorption (DVS), thermally stimulated current spectrometry, density measurements, dynamic mechanical analysis (DMA), inverse gas chromatography (IGC), dissolution, infrared spectroscopy, FT-Raman spectroscopy, and ^{13}C SSNMR spectroscopy. The capabilities and limitations of some of the techniques will be discussed briefly.

PXRD is one of the most widely used techniques for solid-state characterization and quantitation. PXRD patterns of crystalline samples have sharp peaks. Amorphous materials have very broad, featureless peaks, often referred to as halos. Because PXRD is sensitive to long-range order in a crystal lattice, it indirectly measures the amorphous content of a sample by determining the fraction of intensity in the halo. Quantitation limits for amorphous pharmaceuticals of approximately 10% are typically reported for PXRD.[1,5]

Multiple researchers have used DSC to quantitate amorphous material.[5-8] In conventional DSC, the sample temperature is raised to cause recrystallization. The area under the crystallization exotherm is proportional to the amorphous content

present in the sample.[5] Conventional DSC has detection limits of approximately 10%, comparable to that of PXRD. Another approach to quantitate amorphous material with DSC is to measure the change in the heat capacity (C_p) at the glass transition. The magnitude of the ΔC_p is proportional to the amorphous drug present. To measure the ΔC_p, modulated-temperature DSC (MTDSC) or hyper-DSC must be used.[9-11] The use of these techniques creates large gains in sensitivity over the use of conventional DSC: the limits of detection can be lowered from 10% to 1% or below. Unfortunately, the increased sensitivity comes at a cost: the use of MTDSC and hyper-DSC requires calibration curves made from pure standards. Similar to PXRD, DSC does not directly measure the amorphous state. The area of the recrystallization exotherm or heat capacity of the material is measured and attributed to the relative percentage of amorphous material. Other calorimetric techniques, such as IMC and SC, measure the amount of amorphous material in samples based on the same properties as DSC. The heat from the recrystallization is proportional to the amorphous material present in the sample.

Dynamic vapor sorption (DVS) has also been used to quantitate amorphous material in a crystalline sample. Typically, amorphous material is much more hygroscopic than crystalline material; therefore, the amount of water taken up by the sample is proportional to the amount of amorphous material present. In order to quantitate the amorphous content, the amount of water taken up by both the pure crystalline and amorphous forms must be known. DVS can exhibit a very low level of detection, but it can typically be applied only to drug substances and not

formulations. FT-IR and Raman spectroscopy have been used to identify amorphous material. Often the amorphous peaks will have different absorption frequencies from those of the crystalline. If not, quantitation can be difficult.

Many of the techniques described here do not directly measure the crystalline to amorphous ratio, but assume that the measured parameter is related to the amount of one of the species present. For example, in water vapor sorption, it is assumed that the increase in water content is due solely to the amorphous material present, and that the crystalline material does not absorb water. If this assumption fails, then the technique can give an incorrect measurement of that particular parameter. Using an indirect parameter to measure the amorphous state can lead to inconsistent results when the same system is quantitated with a variety of techniques. For example, Lehto et al. used seven different techniques (PXRD, DSC, StepScan DSC, IMC, solution calorimetry, Raman Spectrometry and gravimetric moisture sorption) to quantitate amorphous lactose.[8] The study concludes that the percentage of measured amorphous impurity may vary depending on the technique used for quantitation; therefore, the researchers suggest several different methods should be employed to achieve a more accurate value.

Each technique has limitations in its ability to quantitate crystalline and amorphous forms based upon the technique itself. For example, many techniques require a calibration curve, and many are highly insensitive. Some techniques require the use of pure amorphous and crystalline forms as standards and creating a standard curve of various relative percentages. A common disadvantage of all of the described

techniques is that they fail when attempting to quantitate amorphous impurity in a drug product. The background signal from an excipient prohibits the use of common solid characterization techniques (e.g. PXRD and DSC), when studying a solid drug formulation. SSNMR spectroscopy is an alternative technique that can be used to monitor the API within a formulation.

5.1.3 ^{13}C SSNMR spectroscopy

Unlike many of the techniques detailed in the previous section, the signal from amorphous material is directly observed in a SSNMR spectrum. ^{13}C SSNMR has been routinely used to study low levels of crystalline API in a drug product.[12] Byrn et al. have shown that formulations of crystalline prednisolone can be readily observed at loading levels below 5%. Three formulations from different vendors were examined, and researchers reported finding a different polymorph in one of the formulations by ^{13}C SSNMR.[12] This demonstrates that SSNMR can discriminate between different crystalline solid forms at load levels of drug loading. There are many challenges for observing amorphous content using ^{13}C SSNMR. Typically a SSNMR peak of the amorphous form is an order of magnitude broader than a crystalline peak. The breadth of the peak reduces the overall intensity of the signal. For example, if an NMR peak of the amorphous form was 10 times broader than the crystalline peak, a sample with 10% amorphous content would correspond to a peak with ~1% of the crystalline peak intensity. The breadth of the NMR peak makes it much more likely that separation with the crystalline peak is limited. Polymorphic

impurities are usually easier to detect because of the sharpness of the lines and changes in chemical shift.

^{13}C SSNMR has been used in several studies to quantitate the amorphous state.[2,6,8,13] Gustafsson et al. used partial least squares analysis to determine the percentage of amorphous lactose in the physical mixture. Pure crystalline and amorphous standards were used and a calibration curve was made. The detection limits were approximately 0.5% for amorphous lactose. Although low levels of detection were reached, the data acquisition parameters used were non-quantitative. This can create a problem when the relaxation times for the material being studied are different than those of the standards. Lefort et al. studied trehalose using DSC and SSNMR. To determine the percentage of amorphous trehalose, a standard linear regression procedure was used. The procedure quantitated amorphous trehalose to levels of approximately 20%.

Offerdahl et al. used ^{13}C SSNMR to quantitate amorphous material present in crystalline physical mixtures of neotame.[13] The lowest percentage physical mixture prepared was 20%. A plot of the SSNMR calculated wt.% vs. the weighed wt.% resulted in a non-zero y-intercept. The intercept occurred because the bulk crystalline material had a significant level of amorphous material present. The amorphous material was not easily seen in the spectra of the physical mixtures or of the "pure" crystalline material because the crystalline peaks are much more intense than the amorphous peaks, making it difficult to observe the amorphous peak at the base of the crystalline peak. The time frame of these experiments was reasonable due

to the number of scans and short relaxation rates of the amorphous and crystalline forms. If the sample were diluted, the length of the experiments would have risen to unreasonable levels in order to achieve acceptable signal to noise ratio (SNR). Thus, the presence of excipients effectively limits the ability to perform quantitation experiments.

The downside of SSNMR for quantitation of amorphous material is that it is relatively insensitive compared to other analytical techniques. The primary reason is the low-energy transitions, which means that the population difference is very small between transition states.[14] Another reason is the low (1.1%) natural abundance of ^{13}C. In addition, the broadness of the amorphous peaks lessens the peak sensitivity even further. Low sensitivity leads to unrealistic analysis times required to observe low levels of amorphous drug. Low-level loading in a drug product would greatly increase these analysis times.

5.1.4 ^{19}F SSNMR spectroscopy

There are several advantages to using ^{19}F SSNMR spectroscopy over ^{13}C SSNMR spectroscopy to detect small amounts of amorphous API in the presence of crystalline API, especially within a formulated product. The ^{19}F nucleus is 100% naturally abundant, compared to the 1.1% natural abundance of the ^{13}C nucleus. The higher abundance is important because that means a ^{19}F spectrum with a higher SNR can be obtained in a fraction of the time necessary to collect a ^{13}C spectrum with a similar SNR. The number of fluorine atoms is always much lower than the number of

carbon atoms in a molecule. This means that the ^{19}F NMR spectrum will be much less complicated than the corresponding ^{13}C NMR spectrum because it has fewer peaks. The fewer number of peaks allows for easier spectral interpretation, but it provides us with fewer opportunities to find chemical shift resolution between the solid forms. The greatest potential advantage of using ^{19}F SSNMR to look at solid forms is the lack of signal from the excipients. No commonly used excipients contain fluorine, so they will not be detected in the spectrum, which means that the only signals will come from the API. ^{19}F SSNMR will observe just the API.

There are some disadvantages for using ^{19}F SSNMR to quantitate crystalline and amorphous fractions in pharmaceutical materials. First, samples must be spun at high magic-angle spinning (MAS) rates of 15-25 kHz to eliminate the broadening effects of strong $^{19}F/^{19}F$ homonuclear couplings and reduce spinning sidebands. The air-generated friction due to extremely fast spinning induces sample heating. Sample heating will vary based on rotor size, spinning speed, and type of module used. This group has reported that spinning with a 3.2-mm Chemagnetics spinning module at rates as high as 20 kHz caused temperature changes of 40 °C.[15] Sample heating could have several unintended consequences that can be problematic if the temperature is not adequately controlled and monitored, such as water loss, and/or changes in the thermal history of an amorphous solid. Second, ^{19}F SSNMR line widths are typically much broader than in ^{13}C spectra. The peak broadness can cause additional resolution issues between the crystalline and amorphous peaks. Lastly, ^{19}F and ^{1}H have close

resonant frequencies; therefore, decoupling ^{1}H spins from ^{19}F requires a special probe configuration.

5.1.5 Prevalence of fluorine in pharmaceuticals

The obvious drawback to studying amorphous systems with ^{19}F SSNMR spectroscopy is its limitation to compounds containing one or more fluorine atoms. No fluorine-containing drugs had been developed prior to 1957. Fluorine is commonly substituted for hydrogen because of its similarity in size but large difference in electronegativity. There should be little or no steric effect; however, the electronic environment, pK_a, dipole moment, and ultimately the chemical stability and reactivity of nearby functional groups will be affected.

Recently, studies have shown that fluorine has the ability to enhance metabolic stability by lessening the susceptibility of nearby moieties to the enzymatic oxidation of cytochrome P450.[16] Substitution of fluorine can also influence lipophilicity and affect partitioning of the drug across membranes.[16] Hydrophobic interactions can also influence binding with enzymes or receptor sites. The substitution or addition of fluorine to a drug compound has produced many drug compounds in the past 50 years. Currently, estimates suggest that 5-15% of all drugs launched worldwide over the past half century contain one or more fluorine substitutions.[17] It is estimated that 20% of all drugs marketed today contain fluorine.[18] This number could be even higher for the past decade when agrochemicals are considered, which could be an additional application of ^{19}F

SSNMR. Some key pharmaceuticals that include fluorine are Prozac, Ciprobay, and Lipitor. The growing presence of fluorine in pharmaceuticals makes ^{19}F SSNMR an appropriate and invaluable tool for investigating amorphous impurities as well as for standard solution and solid-state characterization.

5.1.6 NMR quantitation

NMR spectroscopy has a unique advantage over many other analytical techniques for the analysis of pharmaceutical formulations. An NMR spectrum can be inherently quantitative because the signal observed in a spectrum is directly proportional to the number of nuclei present in the sample. In pharmaceutical applications, the ^{13}C nucleus is most frequently studied.

The first step in quantitation is to measure the spin-lattice relaxation times of the species of interest. When using cross polarization (CP), it is necessary to measure the spin-lattice relaxation rate in the rotating frame ($T_{1\rho}$). The dynamics from cross polarization make quantitation more difficult, so in the following study, direct polarization is used to avoid some of these complexities and to take advantage of ^{19}F relaxation rate differences.

After determining which forms are present, and which forms correspond to specific NMR peaks, the next step is to determine the relaxation rates of the various forms. Spin-lattice relaxation (T_1) times are determined by fitting data to the Equation 5.1.

$$I = (1 - e^{(-\tau/T_1)}) * I_o \quad (5.1)$$

Where I is the observed intensity of the NMR peak, and I_o is the magnetization available once an external magnetic field is applied. When $I = I_o$, the sample is fully relaxed. Tau (τ), often referred to as the pulse delay, is the delay between radio-frequency pulses in signal averaging. In the studies reported here, the ^{19}F T_1 relaxation time is measured and ^{19}F spectra are collected. Processing history, water content, lot, or the presence of oxygen can influence the T_1 of a sample. To obtain reliable quantitative data, the relaxation time must be monitored closely. Traditionally, to be quantitative, a pulse delay that is five times the longest relaxing component in a mixture or formulation is used. Under these conditions, 99.3% of the possible nuclear magnetization is observed. This is usually considered to be quantitative for NMR spectroscopy. Any spectrum collected with a pulse delay shorter than this is often considered non-quantitative. However, if the relaxation rate and pulse delay are taken into consideration, a quantitative value can be obtained at τ values less than five times the T_1 value.

In many cases, when using traditional quantitative conditions, resolution between NMR peaks is not adequate to detect low levels of amorphous material. When that is the case, other NMR parameters can be manipulated to enhance the signal from the amorphous component at the expense of the crystalline component. If the components in a mixture have significantly different relaxation times, the difference-NMR technique can be used to enhance the amorphous signal.[19]

The difference-NMR technique is a spectral subtraction of two or more spectra acquired with different pulse delays to selectively eliminate a component from the spectrum. Before discussing the theory of the difference-NMR technique, it is useful to examine the relaxation profiles that will be described in the following equations. Shown in Figure 5.1 are relaxation profiles for a short (T_1=1.2 s) and a long (T_1=105 s) relaxing component, which may correspond to an amorphous and a crystalline T_1 value, respectively. At five times T_1, or 6 s, the amorphous component is fully relaxed. At longer values of 8 s and 16 s, the amorphous component remains fully relaxed, and the signal intensity from the amorphous component in both spectra will be equivalent. However, the crystalline component has an intensity of 0.073 at 8 s, and an intensity of 0.14 at 16 s. In order to eliminate the crystalline component, the 8-s spectrum is doubled to obtain nearly the same crystalline intensity as the 16-s spectrum. There will be twice as much amorphous component in the doubled 8-s spectrum as in the 16-s spectrum, so subtraction of the 16-s spectrum from the doubled 8-s spectrum will result in an amorphous spectrum with little crystalline component.

At shorter τ values, such as 2 s and 4s, the amount of crystalline component suppressed increases, but the amorphous component is considered non-quantitative, since the signal of amorphous material at 2 s is approximately 84% of the signal at 4 s. The following text will mathematically define the basis of the difference-NMR technique, explaining its basic theory and advantage to expressing short-relaxing components in the presence of long-relaxing components.

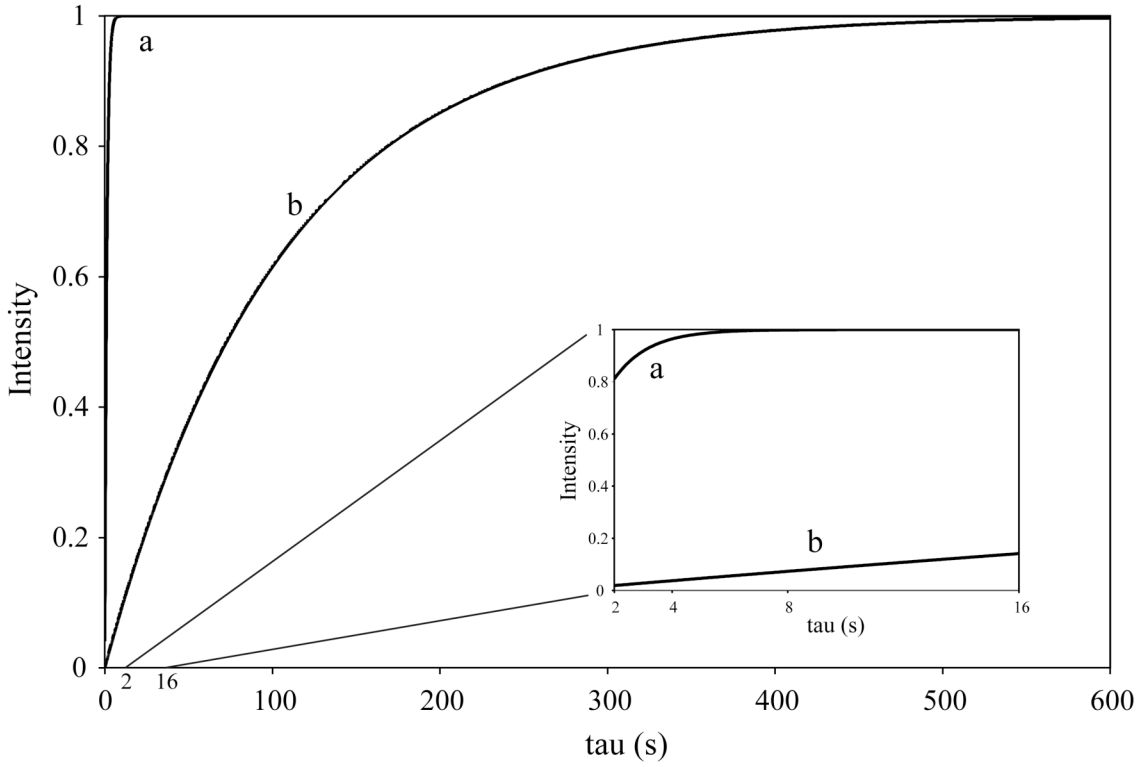

Figure 5.1. The equilibrium magnetization recovery can be plotted against the time allowed to recover (tau). Curve a) represents the relaxation recovery of the spin-lattice relaxation of the amorphous form of triamcinolone (1.2 s) and curve b) represents the recovery of crystalline triamcinolone (105 s). The inset displays the tau region of interest (2-16 s) for the final attempt of the difference-NMR technique.

Assuming exponential relaxation of the NMR signal, Equation 5.1 defines the intensity of the NMR signal with respect to pulse delay and the spin-lattice relaxation rate. A Taylor series expansion of Equation 5.1 establishes the foundation for the difference-NMR technique.

$$I = \frac{\tau}{T_1} - \frac{1}{2}\left(\frac{\tau}{T_1}\right)^2 + \frac{1}{6}\left(\frac{\tau}{T_1}\right)^3 - \frac{1}{24}\left(\frac{\tau}{T_1}\right)^4 + \cdots \tag{5.2}$$

The intensities of two components can be compared by the long division of their respective Taylor series. I_S and I_L are the intensities for the short and long relaxing components of the mixture. The corresponding relaxation rates are T_{1S} and T_{1L}.

$$\frac{I_S}{I_L} = \frac{T_{1L}}{T_{1S}} - \frac{(\tau * T_{1L})}{2T_{1S}}\left(\frac{1}{T_{1S}} - \frac{1}{T_{1L}}\right) + \cdots \tag{5.3}$$

The greatest selectivity will be achieved when the pulse delay, τ, is much shorter than both relaxation rates, T_{1S} and T_{1L}. As τ approaches zero, Equation 5.3 will become:

$$\frac{I_S}{I_L} = \frac{T_{1L}}{T_{1S}} \tag{5.4}$$

The maximum selectivity achievable becomes the ratio of the relaxation rates of the two components. The linearity of the ratio becomes a limiting factor in improving selectivity between two components. To change the linear dependence of the initial

term, some spectral addition is necessary. A spectrum with a pulse delay of $2*\tau$ is subtracted from a doubled spectrum acquired with a pulse delay of τ. The resulting intensity of a single component can be shown mathematically in Equation 5.5.

$$2 * I_{(d = t)} - I_{(d = 2t)} = \left(\frac{\tau}{T_1}\right)^2 - \left(\frac{\tau}{T_1}\right)^3 + \frac{7}{12}\left(\frac{\tau}{T_1}\right)^4 - \cdots \tag{5.5}$$

$$\frac{I_{S((2 * d = \tau) - (d = 2 * \tau)}}{I_{L((2 * d = \tau) - (d = 2 * \tau)}} = \left(\frac{T_{1L}}{T_{1S}}\right)^2 - T_{1L} * \tau\left(\left(\frac{1}{T_{1S}{}^2 - T_{1L}}\right) - \left(\frac{1}{T_{1S}}\right)^3\right) + \cdots \tag{5.6}$$

When comparing $\frac{I_S}{I_L}$ for the spectral subtraction, as in Equation 5.6, the linear term is no longer present; and when τ is much smaller than T_{1S} and T_{1L}, Equation 5.6 reduces to Equation 5.7.

$$\frac{I_{S((2 * d = \tau) - (d = 2 * \tau)}}{I_{L((2 * d = \tau) - (d = 2 * \tau)}} = \left(\frac{T_{1L}}{T_{1S}}\right)^2 \tag{5.7}$$

Equation 5.7 indicates the selectivity benefits of the difference-NMR technique in that the quadratic dependence of Equation 7 allows for greater selectivity of the short-relaxing component. The advantage of the technique is displayed graphically in Figure 5.2. The selectivity of the difference-NMR technique is compared to the

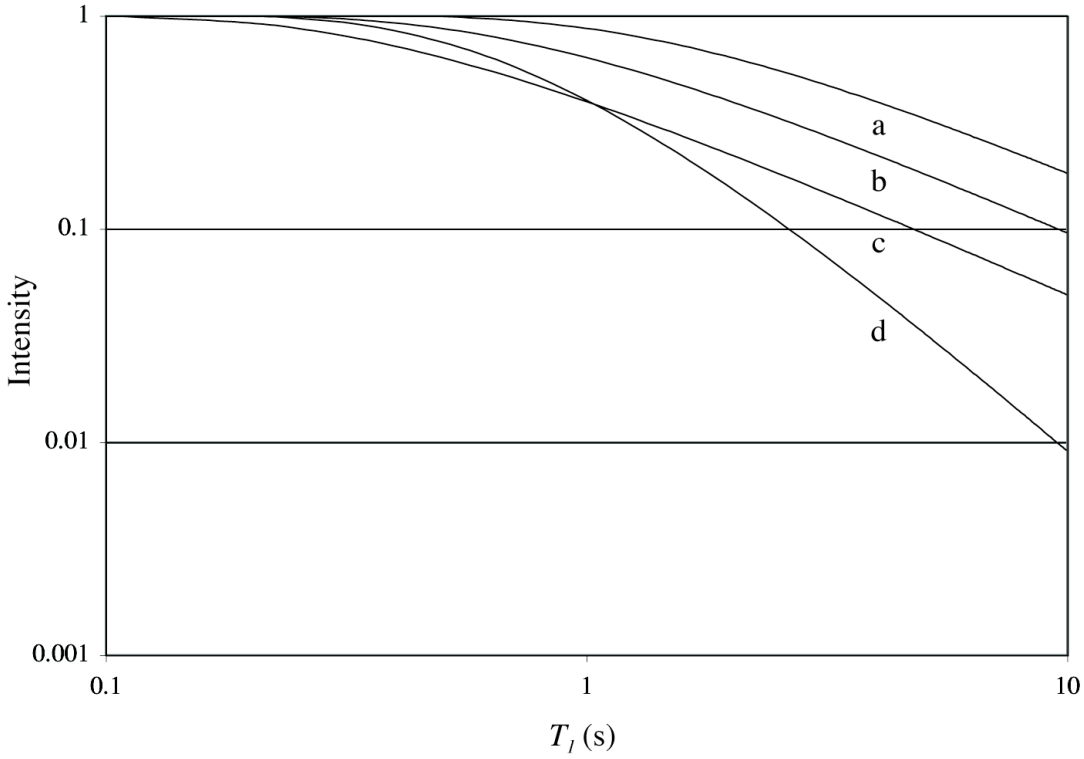

Figure 5.2. Plots of intensity versus T_1 time for a theoretical set of curves to illustrate the increasing efficiency in suppression of long-relaxing components. The intensities of NMR signals from spectra collected with short pulse delays of a) 2 s, b) 1 s, and c) 0.5 s are compared with the efficiency of the d) two-component difference-NMR technique [2*(1s)-2s]. Adapted from reference 19.

selectivity of a single spectra acquired with short pulse delays: 0.5 s, 1 s, and 2 s. Theoretically, the difference-NMR technique should suppress the longer relaxing component to less than 3% intensity when the ratio of T_1 times between the short and long relaxing components is 23:1. When short pulse delays are used, the same suppression is obtainable when the T_1 ratio is 115:1.

To further increase the selectivity of a slow-relaxing component, spectral subtraction can be extended to include three or more component spectra (i.e. $3*1s - 3*2s + 3s$). According to Harris et al., 97% of the short-relaxing component and 3% of the long relaxing component will be retained when the T_1 ratio is only 13:1. The selectivity of the technique increases upon adding an additional component spectrum to the difference-NMR technique, but the noise increases as well. Therefore, there is a balance between selectivity, SNR, and time.

The two-component difference-NMR technique was used in these studies to selectively express the amorphous form in crystalline physical mixtures of triamcinolone. Figure 5.3 shows two examples of the difference-NMR technique. In the illustration, a 45% physical mixture of amorphous and crystalline triamcinolone was used. The amorphous triamcinolone had a ^{19}F T_1 of 1.2 s, and the crystalline component had a ^{19}F T_1 of 105 s. Two subtractions were performed; one subtraction was performed to obtain a quantitative value of the amorphous component (Figure 5.3a-c), and the other was performed under conditions that achieved greater selectivity of the amorphous form (Figure 5.3d-f). Two component spectra were acquired for each set of subtractions. For the first subtraction, component spectra

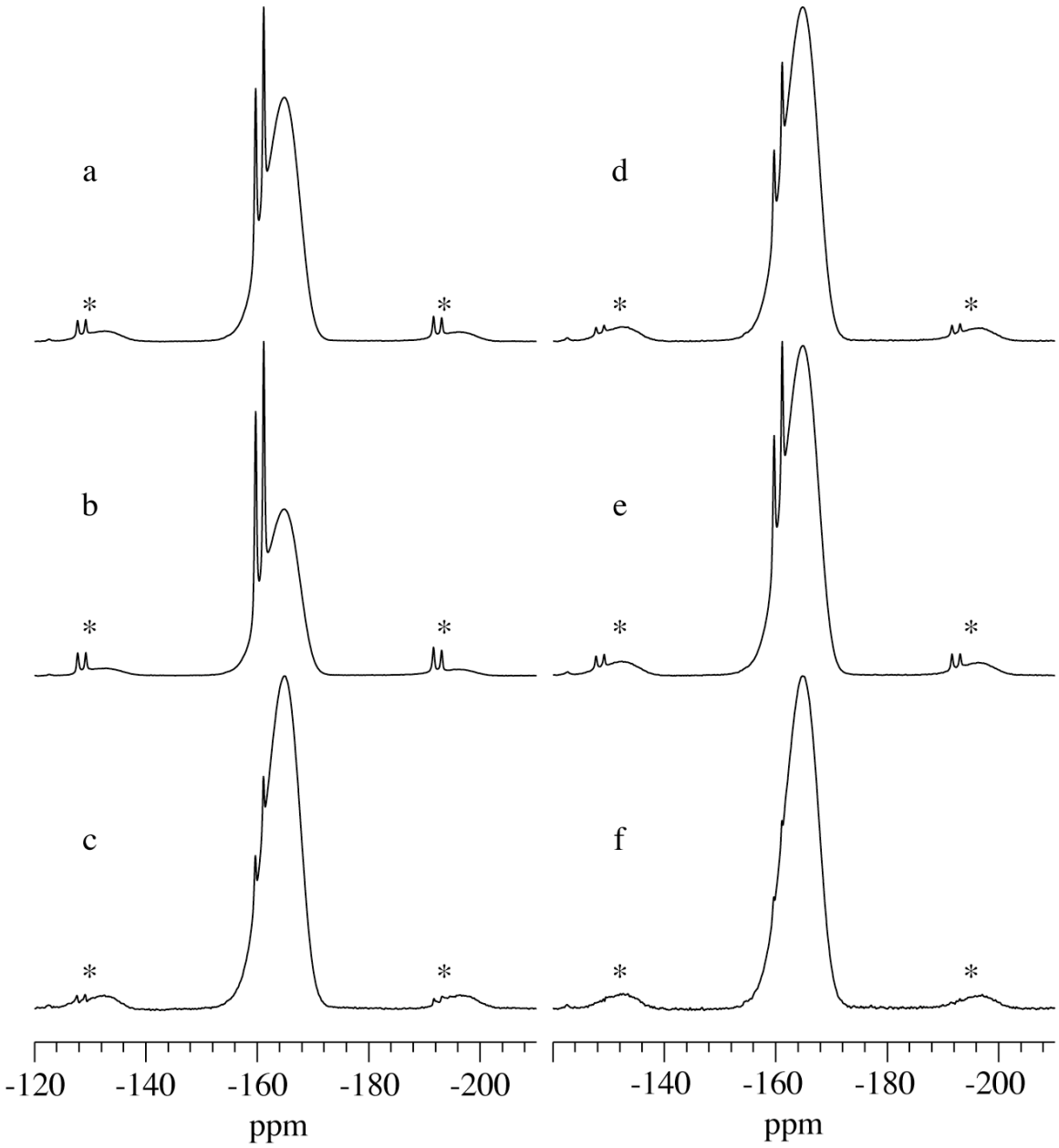

Figure 5.3. An example of the difference-NMR technique being applied to a physical mixture of crystalline and amorphous solid forms with two sets of NMR acquisition parameters. The component spectrum acquired with an a) 8-s pulse delay, b) 16-s delay, and c) the quantitative (for amorphous content) subtracted [(2*(a) – b] spectrum. Non-quantitative spectra acquired with d) a 2-s delay e) 4-s delay, and f) the subtracted [(2*d– (e)] spectrum. Asterisks denote spinning sidebands.

with pulse delays of 8 s and 16 s were acquired, and for the second subtraction, component spectra with delays of 2 s and 4 s were collected. In both cases, the difference-NMR technique suppressed the long-relaxing crystalline component. The component. To obtain a quantitative value for the crystalline component, an additional spectrum must be acquired with a pulse delay greater than five times the relaxation time of all components in the mixture.

5.1.7 Triamcinolone as a model compound

The search for a fluorine-containing compound to study low-level amorphous quantitation using ^{19}F SSNMR spectroscopy is detailed extensively in Chapter 4. The model compound must have the characteristics of both a stable amorphous form and chemical shift resolution of the crystalline and amorphous forms. For this study, the glucocorticoid steroid triamcinolone was selected. Crystalline and amorphous forms of triamcinolone will be used to test the limits of detection of amorphous quantitation using ^{19}F SSNMR spectroscopy. The molecular structure of triamcinolone is shown in Figure 5.4.

5.1.7 Strategy for quantitating mixtures using ^{19}F SSNMR

The general strategy for quantitation was to prepare physical mixtures of the crystalline and amorphous forms of triamcinolone and determine the limit of detection and quantitation. Although not required, the ability to differentiate the crystalline and amorphous components based upon NMR parameters such as

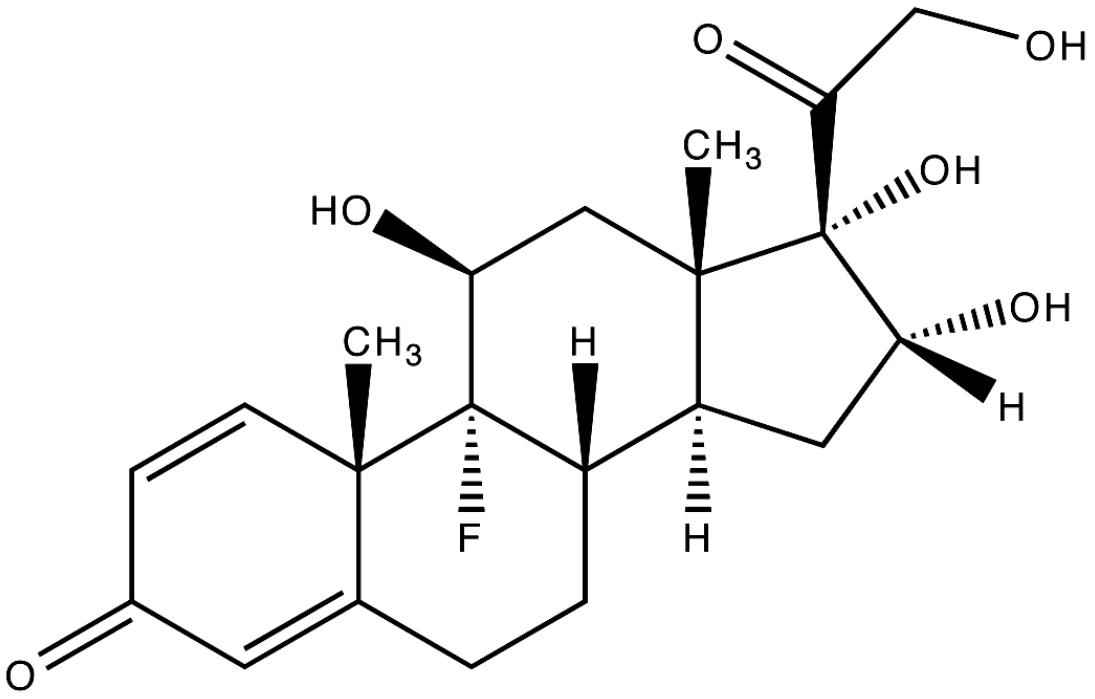

Figure 5.4. Molecular structure of triamcinolone.

relaxation or chemical shift was considered. Quantitation limits below 1% are considered reasonable, with detection limits of up to an order of magnitude below that anticipated.

5.2 Experimental

5.2.1 Materials

Triamcinolone was purchased from Sigma Aldrich (St. Louis, MO) and was analyzed by ^{13}C (not shown) and ^{19}F SSNMR. Further purification was necessary to generate the various crystal forms. Pure polymorph B was obtained by crystallization from methanol. Approximately 1 g of triamcinolone was dissolved in 100 mL of boiling methanol. The solution was concentrated approximately two-fold by evaporation. Then the solution was stirred at room temperature for several hours, while the material crystallized. The crystals were vacuum filtered and dried overnight while exposed to a vacuum at ambient temperature.

The monohydrate was produced by crystallization from an acetone and water solution. Approximately 500 mg of as-received triamcinolone was dissolved in 200 mL of warm acetone. As the solution was cooling in an ice bucket, ice fell into the beaker. The unknown combination of acetone and ice produced a pure monohydrate (according to ^{19}F SSNMR). Although pure hydrate was formed once, attempts to reproduce the pure monohydrate from an acetone and water solution were

unsuccessful. In successive attempts of crystallizing the monohydrate form, polymorph B was also present at various levels.

Physical mixtures were prepared three different times for quantitation with ^{19}F SSNMR. In the first attempt, polymorph B and a cryoground amorphous form were the prepared solid forms. For quantitation using the conventional approach, five times T_1, approach, physical mixtures were prepared with polymorph B (crystallized from methanol) and the amorphous form. The amorphous form was prepared by cryogrinding the as-received triamcinolone for 60 min. Four physical mixtures of approximately 30%, 11%, 3%, and 1.5% amorphous were prepared through serial dilution. The 30% and 3% were produced through one series, and the 11% and 1.5% were produced in another. For the 30% mixture, approximately 30 mg of amorphous triamcinolone was added to 70 mg of crystalline triamcinolone. The 3% mixture was generated by measuring approximately 10 mg of the 30% mixture and diluting with 90 mg of crystalline triamcinolone. All of the mixtures were vortexed in a scintillation vial for 5 min to ensure proper mixing. The same method of dilution was applied to the second dilution series of 11% and 1.5%. Physical mixtures were stored under vacuum at ambient temperature.

For the initial attempt using the difference-NMR technique approach, a set of physical mixtures was prepared with cryoground amorphous triamcinolone and triamcinolone monohydrate. The monohydrate with polymorph B impurity was the crystal form used for the physical mixtures. Two physical mixtures, 45% and 4.5%, were prepared through serial dilution. For the 45% physical mixture, amorphous and

crystalline forms of triamcinolone were weighed to approximately a 1:1 mixture. The 4.5% mixture was produced by taking 10 mg of the 45% mixture and adding 90 mg crystalline material. The samples were stored at ambient temperature in a desiccator.

Using the difference-NMR approach, the crystalline and amorphous triamcinolone were prepared differently in order to generate more stable/purer standards. Polymorph B obtained by crystallization from methanol for the second attempt at the difference-NMR technique. The amorphous form was produced via spray drying, and six physical mixtures were prepared through two serial dilutions. The mixtures containing 45%, 5%, and 0.5% amorphous material were prepared via one series, and the mixtures containing 10%, 1%, and 0.1% amorphous material were prepared through a second dilution. Initially, pure amorphous and pure crystalline materials were weighed to approximately a 1:1 mixture by mass. Roughly 10 mg of this first dilution was used with an additional 90 mg of pure crystalline material to form the 5% mixture. Roughly 10 mg of the 5% dilution was mixed with approximately 90 mg of the crystalline mixture to form the 0.5% sample. Each physical mixture was weighed in a scintillation vial and mixed for 10 minutes with a Turbula mixer (Glen Mills; Clifton, New Jersey). The physical mixtures were stored under vacuum at ambient temperature.

5.2.2 Cryogrinding

Cryogrinding was performed with a SPEX CertiPrep 6750 Freezer/Mill (SPEX CertiPrep, Inc., Metuchen, NJ). Approximately 500 mg of as-received

triamcinolone was loaded into the cryovial for each process. Samples were pre-cooled for 15 minutes, followed by 30 cycles. Each cycle consisted of 2 min of impaction and 2 min of cooling time. The impaction rate was 10 impacts/s. After grinding, the cryovial with sample returned to ambient temperature under vacuum in order to prevent condensation upon removal from the vial.

5.2.3 Spray drying

Spray drying was performed with a custom-built spray dryer (Bend Research, Inc., Bend, Oregon). Approximately 200 mg of drug was dissolved in 10 g of warm methanol, producing approximately a 2% wt/wt solution. The solution was injected into the spray dryer at a rate of 1.3 mL/min with an inlet temperature of 70 °C. The material was collected on a piece of 110-mm Whatman filter paper, and a static gun was used to discharge any electrostatic charge. The spray-dried material was exposed to a vacuum for one hr at ambient temperature to remove any methanol.

5.2.4 SSNMR spectroscopy

Quantitation by waiting 5x the T_1 value was performed on a Tecmag (Houston, TX) Apollo three-channel spectrometer operating at 284.1 MHz for ^{19}F and 301.9 MHz for ^{1}H. A Chemagnetics (Varian, Inc., Fort Collins, CO) double-resonance $^{1}H/^{19}F$ probe was used to collect the data. The samples were packed in 3.2-mm o.d. zirconia rotors with torlon endcaps and a Vespel drive tip. Samples were spun at a rate of 10-20 kHz. The samples were cooled to -70 °C using a variable-

temperature accessory that delivered liquid-nitrogen cooled air directly to the spin module housing. ^{1}H to ^{19}F cross polarization (CP) was employed along with two-pulse phase modulated (TPPM) proton decoupling. A ^{1}H 90° pulse of 2.9 μs, and a contact time of 2 ms were used. A spectral sweep width of 100 kHz was used. The ^{19}F and ^{1}H spin-lattice relaxation times (T_1) were measured using a saturation recovery pulse sequence with at least eight increments. The 10-s pulse delay used was more than five times the measured ^{1}H T_1 value for polymorph B and the amorphous form of triamcinolone. All spectra were referenced to Teflon at -121.1 ppm.

^{19}F SSNMR spectra on all solid forms of triamcinolone and the difference-NMR studies were performed on a Bruker (Bruker, Billerica, MA) Avance 500 three-channel spectrometer outfitted with an $^{1}H/^{19}F/X$ triple-resonance probe and operating at 469.8 MHz for ^{19}F and 499.3 MHz for ^{1}H. Samples were packed in 4-mm zirconia rotors and spun at a rate of 15 kHz. A 2.7-μs ^{19}F 90° pulse-width was used in direct polarization of the ^{19}F nucleus with TPPM proton decoupling. The spectral width was 100 kHz (212.9 ppm), 3072 points were collected in all cases, and acquisition times were between 10 and 16 ms. ^{19}F T_1 relaxation data was collected on all samples. Eleven points were acquired and fit to a monoexponential decay with a good fitting parameter. All samples acquired on the Bruker Avance 500 were referenced to a 1:1 solution of trifluoroacetic acid (TFA) and water at -76.54 ppm.

During the initial attempt at the difference-NMR technique, Vespel drive tips were used to seal the rotors. Two component spectra were acquired for each physical

mixture (45% and 4.5%) for a total of four spectra. The component spectra were collected with identical acquisition parameters with the exception of pulse delay and number of scans. For the 45% physical mixture, a spectrum was acquired with a 14-s pulse delay and 128 scans and another component spectrum with a 28-s pulse delay and 64 scans. The same conditions were used for the component spectra acquired for the 4.5% physical mixture. No post-acquisition modifications were made to the FID.

In the second attempt at the difference-NMR technique, the rotors were purged for one min with medical-grade oxygen gas and sealed with Vespel end caps. The Vespel end caps have two Teflon O-rings (Revolution NMR, Fort Collins, CO) and provide a gas-tight seal. For each of the six physical mixture, eight data sets were acquired in this order: crystalline ^{19}F T_1 (11 increments, 1 scan) measurement, amorphous ^{19}F T_1 (11 increments, 12 scans) measurement, four component spectra (pulse delays of 2 s, 4 s, 8 s, and 16 s), a spectrum that is five times the crystalline ^{19}F T_1 time (600-s pulse delay and 4 scans), and an additional amorphous ^{19}F T_1 measurement. The four component spectra are used in the two difference-NMR subtraction [2*(2s)-4s] and [2*(8s)-16s]. The spectrum acquired with five times the crystalline ^{19}F T_1 time is used to determine the amount of crystalline material present by SSNMR, and the three relaxation measurements were made to ensure relaxation stability throughout the experiments. Twenty dummy scans were used to equilibrate the magnetization in the sample prior to data collection of the four component spectra to minimize differences in the starting magnetic equilibrium. The corresponding component spectra of the six physical mixtures (45%, 10%, 5%, 1%, 0.5%, and 0.1%)

were acquired with identical parameters other than the number of scans (1024, 1024, 1024, 4096, 2048, and 8192, respectively). It was determined that processing the NMR data using Spinsight was the preferred method for deconvolution of the various peaks. Spinsight is the software that comes with the Chemagnetics (now Varian) spectrometers. The FIDs were processed with 100 Hz Gaussian line broadening, 1024 data points, and baseline correction was applied after the component spectra were subtracted.

5.2.5 Data conversion XWin-NMR to Spinsight

SSNMR data collected on the Bruker Avance 500 with XWin-NMR software were transferred to a Sun workstation, and the data were converted into Spinsight format with in-house software. The digital free induction decays (FIDs) from Bruker were processed within Spinsight by a macro written to handle the additional steps required to process the data. [Note: Bruker can convert the FIDs into an analog form. In the present case, there were hundreds of data files, which means that writing a conversion program was preferred]. To treat the digitally filtered Bruker data, the DC offset must be corrected first, followed by any desired zero filling. Next, there is an artifact at the beginning of the Bruker FID that arises as a consequence of the digital filtering. Those points must be circularly shifted to the end of the FID (i.e., the first X points in the FID become the last X points of the baseline-corrected and zero-filled FID). Then the FID was Fourier transformed and phased.

5.3 Results

5.3.1 Solid forms of triamcinolone

The solid-state ^{19}F NMR spectra of the three crystalline forms and one amorphous form of triamcinolone are shown in Figure 5.5. In all spectra, the smaller peaks, denoted with asterisks, are spinning sidebands. Spinning sidebands are artifacts of spinning the samples and occur at frequencies proportional to the spinning speed.

A ^{19}F SSNMR spectrum of the as-received triamcinolone lots is shown in Figure 5.5a. Several lots were received and analyzed, and the bulk as-received material usually consisted of mixtures of polymorphs A and B. The two downfield peaks (-159.7 and -161.2 ppm) were assigned to polymorph B, and the two upfield peaks were assigned to polymorph A (-163.2 and -164.0 ppm). Both polymorphic forms A and B produced two NMR peaks for a single fluorine atom in the molecule. In these cases, the unit cell consists of two crystallographically inequivalent molecules. Each unique molecule has a different molecular environment and therefore a unique chemical shift. This is supported in the ^{13}C SSNMR spectrum (not shown), where two peaks were also present in the spectrum for each carbon in triamcinolone.

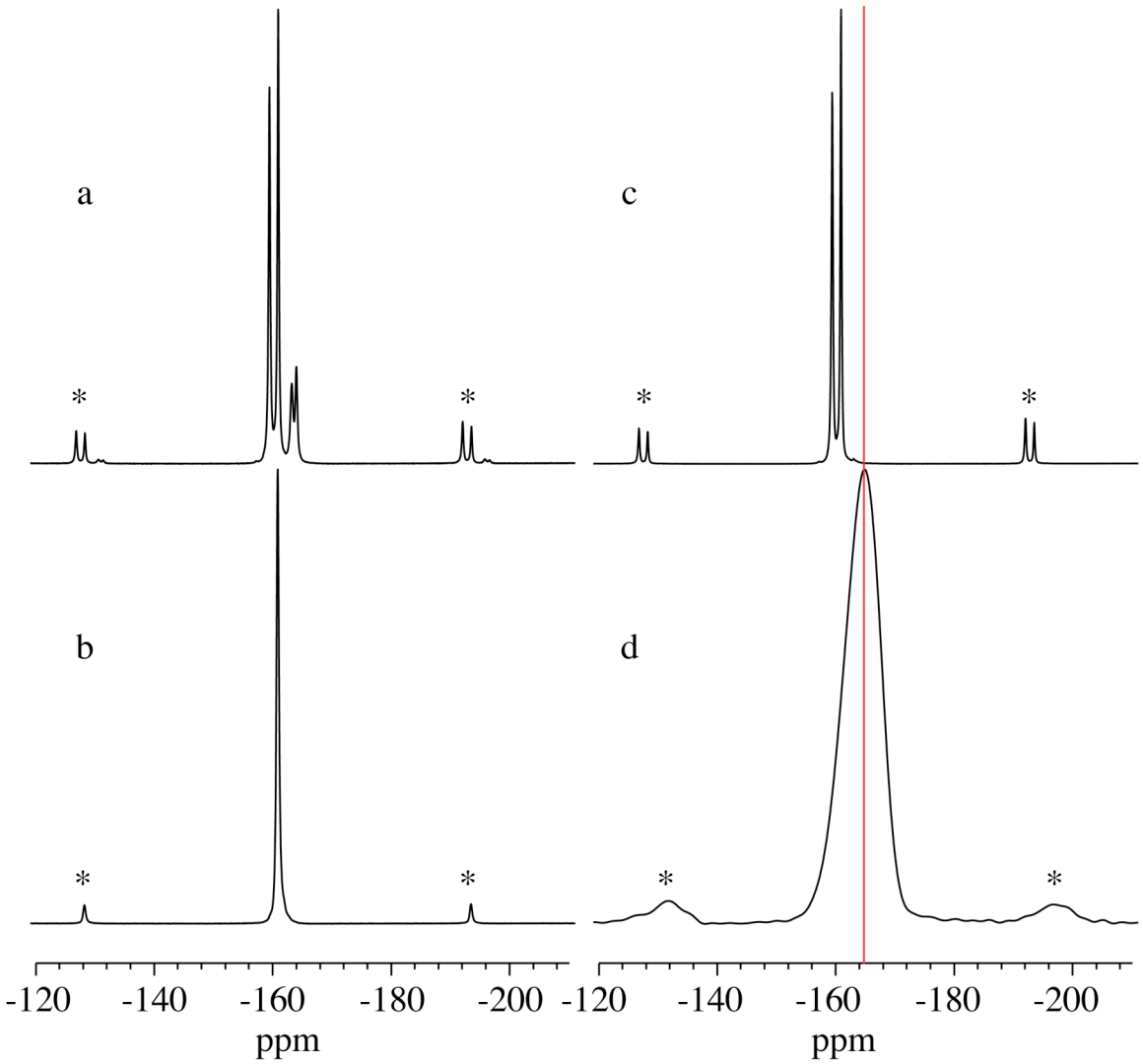

Figure 5.5. ^{19}F SSNMR spectra of the different forms of triamcinolone: a) as-received triamcinolone from Sigma-Aldrich containing polymorphs A and B, b) the monohydrate form, c) polymorph B, and d) amorphous triamcinolone. The asterisks denote spinning sidebands. The red line indicates the chemical shift resolution between polymorph B (figure 5.5c) and the amorphous form (figure 5.5d).

Polymorph A was present in the majority of lots received from Sigma Aldrich. Polymorph A is a metastable polymorph of triamcinolone that can be produced by dehydrating the monohydrate or crystallization from the amorphous form. The peaks of polymorph A significantly overlap with the chemical shift region of the amorphous form, making it an unsuitable crystalline form for this study. Despite not being an appropriate crystalline form, polymorph A was helpful in monitoring the physical stability of the model forms in the physical mixtures studied in these experiments.

The ^{19}F SSNMR spectrum of the monohydrate form is shown in Figure 5.5b. The monohydrate was produced by crystallization from an acetone and water solution. The weight loss from the thermogravimetric analysis (TGA) (not shown) thermogram was consistent with a stoichiometric loss of a single water molecule per molecule of triamcinolone. The ^{19}F SSNMR spectrum of the monohydrate had a single peak at -160.9 ppm with a line width of 223 Hz. Upon exposure to a vacuum overnight, the monohydrate partially converted to polymorph A. The ^{19}F T_1 time of monohydrate triamcinolone was 110 s. Because the chemical difference between the monohydrate and amorphous forms were substantially different, the monohydrate form was used as the model crystalline form for the initial attempt at quantitation using the difference-NMR technique.

The ^{19}F SSNMR spectrum of pure polymorph B is shown in Figure 5.5c. Polymorph B was recrystallized from methanol for these studies, and it readily crystallizes from a number of organic solvents. There are two peaks in the spectrum,

at -159.7 and -161.2 ppm, with line widths of 145 and 122 Hz, respectively. The ^{19}F T_1 time was 105 s, and the measured ^{1}H T_1 time was approximately 1 s.

In these studies, amorphous triamcinolone was generated by cryogrinding and spray drying. Both processing techniques generated an amorphous form with similar ^{19}F SSNMR spectra and comparable relaxation times between 2-5 s. The spectrum of the amorphous form of triamcinolone is shown in Figure 5.5d. The peak had a chemical shift of -164.9 ppm and a line width of 3300 Hz, which was 22x and 27x broader than the line widths of the two NMR peaks of polymorph B. The dashed line helps illustrate the chemical shift resolution between polymorph B (figure 5.5c) and the amorphous form (figure 5.5d). For these quantitation studies, increased chemical shift resolution improves the ability to quantitate the solid forms. The ^{19}F NMR peak shape of the amorphous form was visibly asymmetric. Typically NMR line shapes are symmetric, so this observation is notable. The cause of the asymmetry is unknown, but it did not depend on spectrometer or field strength, because it was exhibited at both 300 MHz and 500 MHz on two different solid-state NMR spectrometers. The asymmetry was also present for amorphous samples produced from cryogrinding and spray drying processes.

Amorphous triamcinolone generated by cryogrinding was used to prepare the physical mixtures for the first and second quantitation attempts. For the third and final quantitation, the physical mixtures were prepared with spray-dried amorphous triamcinolone.

5.3.2 Quantitation attempt one

The initial attempt at quantitation was performed using $^{1}H/^{19}F$ cross polarization with a pulse delay longer than 5× the ^{1}H T_1 times of the crystalline and amorphous forms. Two series dilutions produced four physical mixtures with varying percentages of amorphous triamcinolone (30%, 10%, 3%, and 1%). The ^{19}F SSNMR spectra of the four physical mixtures and the crystalline polymorph B standard are shown in Figure 5.6. Each spectrum is zoomed in on the chemical shift region of the amorphous form to show the presence of low-level amorphous material. A dashed line is positioned at the chemical shift of the peak to aid the eye for observing the low-level presence of amorphous triamcinolone. The amorphous form was readily visible in the full NMR spectrum of the 30% physical mixture as shown in Figure 5.6a. The amorphous form was not readily visible in the full spectrum for the other physical mixtures, Figure 5.6b-d. When the spectra are expanded, the spectrum of the 10% physical mixture appears to have a small but distinguishable signal from amorphous triamcinolone. The amorphous form was not observed in the spectra of the 3% and 1% physical mixtures. The ^{19}F SSNMR spectrum of polymorph B is shown in Figure 5.6e. The intensity of the crystalline peaks decreases the resolution with the amorphous peaks at the base. Acceptable resolution was not achievable for triamcinolone using this approach.

Two unidentified peaks were present in all four physical mixtures and the crystalline polymorph B standard. The two peaks straddled the NMR peaks of

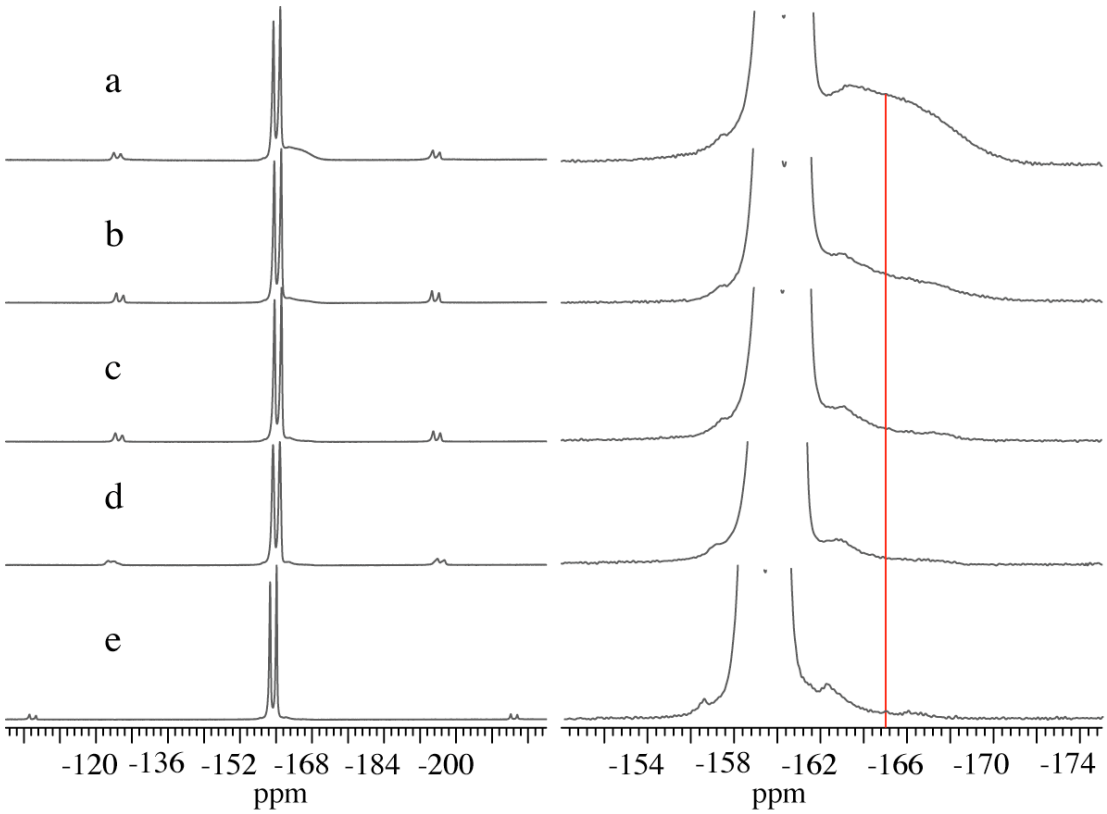

Figure 5.6. Traditional quantitation attempt of the physical mixtures of polymorph B and amorphous triamcinolone. ^{19}F SSNMR spectra of the four physical mixtures: a) 30%, b) 10%, c) 3%, d) 1% and e) pure polymorph B. Each of the spectra are expanded to zoom in on the region of the amorphous impurity. The vertical line is located
at -164.9 ppm to help follow the amorphous peak.

polymorph B. They are only observed in the spectra of polymorph B and were consistent in intensity from various lots of polymorph B crystallized from methanol. There are several potential explanations for these two peaks. One explanation for these peaks is that they could be due to ^{13}C-^{19}F spin-spin couplings. This explanation, while possible, is inconsistent with the fact that the peaks have the same chemical shift (in ppm) on both 300 and 500 MHz spectrometers. The peaks could also be signal from a polymorphic or chemical impurity generated during crystallization from methanol. Although the source of the peaks is unidentified, they are irrelevant to the quantitation studies. Detection of low-level amorphous impurity was not possible with the traditional quantitation approach, and another approach is necessary, which suppresses the signal of the crystalline form.

5.3.3 Quantitation attempt two

Amorphous levels below 10% could not be detected with the traditional quantitative approach; therefore, the difference-NMR technique was used to increase the detection of low-level amorphous impurity. The difference-NMR technique separates forms based on differences in spin-lattice relaxation times. In the case of triamcinolone, the ^{1}H T_1 times for the amorphous and crystalline forms are both on the order of a few seconds. However, the ^{19}F T_1 times differ by nearly two orders of magnitude between the crystalline and amorphous forms. The ^{19}F T_1 time of the cryoground amorphous form used in this experiment was determined to be 2.8 s, yet the ^{19}F T_1 time of the mononhydrate was measured to be 110 s, nearly 40 times

longer. The difference means that this system is very amenable to use the difference-NMR technique.

The amorphous form was physically mixed with the crystalline monohydrate to demonstrate the difference-NMR technique. Two physical mixtures, containing 45% and 4.5% amorphous, were prepared through serial dilution. Two SSNMR component spectra were acquired for each blend using identical NMR parameters except pulse delay and number of scans. To maintain quantitative conditions for the amorphous form, both component spectra were collected with pulse delays greater than 5× the ^{19}F T_1 time. One of the component spectra was acquired with a 14-s pulse delay and 128 scans, and the other was collected with a 28-s delay and 64 scans. The individual component spectra and the subtraction for the two physical mixtures are shown in Figure 5.7. Figure 5.7a-c shows the component spectra and subtracted spectrum of the 45% physical mixture. In each of the three spectra, three solid forms of triamcinolone are visible: polymorph B (-159.7 ppm), the monohydrate (-160.9 ppm), and the amorphous form (-164.9 ppm). The monohydrate still had a large impurity of polymorph B after crystallization. As would be expected, the amorphous intensity in the spectrum acquired with a 14-s pulse delay (Figure 5.7a) is greater than the amorphous intensity in the 28-s component spectrum (5.7b). This is because the NMR signal from the crystalline form is suppressed more at shorter pulse delays, and the number of scans acquired is larger for the 14-s component spectrum.

The component ^{19}F SSNMR spectra of the 4.5% physical mixture and the difference-NMR subtraction are displayed in Figure 5.7d-f. In each of the three ^{19}F

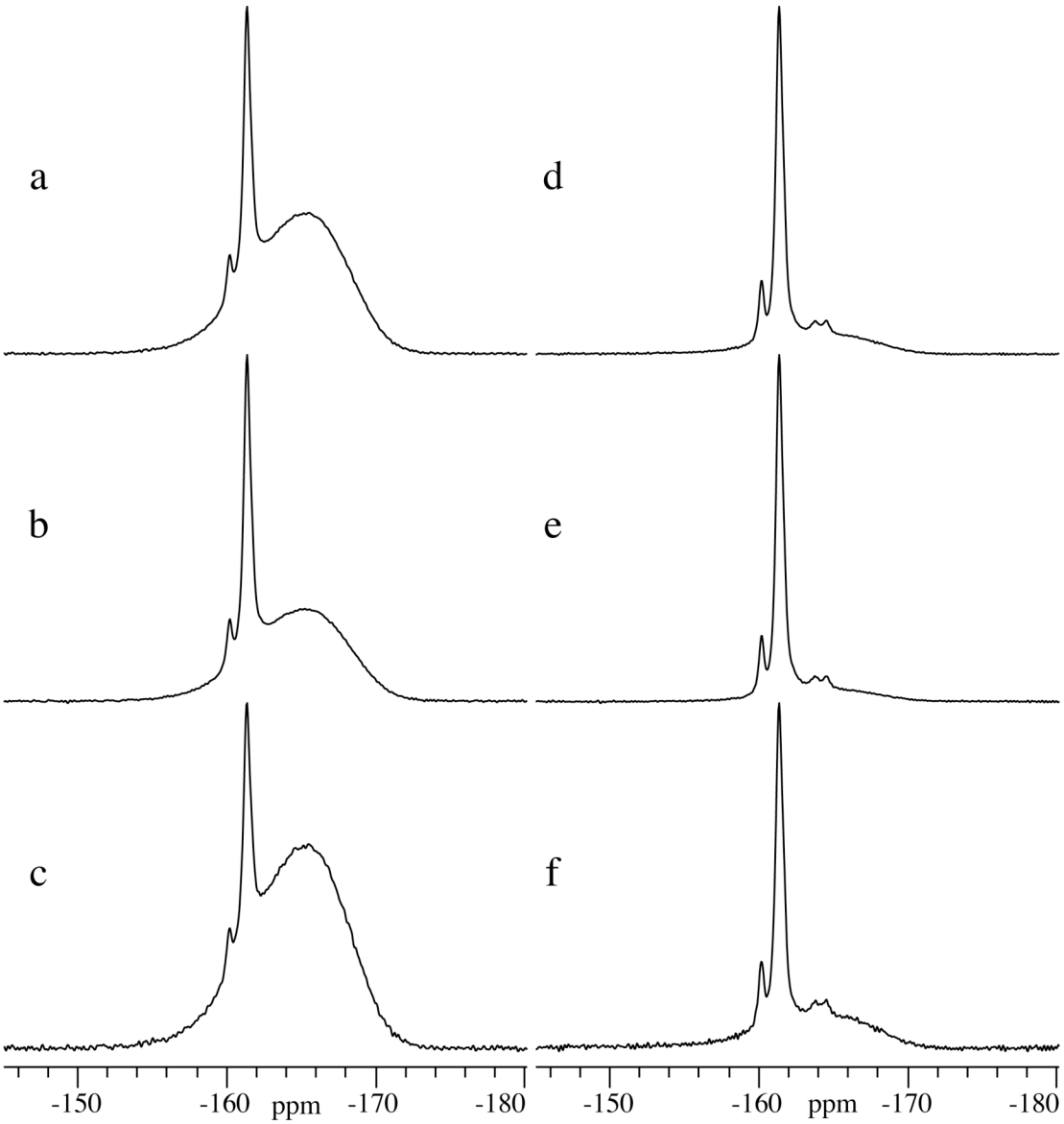

Figure 5.7. ^{19}F SSNMR spectra of the component and subtraction spectra for each physical mixture in the first attempt using the difference-NMR technique. The spectra of the 45% physical mixture were acquired with a a) 28-s pulse delay and a b) 14-s delay, and the c) the subtracted spectrum. [2*(28s)–14s]. The same conditions apply for the 4.5% physical mixture: a) component spectrum with a 28-s delay, b) 14-s delay and c) the subtracted spectrum, [2*(28s) –14s].

SSNMR spectra, four forms are now visible. In addition to the NMR peaks corresponding to the three forms anticipated to be present, two small sharp peaks of corresponding to polymorph A have appeared. This indicates that the physical forms present in the sample changed some time during preparation, storage, and/or data acquisition. Both recrystallization of cryoground triamcinolone and dehydration of the monohydrate form have been shown to generate polymorph A. For this reason, both the monohydrate and the cryoground amorphous form were determined to be physically unstable for quantitation.

Despite the form conversion, both the subtractions for each physical mixture show a higher ratio of the amorphous form in comparison to the individual component spectra. Afterwards, the ^{19}F T_1 time of the amorphous form was monitored over several hours to determine if the relaxation time had changed, and it was found that it increased from the initially measured value of 2.8 s to nearly 20 s. Through a series of experiments detailed in Chapter 6, it was determined that the nitrogen gas used to spin the samples purged oxygen from the rotor. Oxygen is a paramagnetic relaxation agent, and as it is removed, the relaxation time of amorphous triamcinolone increased by more than an order of magnitude. Changes in partial pressure of oxygen had no visible affect on the ^{19}F T_1 times of the crystalline forms of triamcinolone or the line widths and chemical shifts of both forms. During the acquisition of the component spectra, the ^{19}F T_1 time increased for the amorphous form. If the ^{19}F T_1 time increased to more than 5.6 s, the 28-s component spectra

would have considerably less NMR signal from the amorphous form; therefore, the subtracted spectrum would have more amorphous signal than anticipated.

This attempt at quantitation using the difference-NMR technique raised several concerns. First, the spin-lattice relaxation times of each component in the mixture must be measured because the values remaining constant is paramount to the accuracy of the difference-NMR technique. Second, the ^{19}F T_1 times of the crystalline and amorphous forms need to be monitored throughout the course of the experiments. Lastly, the crystalline and amorphous solid forms should be closely monitored for form conversion, which could also skew quantitation results. The monohydrate form can potentially dehydrate during the experiment and convert to polymorph A. A more physically stable amorphous form needs to be prepared to ensure physical stability throughout the experiments. The final quantitation attempt is designed to account for these shortcomings.

5.3.4 Quantitation attempt three

In the previous quantitation attempt, the ^{19}F T_1 times increased during some of the acquisition of the component spectra, and the solid forms exhibited physical instabilities. The concerns that arose in the previous attempt were addressed with several changes. First, the solid forms of triamcinolone were prepared in a more reproducible manner. Spray drying was used to generate amorphous triamcinolone rather than cryogrinding. Chapter 4 provides a more detailed discussion on the physical stability of the differences between spray-dried and cryoground amorphous

triamcinolone. Polymorph B crystallized from methanol was used as the model crystalline form. Reproducibly crystallizing the monohydrate form was difficult, and it was physical instable, which were both reasons to return to using polymorph B as the crystalline standard. Second, the physical mixtures were purged with oxygen gas, and gas-sealed with an MAS drive tip containing two O-rings, which would prevent the sample from being purged by nitrogen gas while spinning. Third, the ^{19}F T_1 times of the crystalline and amorphous forms were closely monitored (when possible) during the course of the experiments to ensure relaxation time stability and accuracy. Fourth, dummy pulses were added to minimize differences in the magnetic equilibrium of the individual component spectra. Lastly, an additional spectrum was acquired to provide a quantitative value for the crystalline form.

Prior to quantitation, the ^{19}F T_1 times of the amorphous and crystalline standards were measured. Pure spray-dried amorphous triamcinolone was purged with oxygen gas and sealed. After purging and sealing a sample of amorphous triamcinolone, the measured ^{19}F T_1 time was 1.6 s. After spinning for 48 hrs in a sample spinner, the ^{19}F T_1 time was 1.5 s. The relaxation time had not increased, and the drive tips provided a reliable seal. The 1.6-s ^{19}F T_1 time was less than the 2.8-s ^{19}F T_1 time measured during the previous quantitation attempt. The drop in relaxation time was attributed to increased partial pressure of oxygen gas in the rotor. The ^{19}F T_1 time of pure polymorph B was also monitored after purging with oxygen gas. The T_1 time of polymorph B was 105 s, and did not change after spinning for 48 hrs. The relaxation time of the amorphous form had dropped, yet the crystalline form was

unchanged. This was likely due to the crystal lattice preventing penetration of the oxygen molecules. Because the increased partial pressure of oxygen only affected the amorphous form of triamcinolone, the T_1 ratio of our forms was increased. Increasing the T_1 ratio improves selectivity of the difference-NMR technique.

During the quantitation experiments, four relaxation measurement experiments were performed for each physical mixture. Due to the large differences in relaxation times, the ^{19}F T_1 times of the crystalline and amorphous forms were measured separately. A T_1 measurement was performed for the amorphous and crystalline forms both before and after the component spectra were acquired. The measurements ensured that the T_1 times had not increased during the experiment due to sample annealing or healing and/or loss of partial pressure of oxygen gas. The ^{19}F T_1 time of polymorph B was 105 s (+/- 5 s) in the six physical mixtures. The ^{19}F T_1 time of the amorphous form was 1.2 s for the 45% and 10% physical mixtures before and after collection of the component spectra. The NMR signal of the amorphous form was too low to measure in the other physical mixtures. The ^{19}F T_1 time dropped from 1.6 s for the pure amorphous standard to 1.2 s for the 45% and 10% physical mixtures. The reduction in T_1 could be attributed to additional disorder of the amorphous state in the physical mixtures or an increased partial pressure of oxygen gas relative to the standard.

Along with the three relaxation experiments, five ^{19}F SSNMR spectra of each physical mixture were acquired. Of the five spectra acquired, four spectra were acquired as component spectra for the difference-NMR subtractions with pulse delays

of 2 s, 4 s, 8 s, and 16 s. All other experimental NMR parameters remained the same, including the number of scans. These four component spectra were spectrally subtracted in three different ways. A spectral subtraction, [2*(2s)-4s], was performed that yielded the best crystalline suppression. The subtraction is considered qualitative (**QL**), because the component spectra (2 s and 4 s) were collected with pulse delays shorter than five times the ^{19}F T_1 time (1.2 s) of the amorphous form,. The other two subtractions combined component spectra with pulse delays of 8 s and 16 s. The pulse delays of these component spectra were greater than five times the ^{19}F T_1 time of the amorphous form, and are considered quantitative. The two component spectra were combined in two different ways. First, a straightforward application of the difference-NMR technique [2*(8s)-16s] provided a spectrum with a quantitative value for the amorphous drug. This subtraction is referred to as the first quantitative subtraction (**QT1**). The third subtraction, [1.927*(8s)-16s], accounted for the exponential nature of the crystalline ^{19}F T_1 curve between 8 and 16 s. The subtraction was still quantitative for the amorphous and is referred to as the second quantitative subtraction (**QT2**).

The three subtractions using the difference-NMR technique did not return a quantitative value for the crystalline form. The fifth spectrum was acquired to obtain NMR peak areas for the crystalline material in each mixture. The spectrum was acquired with a 600-s pulse delay that allowed for full relaxation of both solid forms, specifically the crystalline form. This is referred to as the quantitative crystalline (**QTC**) spectrum.

Table 5.1. Descriptions of the four spectra (three subtractions and the **QTC**) used to measure the amorphous content in the six physical mixtures.

Abbr.	Description	Component Spectra	Subtraction	Notes
QL	Qualitative subtraction	2 s, 4 s	2*(2s)-4s	Best crystalline suppression. Amorphous material significantly suppressed as well.
QT1	Quantitative subtraction 1	8 s, 16 s	2*(8s)-16s	Component spectra collected with 5x T_1 of amorphous material. Quantitative amorphous value with no additional corrections.
QT2	Quantitative subtraction 2	8 s, 16 s	1.927*(8s)-16s	Coefficient (1.927) used to mathematically account for residual crystallinity. Quantitative for amorphous drug.
QTC	Quantitative crystalline	none	none	Spectrum acquired with 4 scans a 600-s pulse delay to obtain a quantitative value for polymorph B.

The **QTC** and component spectra were transferred to Spinsight for subtraction and deconvolution. Isotropic peak areas of the amorphous peak in the difference-NMR subtraction spectra (**QL**, **QT1**, and **QT2**), and crystalline peaks in the **QTC** spectrum were measured. The areas of the spinning sidebands were not deconvoluted, yet the signal loss from the sidebands was taken into account. The following procedure outlines the deconvolution scheme applied to the NMR data of the six physical mixtures.

Initially, the ^{19}F SSNMR spectra of pure amorphous and crystalline spectra were deconvoluted to determine the values of the principle parameters that define a peak in a SSNMR spectrum: chemical shift (ppm), line width (Hz), and line shape (Gaussian/Lorentzian ratio, %GL). The defined parameters limited the ability of the user to adjust parameters for a better fit, especially when peaks were difficult to deconvolute due to relatively low intensities. In Figure 5.8, an example of the deconvolution scheme for one of the physical mixtures is shown. There are five traces in this figure: two peaks for the crystalline form (*c1* and *c2*), two peaks for the amorphous form (*a1* and *a2*), and a trace of the deconvoluted sum. The trace of the deconvoluted sum is difficult to distinguish from the acquired spectrum. Because of the asymmetry of the amorphous NMR peak, two peaks were required for deconvolution.

The parameters used to define the four peaks in the deconvolution scheme are presented in the table in Figure 5.8. The peaks of the crystalline form had chemical shifts of -159.7 and -161.2 ppm, and line widths of 202 and 185 Hz, respectively.

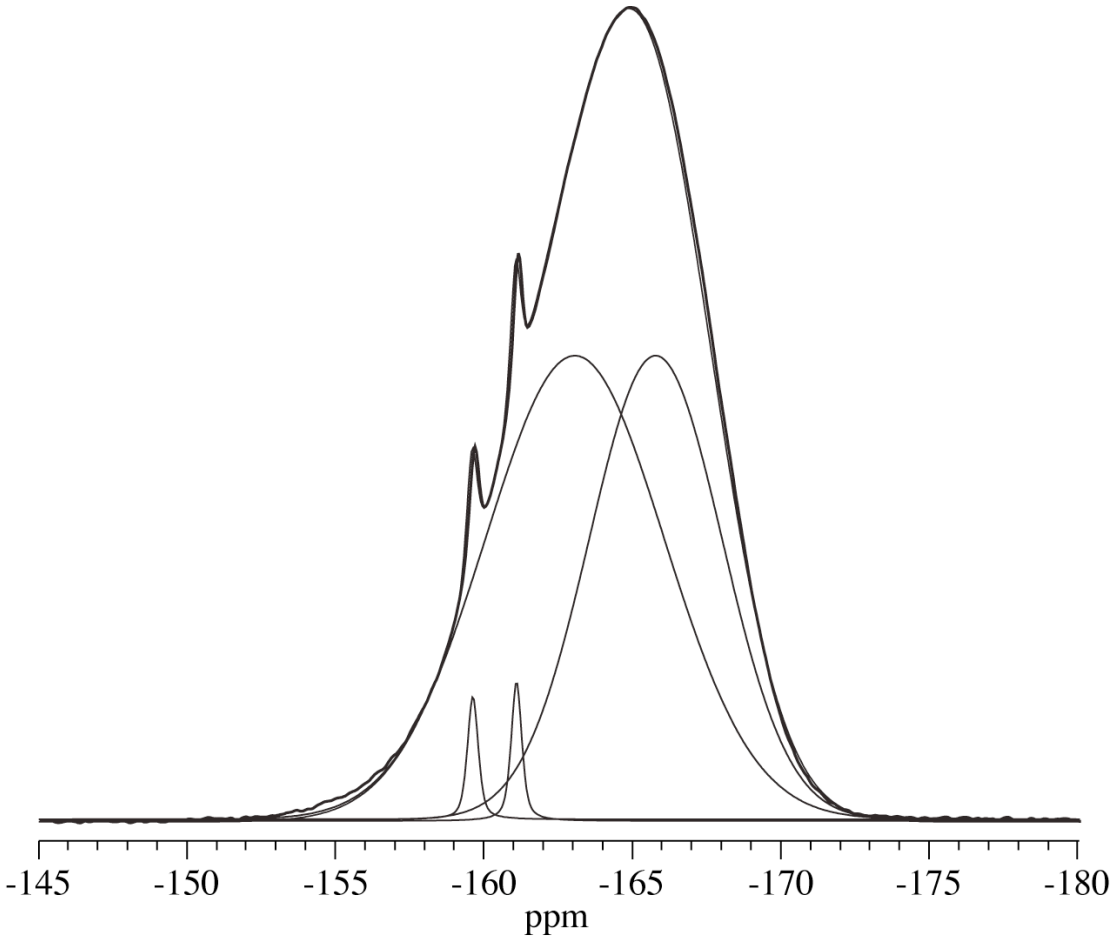

Crystalline	Chemical Shift (ppm)	Width (Hz)	%G/L	Ratio c1:c2
c1	-159.7	202	49	1:1
c2	-161.2	185	42	
Amorphous	**Chemical Shift (ppm)**	**Width (Hz)**	**%G/L**	**Ratio c1:c2**
a1	-163.1	3315	100	1.35:1
a2	-165.8	2462	100	

Figure 5.8. Shown is an example of the deconvolution scheme applied to a ^{19}F SSNMR spectrum. The scheme was applied to each spectrum of the six physical mixtures

The line shapes were determined to be 49 and 42% Gaussian. The two peaks used to deconvolute the amorphous form were at chemical shifts of -163.1 and -165.8 ppm with corresponding line widths of 3315 and 2462 Hz. Both amorphous peaks were fit with a 100% Gaussian line shape, and the ratio between the two peaks was 1.35:1. The ratio of amorphous peaks was maintained within the limitations of the Spinsight software to maintain the integrity of the deconvolution. The chemical shifts and line widths were controlled within 0.05 ppm and 5 Hz, respectively. The assumption was made that these deconvolution parameters did not change. It is possible that line widths might be affected by the dilution of the amorphous material in the crystalline material. Barich *et al.* have studied the effects of dilution of ibuprofen in excipients that cause anisotropic bulk magnetic susceptibility (ABMS).[20] ABMS produces line broadening due to changes in the local electronic environment. ^{19}F SSNMR line widths of the different forms of triamcinolone have not been fully investigated; therefore, the line widths are assumed to be constant, with respect to the bulk forms, throughout all physical mixtures.

The deconvolution procedure provided peak areas for the three subtraction spectra, and the **QTC** spectrum for each of the six physical mixtures. Because of the acquisition and subtraction conditions, quantitation was not straightforward. For example, a deconvoluted amorphous area of the **QL** subtraction spectrum was obtained, yet the component spectra of **QL** were acquired using non-quantitative conditions. The amorphous area measured is less than the representative amount of amorphous drug in the mixture. Table 5.2 can be used to account for the percent of

Table 5.2. The percent of crystalline (%C) and amorphous (%A) material was calculated for the individual component spectra and the spectral subtraction based on the relaxation profiles for the amorphous and crystalline forms. The correction factor is used to achieve 100% of the amorphous intensity.

	Component Spectra		Subtraction	Correction Factor
	8-s	**16-s**	**2*(8s)-16s**	
QT1 (%C)	7.34	14.1	0.538	
QT1 (%A)	100	100	100	
	8-s	**16-s**	**1.927*(8s)-16s**	
QT2 (%C)	7.34	14.1	0	
QT2 (%A)	100	100	92.7	1.08
	2-s	**4-s**	**2*(2s)-4s**	
QL (%C)	1.89	3.74	0	
QL (%A)	81.1	96.4	65.8	1.52

the total amorphous and crystalline area in each sample. For the case of the three subtractions listed, the amorphous form should be 100%. The crystalline form is suppressed, and will have a much lower percentage.

Using the relaxation profiles for the two forms in Figure 5.1, the relative intensity of each form was determined for each component spectrum. For the **QT1** subtraction, the amorphous form was completely relaxed during the acquisition of each of the component spectra yielding 100% amorphous intensity. Because the crystalline ^{19}F T_1 time was much longer than the pulse delays used for the component spectra, the two component spectra contained 7.3 and 14% of the total crystalline signal. When the difference-NMR technique was applied for the **QT1** subtraction, there was a calculated residual crystalline signal (0.54%) remaining, and 100% of the total amorphous signal. The **QT2** subtraction spectrum was performed to adjust for the residual crystalline signal. A coefficient of 1.927 was used for the **QT2** subtraction to mathematically eliminate the residual crystalline signal. During the subtraction, the resulting %A was less than 100%. The deconvoluted areas of the amorphous peaks were multiplied by a correction factor of 1.08 to account for the loss in amorphous signal.

The **QL** component spectra were acquired with conditions that did not allow full relaxation of either solid form. According to the relaxation profile, the relative percentages for the amorphous form were less than 100 for both the 2-s and 4-s component spectra. Even though the amorphous form was not fully relaxed, quantitation was performed. Based on the measured 1.2-s ^{19}F T_1 time, the amorphous

signal observed in each component spectrum was calculated. The 2-s component spectrum had 81.1% of the total amorphous signal remaining, and the 4-s component spectrum had 96.4% of the signal. After performing the **QL** difference-NMR subtraction, only 65.8% of the total amorphous signal remained. The deconvoluted areas were multiplied by a correction factor of 1.52 to account for the loss in signal.

Last, the sideband areas needed to be calculated to finalize the quantitative amorphous signal. If the crystalline and amorphous peaks lose the same percentage of signal to their sidebands, the sideband areas can be ignored. The sideband areas were deconvoluted for the pure amorphous and crystalline forms. The spinning sidebands of the amorphous peak represented 7.7% of the total amorphous signal, whereas, the sidebands of the crystalline peaks represented 14.3% of the crystalline signal. Because of the difference, the area values need to be adjusted. After the corrections for magnetization for the subtractions, another coefficient (1.08) was multiplied to the amorphous area in each of the three subtractions to account for the amorphous signal lost to the spinning sidebands. Thus far, the deconvolutions and mathematical adjustments have provided a quantitative value for the amorphous form but not the crystalline.

The difference-NMR subtractions were performed to obtain a quantitative value for the amorphous form. The **QTC** spectrum for each physical mixture was acquired to determine the quantitative value for the crystalline form. Similar to the amorphous form, the deconvoluted area was multiplied by an adjustment factor (1.17) to account for the signal lost to the spinning sideband intensity. Before a quantitative

value can be obtained for the physical mixtures, one final correction was made. As mentioned previously, the **QTC** spectrum allowed time for full relaxation of all forms, specifically the crystalline form. The intensity of a spectrum is directly proportional to the number of scans acquired, and the amorphous and crystalline peak areas were collected with different scan counts. The deconvoluted peak areas of the **QTC** spectrum were multiplied by the ratio of scans used in acquiring the component spectra and the **QTC** spectrum. For example, if 1024 scans were used to acquire the component spectra, and four scans were used to acquire the **QTC** spectrum, then the area of the crystalline peaks in the **QTC** spectrum would be multiplied by 256 to account for the difference in relative signal.

Table 5.3 lists the quantitation data for the six physical mixtures of the amorphous and crystalline forms of triamcinolone. The (measured) wt% by SSNMR spectroscopy and (known) wt% by mass values in Table 5.3 agree well for each physical mixture. Quantitative values were calculated for all six physical mixtures using each of the three subtraction techniques. At the 0.1% the amorphous signal present in the **QT1** and **QT2** subtraction spectra was so low that only the **QL** subtraction data were presented. The three subtractions agree well with each other.

The error for each physical mixture could arise from a variety of places. The physical mixtures were prepared with amorphous and crystalline standards. The standards could be less than 100% pure. The particle size of each form could contribute to less than homogenous mixing. When collecting the data, the component spectra were collected in series. If probe tuning fluctuates or the probe arcs, each

Table 5.3. Quantitation of the six physical mixtures using three subtractions of the difference-NMR technique: **QT1**, **QT2**, and **QL**.

Physical Mixture	Diff. NMR Subtraction	A1 and A2 Peak Areas	C1 and C2 Peak Areas (QTC)	Wt% by SSNMR	Wt% by Mass	Diff. Abs.
45%	QT1	4024	5510	42.2	45.1	2.9
	QT2	4014	5510	42.1	45.1	3.0
	QL	4266	5510	43.6	45.1	1.5
10%	QT1	755	7366	9.3	10.0	0.7
	QT2	754	7366	9.3	10.0	0.7
	QL	760	7366	9.3	10.0	0.6
5%	QT1	433	8835	4.7	5.0	0.3
	QT2	409	8835	4.4	5.0	0.6
	QL	400	8835	4.3	5.0	0.7
1%	QT1	429	33541	1.3	1.0	0.3
	QT2	397	33541	1.2	1.0	0.2
	QL	459	33541	1.3	1.0	0.4
0.5%	QT1	161	17619	0.9	0.5	0.4
	QT2	105	17619	0.6	0.5	0.1
	QL	101	17619	0.6	0.5	0.1
0.1%	QL	169	66779	0.3	0.1	0.2

component spectrum would be affected differently. Prior to acquisition, 20 dummy pulses were applied to each component spectrum in an attempt to achieve a common magnetic equilibrium for the individual component spectra. The dummy scans were pulsed at the pulse delay time values, so each component spectrum used a dummy pulse with a different delay. The delay could contribute to changes in the observed crystalline signal. The ^{19}F T_1 times for both forms are relied upon heavily in acquisition and mathematical adjustments made to the deconvoluted peak areas. If the relaxation rates were not measured precisely or changed during the experiments, the effects could contribute to error in the quantitation values. Error could also occur during deconvolution. The deconvolution scheme was heavily restrictive, and in some cases left significant residual signal. Error occurs at some level in all of the steps of quantitation. Each spectrum was only acquired once. A change in one of the four scans of the **QTC** spectrum could result in distorted crystalline peak areas. Despite the potential error, the wt% by SSNMR and wt% by mass agree well.

Figure 5.9 shows the plot of amorphous wt% by SSNMR versus the amorphous wt% by mass for the **QL** subtraction data. The trend line has a R^2 value near one, a slope less than 1, and a small negative y-intercept. The slope indicates that in most cases the wt% by SSNMR is underestimating the amorphous content or overestimating the crystalline content. The value of the intercept (0.067) is on the order of the lowest value intended to quantitate. The quantitation numbers are easier to appreciate when presented with the ^{19}F SSNMR subtraction spectra. Unlike many techniques used to quantitate amorphous pharmaceuticals, ^{19}F SSNMR allows us to

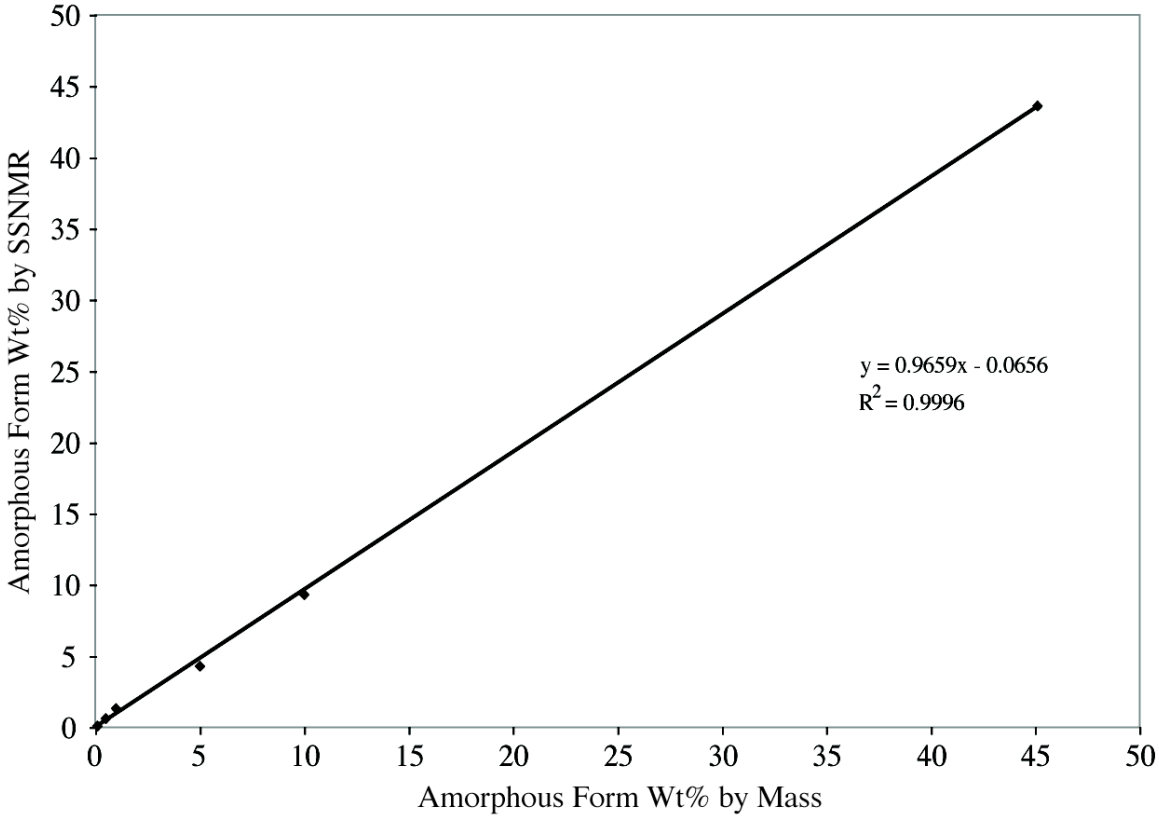

Figure 5.9. Plot of wt% by SSNMR spectroscopy versus wt% by mass of physical mixtures of amorphous and crystalline triamcinolone using the **QL** subtraction.

observe the amorphous signal at low levels. Figure 5.10 displays the ^{19}F SSNMR spectra of the **QT1** and **QL** subtractions for the six physical mixtures. The **QT1** subtraction series is on the left, and the **QL** subtraction series is on the right. In each spectrum, polymorph B and the amorphous form of triamcinolone should be present. For the **QT1** series, amorphous signal is visible down to the 1% (Figure 5.10d) level and quantitated to the 0.5% level.

In the **QL** series, amorphous signal is visible to the 0.5% (Figure 5.10e) level and quantitated to the 0.1% level. In the corresponding spectra for each mixture, the **QL** spectrum has a lower SNR. This is expected because shorter pulse delays were used to acquire the component spectra. The **QL** subtractions of the 1% and 0.5% physical mixtures exhibit phasing anomalies. Each subtraction was performed several times with different phasing conditions of the component spectra. In all of the spectra, a ^{19}F signal from the Teflon O-rings is visible near -121 ppm, and its spinning sideband (-154 ppm) is visible in a few of the subtraction spectra. The peaks from Teflon do not interfere with quantitation. No peaks are present from polymorph A, indicating that the mixtures were physically stable throughout all experiments.

The difference-NMR technique is powerful in suppressing the long-relaxing crystalline component while still being quantitative. Adjusting NMR parameters is a valuable tool for solid-state form quantitation. In Figure 5.11, the ^{19}F SSNMR spectra for the 5% and 0.5% mixtures illustrate how changing the pulse delay and using the difference-NMR technique can suppress the crystalline signal. Each spectrum in the series was acquired on the same sample. Figure 5.11a is the **QTC**

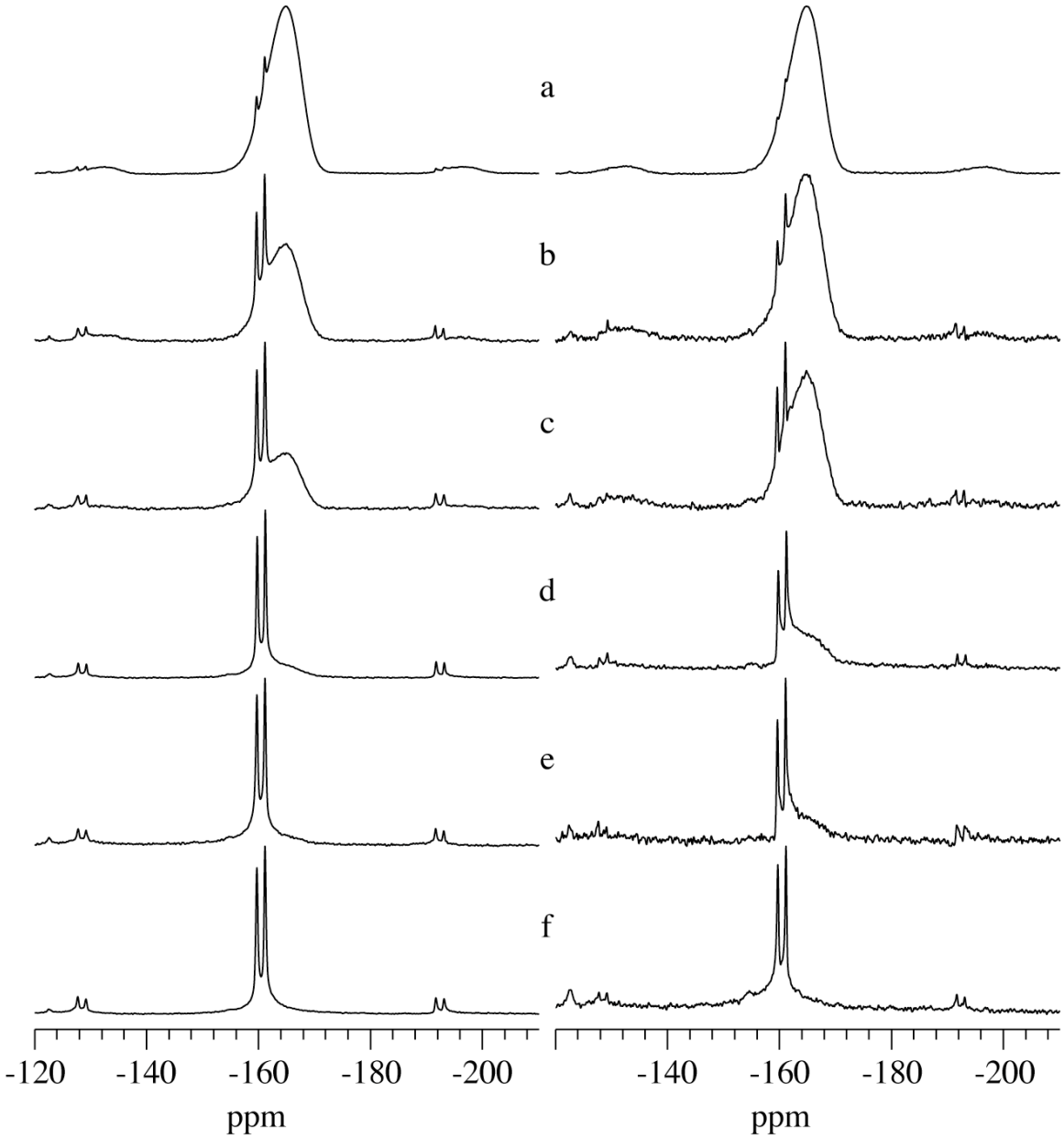

Figure 5.10. ^{19}F SSNMR spectra for the **QT1** and **QL** subtractions of the six physical mixtures. The spectral series on the left consists of the **QT1** subtraction spectra, and the series on the right consists of the **QL** subtraction spectrum for each physical mixture: a) 45%, b) 10%, c) 5%, d) 1%, e) 0.5%, and f) 0.1%.

spectrum of the 5% sample acquired with 4 scans and a 600-s pulse delay. Polymorph B is visible, while the amorphous signal is not. If the presence of amorphous material were not suspected, the SSNMR operator would typically pulse the sample at approximately the T_1 time. Under these conditions, amorphous signal would not be observed. Figure 5.11b and c are the spectra acquired with 16-s and 2-s pulse delays. Simply shortening the pulse delay suppresses the crystalline signal enough to see the amorphous signal. Figure 5.11d and e are the **QT1** and **QL** difference-NMR spectra for the 5% mixture. The amorphous signal becomes even more prevalent. Figure 5.11c and d appear to have similar amorphous content, yet the spectrum in Figure 5.11d is traditionally thought to be quantitative. The spectrum in Figure 5.11c was acquired with a 2-s pulse delay (less than five times the T_1). In the 0.5% series, Figure 5.11f-j, no amorphous signal is visible until the **QL** subtraction spectrum (Figure 5.11j). The **QT2** spectrum is not displayed; however, it exhibits small gains in crystalline suppression.

There is no indication which difference-NMR subtraction (**QT1**, **QT2**, or **QL**) is the best at quantitating the amorphous form of triamcinolone. All three subtraction processes have similar absolute error. Due to the time-intensive nature of acquiring the data, the samples were only analyzed once. For future studies, a pulse sequence should be written that collects two scans at one pulse delay and one scan at twice the pulse delay 180° out of phase. The pulse sequence can acquire the difference-NMR data and eliminate the collection of the individual component spectra.

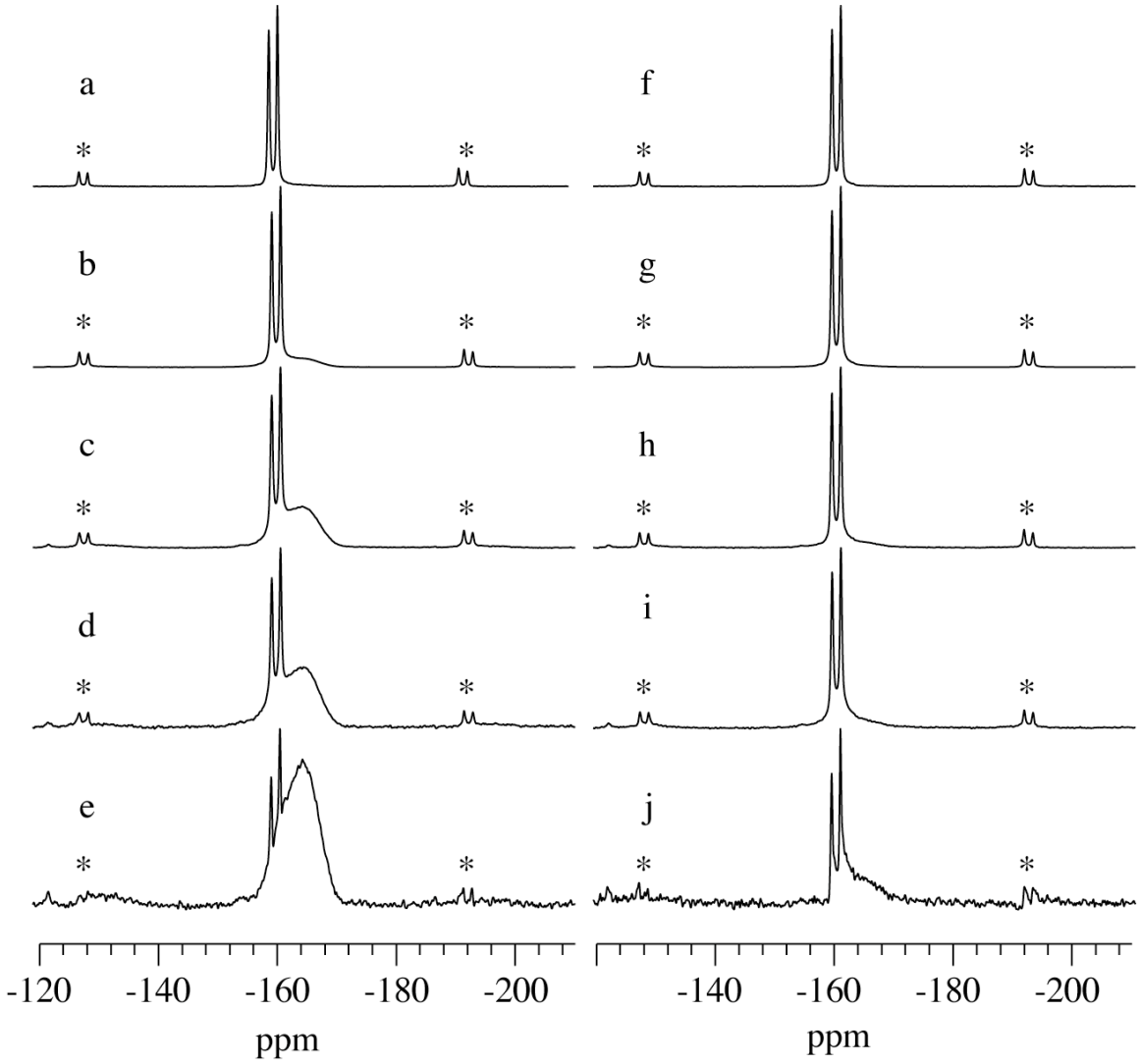

Figure 5.11. Increased expressions of amorphous triamcinolone in the 5% and 0.5% physical mixtures acquired with different parameters. a-e are spectra of the 5% mixture and f-j are spectra of the 0.5% mixture. a) 600-s pulse delay, b) 16-s pulse delay, c) 2-s pulse delay, d) difference-NMR subtraction [2*(8s)-16s], and e) [(2*(2s)-4s]. The 0.5% physical mixture collected with a f) 600-s pulse delay, g) 16-s pulse delay, h) 2-s pulse delay, and the difference-NMR subtractions i) [(2*8s)-(16s)] and j) [(2*(2s)-4s]. Asterisks denote spinning sidebands.

The pulse sequence would minimize the affects of fluctuations of spectrometer operating conditions, eliminate differences in the initial magnetic equilibrium of the component spectra, and any manual phasing errors before spectral subtraction.

5.4 Conclusions

Quantitating amorphous materials is extremely difficult and requires the application of many different techniques depending on the drug substance. When applicable, ^{19}F SSNMR spectroscopy is a powerful addition to the list of techniques.

From the presented work, ^{19}F SSNMR can distinguish and monitor four different forms (two crystalline, one amorphous and one hydrate) of triamcinolone. The ability to simultaneously monitor multiple forms is extremely valuable in understanding the physical nature of a drug substance and product. Mixtures of the crystalline and amorphous forms of the drug can be observed without much difficulty. As the percentage of amorphous content drops, the SSNMR operator can alter parameters to selectively express different components in the sample. Here, the difference-NMR technique was applied and allowed detection of amorphous levels to 0.5%. Potentially, the limits of detection and quantitation could be further decreased with shorter pulse delays, more scans, and a third component in the difference-NMR subtraction. With careful monitoring of the sample and NMR relaxation, reliable quantitative spectra can be obtained for crystalline and amorphous materials.

Although the studies performed here only looked at drug substance, in theory,

the technique can be applied to a formulation without much additional effort. The addition of excipients should not affect the ^{19}F SSNMR spectrum. Of all the techniques currently used to investigate the amorphous state, ^{19}F SSNMR is unique because detection in a formulation should only differ from a physical mixture in the amount of time required to acquire a spectrum. ^{19}F SSNMR proves to be a very powerful technique in detecting low levels of amorphous impurity.

5.5 References

1. Shah B, Kakumanu VK, Bansal AK 2006. Analytical techniques for quantification of amorphous/crystalline phases in pharmaceutical solids. Journal of Pharmaceutical Sciences 95(8):1641-1665.

2. Gustafsson C, Lennholm H, Iversen T, Nystrom C 1998. Comparison of solid-state NMR and isothermal microcalorimetry in the assessment of the amorphous component of lactose. International Journal of Pharmaceutics 174(1-2):243-252.

3. Offerdahl TJ, Salsbury JS, Dong Z, Grant DJW, Schroeder SA, Prakash I, Gorman EM, Barich DH, Munson EJ 2005. Quantitation of crystalline and amorphous forms of anhydrous neotame using ^{13}C CPMAS NMR spectroscopy. Journal of Pharmaceutical Sciences 94(12):2591-2605.

4. Venkatesh GM, Barnett ME, Owusu-Fordjour C, Galop M 2001. Detection of low levels of the amorphous phase in crystalline pharmaceutical materials by thermally stimulated current spectrometry. Pharmaceutical Research 18(1):98-103.

5. Saleki-Gerhardt A, Ahlneck C, Zografi G 1994. Assessment of disorder in crystalline solids. International Journal of Pharmaceutics 101(3):237-247.

6. Lefort R, De Gusseme A, Willart JF, Danede F, Descamps M 2004. Solid state NMR and DSC methods for quantifying the amorphous content in solid dosage forms: an application to ball-milling of trehalose. International Journal of Pharmaceutics 280(1-2):209-219.

7. Bruni G, Milanese C, Bellazzi G, Berbenni V, Cofrancesco P, Marini A, Villa M 2007. Quantification of drug amorphous fraction by DSC. Journal of Thermal Analysis and Calorimetry 89(3):761-766.

8. Lehto V-P, Tenho M, Vaehae-Heikkilae K, Harjunen P, Paeaellysaho M, Vaelisaari J, Niemelae P, Jaervinen K 2006. The comparison of seven different methods to quantify the amorphous content of spray dried lactose. Powder Technology 167(2):85-93.

9. Craig DQ, Barsnes M, Royall PG, Kett VL 2000. An evaluation of the use of modulated temperature DSC as a means of assessing the relaxation behaviour of amorphous lactose. Pharmaceutical research 17(6):696-700.

10. Saunders M, Podluii K, Shergill S, Buckton G, Royall P 2004. The potential of high speed DSC (hyper-DSC) for the detection and quantification of small amounts of amorphous content in predominantly crystalline samples. International Journals of Pharmaceutics 274(1-2):35-40.

11. Guinot S, Leveiller F 1999. The use of MTDSC to assess the amorphous phase content of a micronized drug substance. International Journal of Pharmaceutics 192(1):63-75.

12. Byrn SR, Sutton PA, Tobias B, Frye J, Main P 1988. Crystal structure, solid-state NMR spectra, and oxygen reactivity of five crystal forms of prednisolone tert-butylacetate. Journal of the American Chemical Society 110(5):1609-1614.

13. Offerdahl TJ, Salsbury JS, Dong Z, Grant DJW, Schroeder SA, Prakash I, Gorman EM, Barich DH, Munson EJ 2005. Quantitation of crystalline and amorphous forms of anhydrous neotame using ^{13}C CPMAS NMR spectroscopy. Journal of Pharmaceutical Sciences 94(12):2591-2605.

14. Harris RK. 1989. Nuclear Magnetic Resonance Spectroscopy. 4th ed., Essex, England: Longman Scientific & Technical. p 260.

15. Isbester PK. 1999. Development of an Isolated Flow Variable-Temperature Magic-Angle Spinning (MAS) Nuclear Magnetic Resonance (NMR) Probe for Heterogeneous Catalysis Studies and High-Temperature High-Speed ^{19}F MAS NMR Techniques Applied to Fluoropolymers. Department of Chemistry, ed., Minneapolis: The University of Minnesota. p 179.

16. Park BK, Kitteringham NR, O'Neill PM 2001. Metabolism of fluorine-containing drugs. Annual Review of Pharmacology and Toxicology 41:443-470.

17. Hagmann WK 2008. The Many Roles for Fluorine in Medicinal Chemistry. Journal of Medicinal Chemistry 51(15):4359-4369.

18. Muller K, Faeh C, Diederich F 2007. Fluorine in pharmaceuticals: looking beyond intuition. Science 317(5846):1881-1886.

19. Harris DJ, de Azevedo ER, Bonagamba TJ 2003. Difference-NMR techniques for selection of components on the basis of relaxation times. Journal of Magnetic Resonance 162(1):67-73.

20. Barich Dewey H, Davis Jacob M, Schieber Loren J, Zell Mark T, Munson Eric J 2006. Investigation of solid-state NMR line widths of ibuprofen in drug formulations. Journal of Pharmaceutical Sciences 95(7):1586-1594.

Chapter 6

Effect of Gaseous Oxygen on Solid-State NMR Relaxation Times

6.1 Introduction

6.1.1 Background

In Chapter 5, physical mixtures of crystalline and amorphous forms of triamcinolone were quantitated with ^{19}F solid-state NMR spectroscopy (SSNMR). The physical mixtures of triamcinolone were quantitated by spectral subtraction of two component spectra using the difference-NMR technique. The ability to obtain accurate quantitation data depends in part upon knowing the NMR relaxation times of the components being studied. As mentioned in Chapter 2, there are two relaxation values that need to be accounted for when using cross polarization between two nuclei.[1] In the case of triamcinolone, the NMR experiments were performed with a single-pulse pulse sequence that directly excited the ^{19}F nucleus. Direct polarization simplified the quantitation method because it was unnecessary to account for the two cross-polarization dependent relaxation times. The only relaxation time values to consider were the ^{19}F spin-lattice relaxation times (T_1) of the crystalline and amorphous components.

The difference-NMR technique is based on the assumption that NMR relaxation times are known for each component in the sample. The component spectra of the difference-NMR technique for each physical mixture of triamcinolone were collected over the course of several hours to several days depending on the percentage of amorphous content. It was necessary to ensure that the ^{19}F T_1 times of the crystalline and amorphous forms remained constant throughout the time course of

the experiments. To demonstrate the ^{19}F T_1 times remained constant, the T_1 times were measured on the pure amorphous standard every two hours over a period of 18 hrs. The relaxation time started at ~3 s and increased to ~19 s. Upon sample removal from the NMR probe and reinsertion, the relaxation time returned to ~3 s.

In magic-angle spinning experiments, the spin-lattice relaxation time of a sample rarely changes in the spectrometer. If an increase in relaxation time occurred, the increase is typically non-reversible. Experiments were performed on several batches of differently prepared (cryoground and spray-dried) amorphous triamcinolone and with very similar relaxation time results. The ^{19}F T_1 times increased 3-6 times their original value over a period of 10-20 hours spinning in the magnet. In all cases, the relaxation returned to its original value upon removal from the spectrometer and reinsertion. Before the mixtures of triamcinolone could be quantitated, the mechanism for relaxation change must be examined and then controlled.

6.1.2 Relaxation time changes

NMR relaxation times for crystalline organic solids are often considered to be constant, yet they can change based on processing conditions, thermal history, sample healing, and the presence of NMR relaxation agents. The following is a review of how relaxation times can change based upon processing and environmental conditions.

Lubach *et al.* studied the effects of processing (grinding, lyophilizing, spray drying, and compaction) on the ^{1}H T_1 times of crystalline lactose.[2] The ^{1}H T_1 time was measured, and a ^{13}C SSNMR spectrum was collected for each sample. Compaction of lactose resulted in a three-fold reduction in the ^{1}H T_1 time (243 s to 79 s) from the bulk material. Similarly, cryogrinding lactose for 2 min reduced the ^{1}H T_1 time an order of magnitude (243 s to 23 s). In both cases, there were no form changes readily apparent in the NMR spectra. The researchers suggested that the reduction in T_1 times were due to the increase in several factors that create sites of high mobility: reduction in particle size, introduction of crystal defect sites, and the generation of amorphous material. The ^{1}H T_1 time for a lactose sample cryoground for 60 min was measured over 30 days, and the relaxation time increased from 0.77 s after initially being ground to ~6 s after 30 days with little spectral evidence of recrystallization. The increase in relaxation time was attributed to sample healing.

More recently, unpublished results from our laboratory have shown that the relaxation time for gabapentin changes drastically when the material is processed. The ^{1}H T_1 time of the bulk material was 134 s. After being cryoground for 10 minutes the ^{1}H T_1 time decreased to 7.3 s with no spectral evidence of a solid-state form change. Preliminary research has been performed to study the ^{1}H T_1 times of aspirin after being cryoground for various lengths of time. When cryoground for 10 minutes, the ^{1}H T_1 time dropped from 57 s to 14 s. In the absence of excipients, aspirin is known to remain crystalline. Without amorphous material present in

samples of cryoground aspirin, the decrease in relaxation time was attributed to reduction in particle size and/or an increase in crystal defects.

Although the spin-lattice relaxation times change, the mechanism for how they change can help understand the physical nature of the sample as well as the presence of any additional species (e.g. water). Rigid crystalline solids with no relaxation sinks (e.g. methyl groups) lack the molecular mobility to necessary to transfer energy to the surface and have long spin-lattice relaxation times. When highly mobile regions, such as methyl groups, are present, the magnetization can be transferred via ^{1}H spin diffusion. These regions of increased molecular mobility act as sinks for more efficient relaxation of the entire sample. Cryogrinding lactose reduces particle size while generating crystal defects and amorphous material, all of which can increase the efficiency of spin diffusion. Amorphous material has increased molecular mobility as compared to the crystalline form, and typically has shorter relaxation times.

The drastic changes in the ^{19}F T_1 times of amorphous triamcinolone were a significant cause for concern, as they could have a dramatic impact upon the reliability of the quantitation methods used in Chapter 5. The following sections will present experiments which were designed to eliminate potential changes in relaxation time during quantitation experiments and demonstrate that changes in the partial pressure of oxygen can affect the relaxation rate of several representative pharmaceutical materials.

6.2 Experimental

6.2.1 Materials

Triamcinolone was obtained from Sigma Aldrich (St. Louis, MO) and cryoground and spray dried by the following procedures. Triamcinolone was also crystallized from methanol. Dexamethasone was purchased from Alfa Aesar (Ward Hill, MA) and analyzed without any further processing. Dextran was provided from the laboratory inventory of Dr. Ales Medek (Pfizer Inc., Groton, CT). Acetyl salicylic acid (aspirin) was obtained from Sigma Aldrich (St. Louis, MO). Aspirin was used as received and cryoground for 20 mintes.

6.2.2 Sample preparation and handling

Cryogrinding was performed using a Spex Certiprep 6750 Cryo mill. Thirty milling cycles were performed for triamcinolone and 10 cycles for aspirin with each cycle consisting of two minutes of grinding and two minutes cooling. Prior to the initiation of grinding, the samples were pre-cooled for 15 minutes. After the cryogrinding, the samples were exposed to a vacuum for 45 minutes to allow a return to ambient temperature before the cryovial was opened. If the cryovial was opened too soon after grinding, the sample could still be cold and be at risk of condensation.

Spray drying of triamcinolone was performed on a custom-built spray dryer (Bend Research, Bend, OR). Approximately 200 mg of material was dissolved in approximately 12 mL (10g) of warm methanol for an approximate concentration of

2% (wt/w). A 1.3-mL/min injection rate was used with an inlet temperature of 70 °C The spray-dried material was collected on a 110 mm diameter Whatman filter paper. Harvested product yields were between 70-80%. All solid-state analysis was performed by solid-state NMR spectroscopy.

Unless otherwise noted, triamcinolone, dexamethasone, and dextran were "deoxygenated" by spinning packed samples in the NMR probe at 15 kHz. The drive tips were opened and exposed to ambient oxygen conditions. When "oxygenated," the samples were packed in zirconia rotors and directly exposed to medical-grade compressed oxygen gas for one minute.

Aspirin was oxygenated by exposing the packed NMR rotor to compressed oxygen gas for one minute, then sealing the rotor with a Kel-F drive tip with two O-rings for a gas-tight seal. To deoxygenate, the sample-containing rotor (without endcap) was sealed in the anti-chamber of a glove box and cycled three times in the following manner: vacuum exposure for 10 minutes then nitrogen gas purge for one minute. The rotors were capped inside the glove box under positive nitrogen pressure.

6.2.3 Solid-state NMR spectroscopy

SSNMR data of triamcinolone, dexamethasone and dextran were collected on a Bruker Avance 500 NMR triple-resonance spectrometer (Billerica, MA) operating at 469.8 MHz for ^{19}F and 499.3 MHz for ^{1}H. Spectra were acquired using a Bruker 4-mm $^{1}H/^{19}F/X$ triple-resonance MAS probe. Samples were packed in zirconia rotors

and sealed with Vespel drive tips or a Vespel drive tip with two O-rings (Revolution NMR, Fort Collins, CO). Samples were spun at rates of 10-15 kHz. When low-temperature studies were performed, a Bruker BCU-Xtreme (Billerica, MA) chilling unit was used. Nitrogen gas was used for sample spinning, frame cooling, and low-temperature chilling. All samples acquired on the Bruker Avance 500 were referenced to a 1:1 water and trifluoroacetic acid (TFA) solution at -76.54 ppm. SSNMR data of triamcinolone were collected with $^{1}H/^{19}F$ cross-polarization and direct ^{19}F excitation. ^{19}F and ^{1}H relaxation data were collected primarily with saturation recovery, but inversion recovery was utilized at times for comparison. Relaxation data were collected with 8-11 increments and fit to a mono-exponential decay. For triamcinolone, dexamethasone, and dextran, the relaxation profiles were designed such that a relaxation measurement was made and then followed by the acquisition of the spectrum. The spectrum was collected with a combination of a long pulse delay and specific number of scans such that 2 hrs passed between relaxation measurements (e.g. 60 scans and a 120 s pulse delay).

The ^{13}C SSNMR spectra and ^{1}H T_1 relaxation times of aspirin were collected on a Chemagnetics CMX 300 spectrometer (Fort Collins, CO) operating at 298.7 MHz for ^{1}H and 75.1 MHz for ^{13}C. Samples were packed in custom-made 7-mm zirconia rotors and sealed with a Kel-F purchased from Revolution NMR (Fort Collins, CO). The rotors were open on one end, which was capped with a Kel-F drive tip with two o-rings also from Revolution NMR. The rotors were spun at 4 kHz and data was collected on a double-resonance $^{1}H/X$ probe outfitted with a module

purchased from Revolution NMR. ^{1}H relaxation measurements were made with a saturation recovery pulse sequence with Spinal 64 decoupling. Twenty increments (0.1 s to 350 s) were collected for each relaxation measurement.. Each increment was collected with a 3.4-μs 90° ^{1}H pulse, 512 acquisition points, and 12 acquisitions. The relaxation data was fit with a mono-exponential curve in the Spinsight software.

6.3 Results

6.3.1 Observation of changing NMR relaxation times

Prior to quantitation of the triamcinolone physical mixtures, the following experiments were performed on amorphous triamcinolone to understand the mechanism behind drastic changes in the ^{19}F T_1 times upon exposure to oxygen.

To test the constancy of the measured relaxation times, a sample of spray-dried amorphous triamcinolone was spun overnight and the ^{19}F T_1 time was measured every two hours. The relaxation measurements are plotted in Figure 6.1 and correspond to the initial relaxation profile. At the beginning of the profile, the ^{19}F T_1 time was 3.6 s. After 18 hrs spinning in the magnet at 15 kHz, the relaxation time increased to 19.5 s, more than 5 times its initially measured value. After approximately four hours, the ^{19}F T_1 time appeared to plateau. Based upon this initial observation, the most likely explanation is that the amorphous triamcinolone could have annealed in the NMR rotor due to the heat and pressure produced from spinning at 15 kHz, thereby resulting in a longer relaxation time.

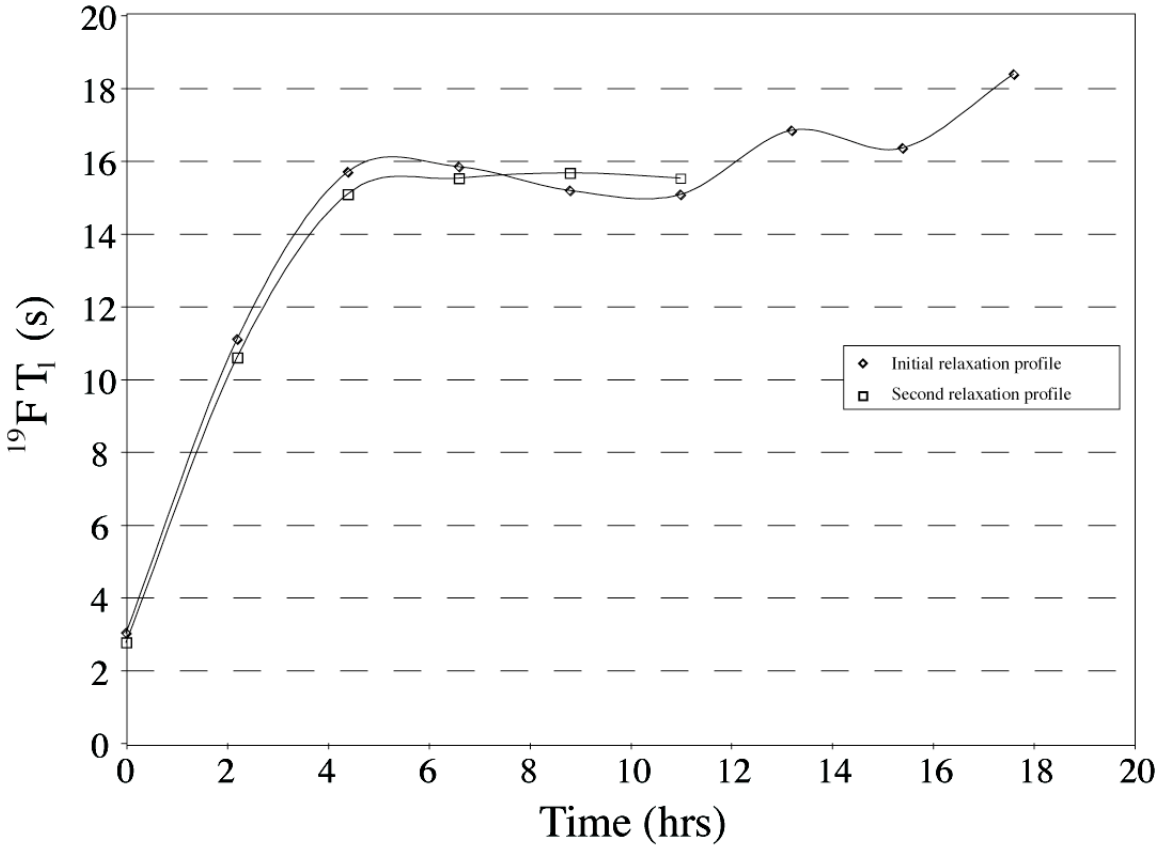

Figure 6.1. The ^{19}F T_1 time of amorphous triamcinolone was monitored over 18 hrs (initial relaxation profile). The ^{19}F T_1 times were measured again (second relaxation profile) a week later.

After acquiring the initial relaxation profile, the sample remained packed and was stored in a desiccator in a laboratory freezer. Several days later, the ^{19}F T_1 time of the same cryoground amorphous triamcinolone sample was measured a second time to determine if the relaxation time had changed. The ^{19}F T_1 time had decreased to 3.6 s. In Figure 6.1, a second relaxation profile followed a similar rise in relaxation time over the next 10 hrs. Typically, NMR relaxation times for a sample only increase with a change in solid form, hydration, or some material processing (e.g. grinding or compression). The initial relaxation time point, the rate of increase in relaxation times, and the maxima reached (~16 s) were remarkably similar for both relaxation profiles. Shown in Figure 6.2 are the ^{19}F SSNMR spectra collected after the 3.6 s and 18 s relaxation measurements. There were no significant changes in chemical shift, line width, or peak shape. The ^{1}H T_1 time was monitored as well and increased from 1.1 s to 1.8 s, an increase of ~65%. Although both T_1 times increased, the relative increase of T_1 times for ^{1}H and ^{19}F nuclei are drastically different. In the initial relaxation profile there was a slight oscillation after the relaxation time had plateaued.

There are several potential causes of the reversible changes in ^{1}H and ^{19}F relaxation times. Some of these include changes in water content, pressure induced from spinning, temperature (between time points and/or during NMR data acquisition), residual solvent (methanol) from spray drying, and paramagnetic oxygen. Before determining which of these potential causes resulted in the changing relaxation times, the possible mechanisms are discussed below.

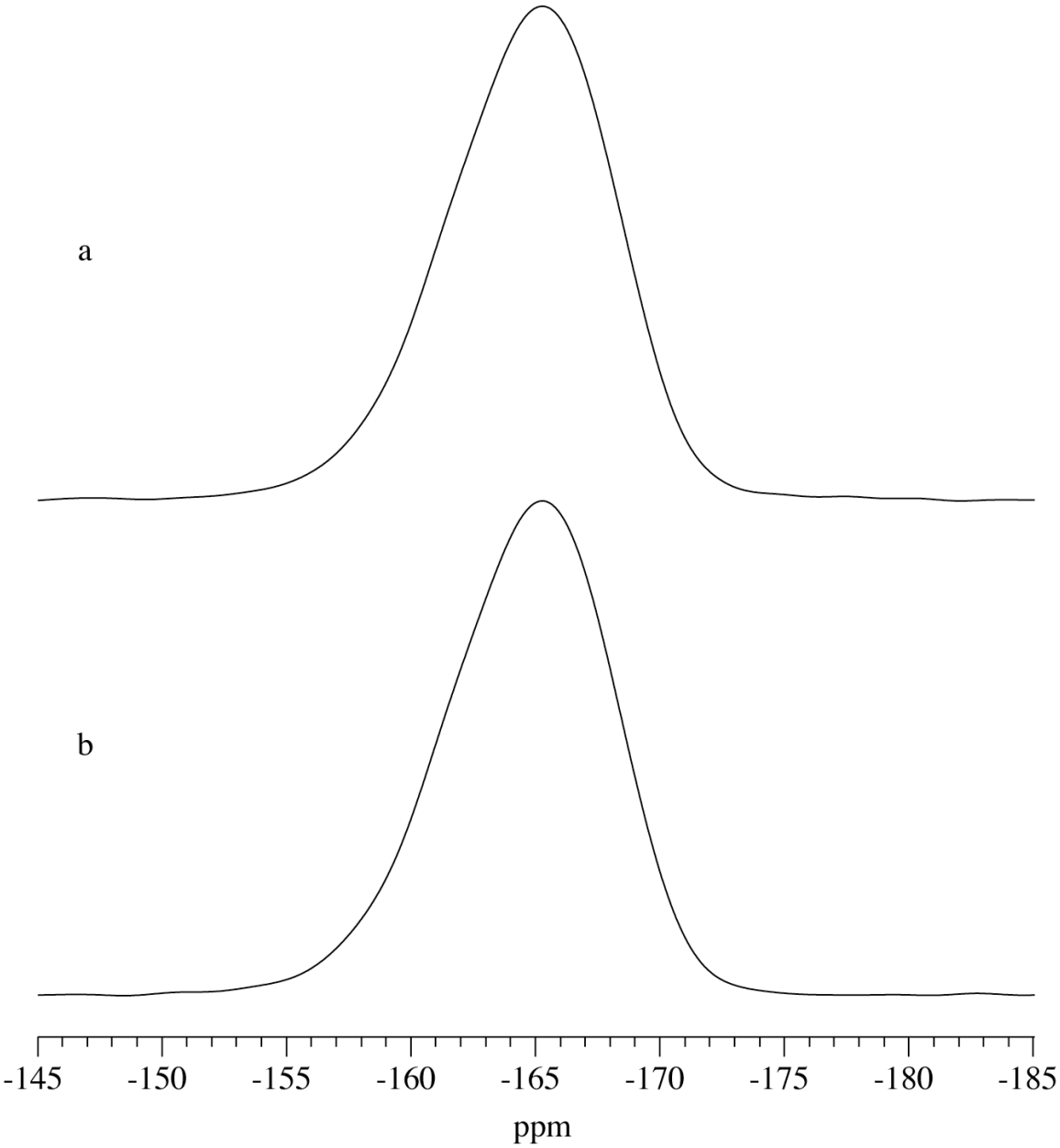

Figure 6.2. Expansion on the single peak in the ^{19}F SSNMR spectra of amorphous triamcinolone, when the measured ^{19}F T_1 time is a) 3.6 s and b) 19.5 s.

It is possible that water content and residual methanol could affect relaxation times by influencing the mobility of the molecules in the amorphous state. When a sample spins at high speeds (~15 kHz), surface water could be expelled from the surface of the sample, effectively drying the sample, yet the water could still be present in the rotor. Hypothetically, when the sample stops spinning, water could return to the surface of triamcinolone. The presence of water would provide greater mobility, which generally corresponds to shorter T_1 times. This hypothesis corresponds to the trends in the data.

The pressure induced from sample spinning could cause changes in relaxation. Barich et al. observed changes in SSNMR line widths of ibuprofen after the NMR samples were packed under different pressures.[3] Compaction could potentially reduce the void space between two molecules. The magnetic susceptibility of air could be lower than that of triamcinolone. The additional magnetic susceptibility due to the increase in density caused ibuprofen lines to broaden. The increased pressure from spinning could compact the sample and increase the spin-lattice relaxation time. After the sample spinning stopped, the material could possibly decompress and relaxation time would decrease.

The sample temperature could also play a role in the changing relaxation times, as temperature is directly correlated with molecular mobility. The sample temperature increases due to spinning over the course of the relaxation profile. In order for the spin-lattice relaxation time to increase as temperature increase, the

extreme narrowing conditions must hold. Also known as the fast-motional regime, extreme narrowing conditions apply when the correlation time is faster than the nuclear precession rate. As the sample warms due to spinning, the relaxation time will rise. Typically solid-state samples are in the slow motional regime, where T_1 time decreases with increasing temperature.

Lastly, oxygen gas has been widely used as a paramagnetic relaxation agent in solution NMR spectroscopy. Prosser et al. have used oxygen to probe membrane immersion depths with solution ^{19}F NMR spectroscopy.[4-6] Oxygen partitions into membranes with increasing concentration at greater depths. The immersion of a fluorinated detergents was determined by changes in relaxation times for individual fluorine groups. The relaxation time of the deepest penetrating groups were the shortest due to an increased exposure to oxygen. Other researchers studied the same effect on ^{1}H spin-lattice relaxation times of aromatic polymers in the solid state.[7-11] Observations were made that adsorption of paramagnetic oxygen on aromatic polymers significantly decreased ^{1}H T_1 times.[7,10] Capitani et al. studied ^{1}H spin-lattice relaxation changes of polymers in solids without magic-angle spinning.[7-11] In one study, the amount of oxygen adsorbed was different between polymorphs and reportedly higher in amorphous fractions of syndiotactic polystyrene.[9] In the case of poly(phenylene oxide) or poly(1-oxy-2-phenyltrimethylene), ^{1}H T_1 times differed up to four orders of magnitude between oxygenated and deoxygenated samples.[9]

Oxygen is uncharged and demonstrates no preference for specific nuclei.[4] In the solid state, oxygen has displayed preferential adsorption to aromatic rings.[7,10]

Oxygen has also been observed to differentially adsorb to amorphous and crystalline domains of polymers.[7] Paramagnetic oxygen has been studied using solution ^{19}F NMR spectroscopy and static ^{1}H solid-state NMR spectroscopy. However, research has not been reported on the effects of oxygen on spin-lattice relaxation times in magic-angle spinning experiments. Additionally, the effect has not been observed or studied for small-molecule solid-state pharmaceuticals. In the case of triamcinolone, oxygen gas could enter the rotor while packing under ambient conditions, and nitrogen gas could purge the sample during spinning elevating the relaxation time. The proceeding studies were designed to examine each potential cause.

6.3.2 Testing the cause of relaxation change

Spray-dried amorphous triamcinolone was used to probe the origin of the change in relaxation. First, the ^{19}F T_1 time was measured every two hours over a 15-hour time period while spinning at 15 kHz, and a similar relaxation profile was produced a third time. As illustrated in Figure 6.3, the ^{19}F T_1 time was initially 3.6 s. The relaxation time increased drastically over the following eight hours. After eight hours, the relaxation continued to increase but at a much slower rate. At 15 hours, the ^{19}F T_1 time was approximately 20 s, and appeared to still be increasing. After the relaxation increase was observed, the following tests were performed to determine which factor caused the ^{19}F T_1 value to decrease below 5 s.

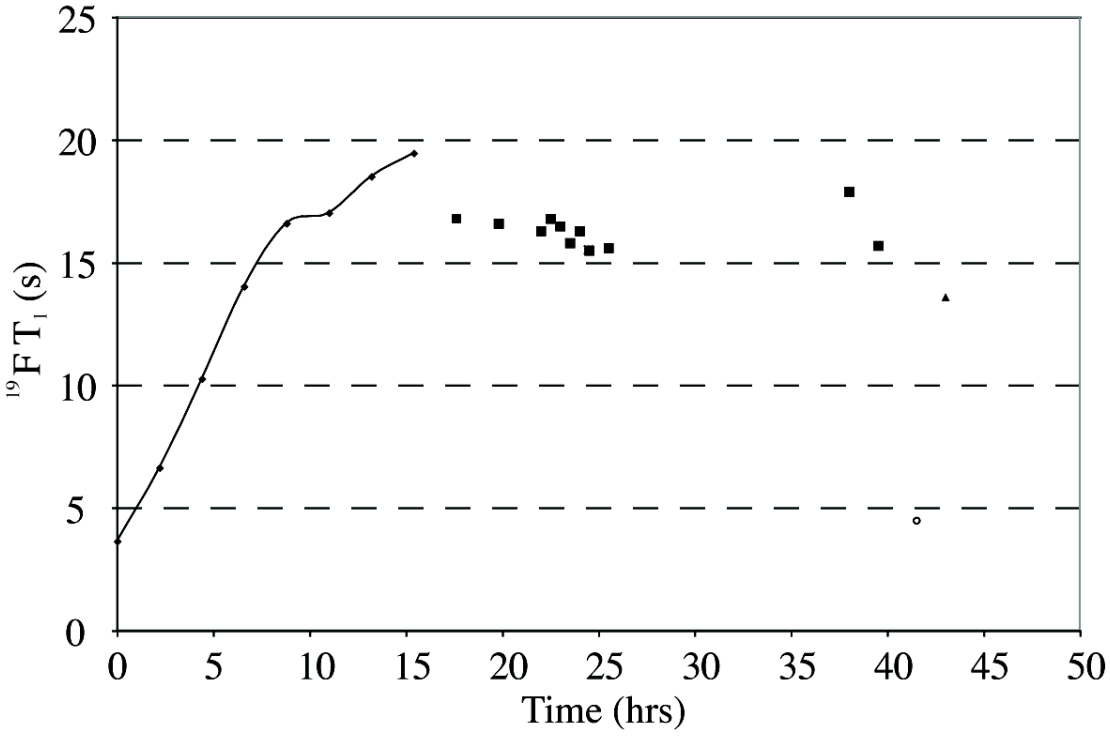

^{19}F T$_1$ (s)	Time (hrs)	Probe Temp. (K)	Storage Temp. (K)	Stored	Spinning
■ 16.6	16	260	260	Probe	15 kHz
■ 16.8	17	260	260	Probe	15 kHz
■ 16.6	18	260	260	Probe	15 kHz
■ 16.6	19	260	260	Probe	15 kHz
■ 16.7	20	260	260	Probe	15 kHz
■ 16.3	20.5	270	270	Probe	15 kHz
■ 16.8	21	270	270	Probe	15 kHz
■ 16.5	21.5	280	280	Probe	15 kHz
■ 15.8	22	290	290	Probe	15 kHz
■ 16.3	22.5	290	290	Probe	15 kHz
■ 15.5	23	290	Ambient	Above Magnet	No
■ 15.6	24	290	Ambient	Above Magnet	No
■ 17.9	36.5	290	Ambient	Above Magnet	No
■ 15.7	38	290	Ambient	Above Magnet	No
○ 4.5	40	290	265	Freezer	No
▲ 13.6	41.5	290	290	Probe	15 kHz

Figure 6.3. Plot of ^{19}F T_1 relaxation time versus time after being exposed to changes in several variables to determine the cause of the relaxation drop. The table describes the physical conditions that the sample was exposed to during collection.

In Figure 6.3, a table and graph show how specific environmental variables were tested that could have been attributed to the reduction in relaxation. The factors adjusted include sample temperature during acquisition, sample temperature during storage (between time point measurements), location of the sample in between relaxation measurements, and spinning between acquisitions. The effects of oxygen gas on relaxation time were not probed during these experiments. After the relaxation was profiled, the sample temperature was lowered to 260 K. Upon cooling, the relaxation time dropped from 19.5 s to 16.6 s. If the NMR conditions are in the fast-motional regime, spin-lattice relaxation time will drop when lowering the temperature. However, it is more likely that amorphous triamcinolone is in the slow-motional regime where the opposite trend would be observed (decreased temperature results in increase relaxation time). Over the next five hours, the ^{19}F T_1 time was maintained a constant value between 16.6 and 16.8 s. Lowering the sample temperature did not elicit a drop in relaxation time of the magnitude that had been observed.

From 20.5 to 22.5 hrs the probe temperature was slowly raised in 10 K increments to 290 K. There appears to be a downward trend in Figure 6.3 during these time points. As probe temperature is raised, the ^{19}F T_1 time drops slightly. This trend is consistent with a sample being in the slow-motional regime.

From 23 to 38 hrs, the probe temperature was kept constant during acquisition (290 K). If the increase in relaxation was related to sample spinning, storing the sample in the auto-sampler between relaxation measurements should have led to a

change in relaxation times by returning to the initial value. During relaxation measurements, the sample was spun at 15 kHz. The relaxation time dropped slightly to approximately 15.5 s, spiking once to 17.9 s. After 38 hrs, no significant drop in ^{19}F T_1 time had occurred despite having spent 12.5 consecutive hours not spinning in the auto-sampler. The sample temperature had been lowered and raised, and the sample was static between relaxation measurements with no dramatic change in relaxation time.

Next, the rotor was removed from the spectrometer and stored in a desiccator in a laboratory freezer (~265 K) for 2 hrs. At 40 hrs from the start of the relaxation profile, the rotor was reinserted in the probe (290 K), spun to 15 kHz, and the ^{19}F T_1 time was measured. The ^{19}F T_1 time dropped to 4.5 s. The two hours the sample was static was a much shorter time then had been previously monitored. The freezer temperature was in the range of temperatures that had not induced a significant relaxation time change. The ^{19}F T_1 time was measured (41.5 hrs) after spinning 1.5 hours to display the increase in relaxation rate (13.6 s)., which was consistent with previous observations.

Sample temperature during acquisition and between measurements caused little or no change to the relaxation time. Although water content and residual methanol had not been directly tested, the hypothesis of their contribution relied on an environment created by spinning at high speeds. When the rotor was static between time points from 23 to 38 hrs, little or no change in ^{19}F T_1 time was observed. The relaxation times were not significantly affected by not spinning the sample between

measurements. The reverse kinetics of the relaxation phenomenon were not well understood, but the ^{19}F T_1 time had dropped from 15.7 to 4.5 s in 1.5 hrs. The set of experiments directly or indirectly illustrated that the relaxation changes observed were not due to spinning, temperature, water content, or residual methanol. However the process method, and the presence of oxygen gas was not eliminated.

Amorphous triamcinolone was prepared again, but this time by cryogrinding to remove any factors due to sample generation. The relaxation time was measured with both inversion recovery and saturation recovery pulse sequences to reaffirm that it was not a systematic error of the pulse sequence. The ^{19}F T_1 time rose from 4.5 to 8.3 s using the saturation recovery experiment, and 4.2 to 7.2 s with the inversion recovery experiment. The relaxation profile had a similar shape to that of the spray-dried amorphous triamcinolone. However, the maximum ^{19}F T_1 time of 8.3 s was considerably lower than the 19.5-s ^{19}F T_1 time of the spray-dried amorphous triamcinolone. The amorphous generation process was not the cause of the effect; however; different samples produced different maxima. All of the proposed hypotheses had been disproved with the exception of the effects of oxygen.

To determine if oxygen played a role in reducing the relaxation, amorphous triamcinolone sample was studied in four oxygen environments: high oxygen gas environment (rotor purged with oxygen gas), medium oxygen gas environment (the rotor was opened to ambient conditions), low oxygen environment (purged with nitrogen gas), and a very low environment (spun at 15 kHz for two hrs). After each change in oxygen concentration, the relaxation time was measured, and reported as

follows: 1.4 s, 3.9 s, 5.1 s, and 9.8 s. When exposed to oxygen, the relaxation dropped to the lowest observed ^{19}F T_1 value for amorphous triamcinolone. As the oxygen concentration decreased, the relaxation time increased.

This result suggested that the changes in relaxation time were caused by a reduction in paramagnetic oxygen by a nitrogen purge during data acquisition. The probe was connected to several lines delivering nitrogen gas; bearing and drive gas for spinning, frame cooling line, variable temperature lines, and nitrogen gas was used to insert and eject rotors from the auto-sampler to the probe. At all points of the study, the sample was exposed to nitrogen levels that were far greater than ambient percentages until the rotor was removed from the spectrometer. Even when the sample was stored in the auto-sampler the positive pressure created from the nitrogen gas in the frame cooling exited through the auto-sampler. The return to the depressed relaxation rate is as quick as it takes ambient gas to reenter the rotor. The rise of the relaxation rate when exposed to nitrogen gas is dependent on sample packing and end cap seals. A tighter drive tip seal could explain the difference in the slope and maxima of the relaxation profiles. The phenomenon was much more dramatic for the ^{19}F T_1 time rather than for the ^{1}H T_1 times for amorphous triamcinolone.

Once changes in partial pressures of oxygen gas were identified as the likely cause of the changes in relaxation time, a sample of spray-dried amorphous triamcinolone was used to test the hypothesis. First, a rotor containing amorphous triamcinolone was purged for one minute with oxygen gas and gas sealed. Under exposure to oxygen, the measured ^{19}F T_1 time was 1.7 s. The sample was spun for 48

hours to purge with nitrogen gas. The measured T_1 time after purging was 27.9 s. Lastly, to demonstrate the reversibility, the sample was purged with oxygen gas a second time, and the ^{19}F T_1 decreased to 1.5 s. This result confirms that oxygen is the source of the changes in relaxation time.

The changes in relaxation time by oxygen was demonstrated on a single solid form of a single small-molecule compound, but there is the question of how generalized this phenomenon is to other solid forms, other NMR nuclei (e.g. ^1H), and polymers. To test this, several other compounds were studied to display the presence or lack of effect in different pharmaceutically related systems. In the following examples the effect is displayed in multiple nuclei, multiple solid forms (crystalline and amorphous), with small molecules, and excipients.

6.3.3 Dextran

Dextran is a polysaccharide consisting of glucose molecules joined in various lengths. The effect was measured on dextran in a similar manner as amorphous triamcinolone. The relaxation time was measured every few hours and plotted against time in Figure 6.4. The sample was spun over a period of 18 hrs and the ^1H T_1 relaxation time was monitored throughout. The relaxation rate climbed from approximately 3.6 s initially to approximately 4.3 s after 18 hrs. The ^1H T_1 time increased approximately 20%. After 18 hrs, the relaxation had not fully reached a maximum as the relaxation time was still climbing. At 19 hrs the sample was ejected and stored in the auto-sampler to demonstrate that being out of the probe/magnet, at

ambient temperature, and static had little effect on relaxation time. The relaxation time dropped slightly (4.2 s), yet not to the original value. The drop in time could be due to a slightly higher concentration of oxygen gas in the auto-sampler. The rotor was removed from the magnet and placed on the lab bench at ambient temperature and pressure. The measured relaxation time had dropped to 3.8 s, near the original value. The effect is reversible and noticeable at changes less than an order of magnitude. Oxygen exposure to dextran changes the ^{1}H T_1 relaxation time. Dextran is a high molecular weight amorphous polymer, with no ^{19}F atoms, aromaticity or conjugated bond systems, yet it still displays the relaxation effects upon exposure to oxygen.

6.3.4 Crystalline dexamethasone

Similar to triamcinolone and dextran, the relaxation time profile of as-received dexamethasone was measured every two hours for 16 hours. The ^{19}F T_1 relaxation time profile is plotted in Figure 6.5. The ^{19}F T_1 time was initially 56.3 s and plateaued at approximately 60.5 s. The ^{1}H T_1 time was also monitored during this experiment, and it did not change appreciably (T_O=2.30 s, T_F =2.29 s) over 16 hours. When the sample rotor was removed from the probe, opened to ambient air, closed, and reinserted, neither the ^{19}F T_1 time (59.9 s), nor the ^{1}H T_1 time (2.26 s) dropped appreciably. The ^{19}F T_1 time did not return to its original measurement of 56.3 s after opening and measuring the sample T_1 again (indicated by the ■ in Figure 6.5). There are several explanations for the ^{19}F T_1 time not returning to its

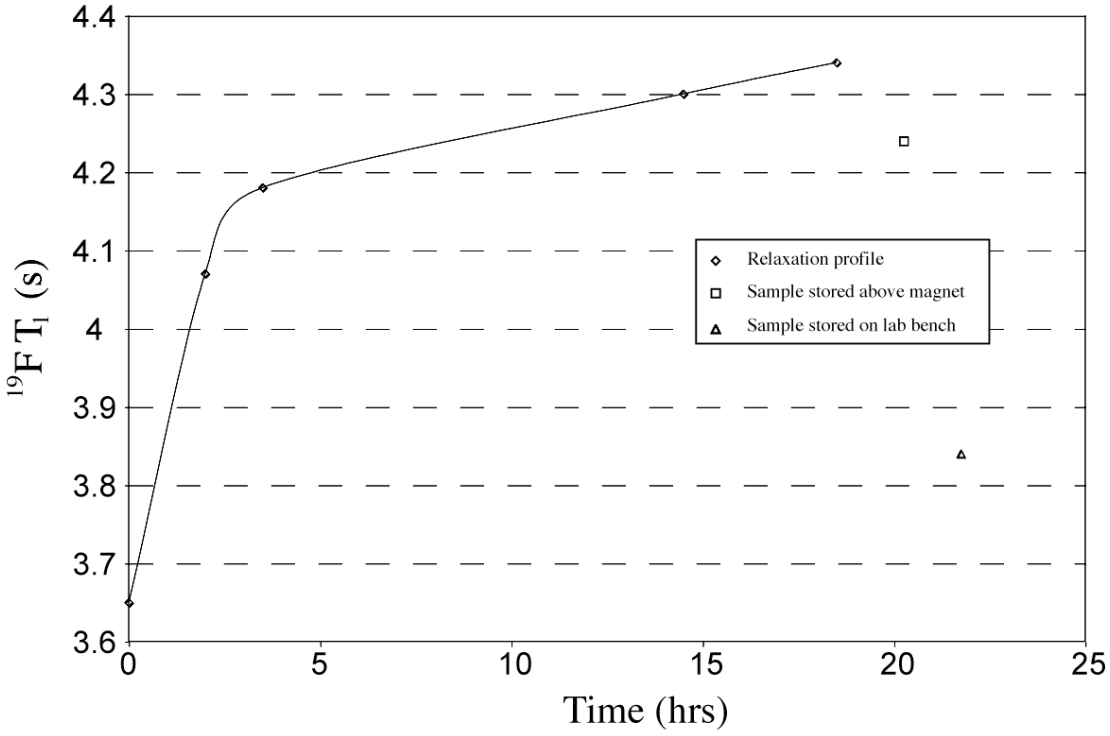

Figure 6.4. Dextran ^{1}H T_1 relaxation time profile.

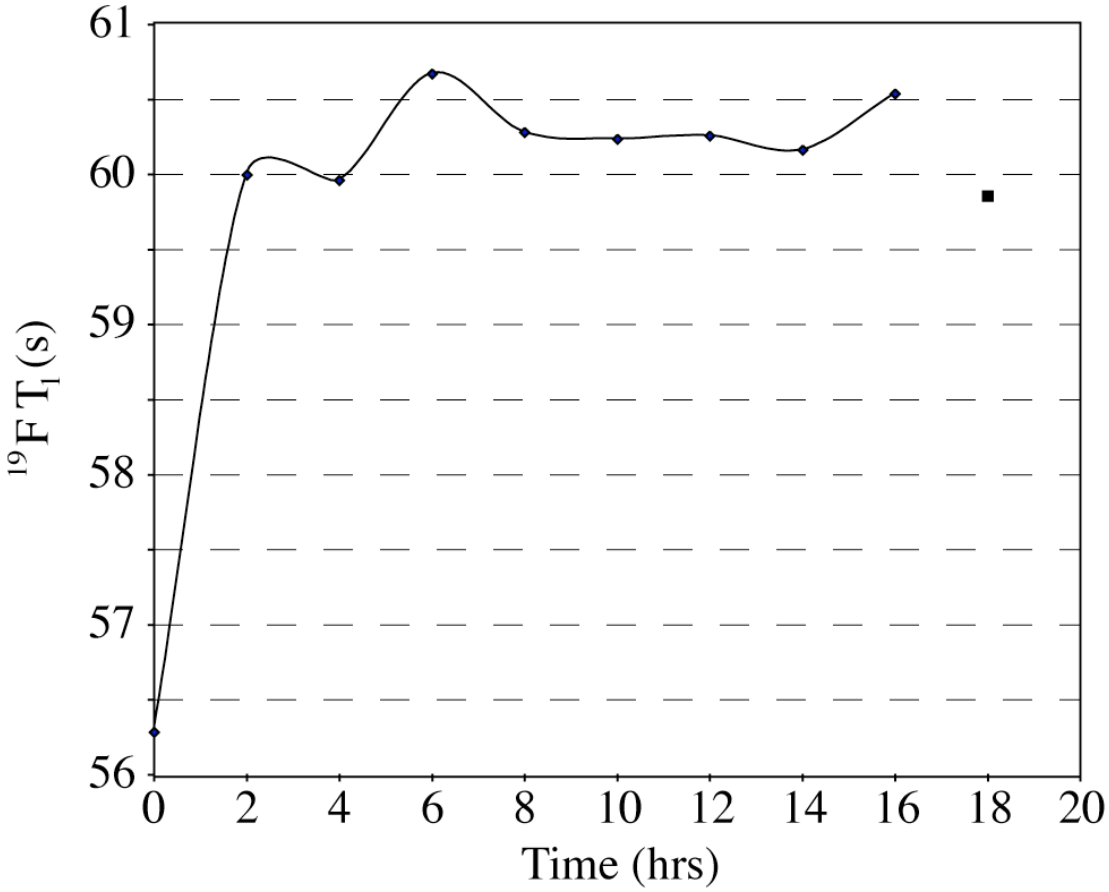

Figure 6.5. a) ◆ ^{19}F T_1 relaxation time profile of as-received crystalline dexamethasone and b) ▪ the same sample measured again after removing from the probe, opening the rotor, and reinserting into the probe.

originally measured value. First, the observed change in relaxation time could have been due to sample healing while spinning at high speeds. Crystal healing would be observed as a non-reversible relaxation change. Secondly, it could be due to instrumental operation error. The probe could have arced causing a change in the SNR of an increment in the relaxation measurement. The arcing could be the reason for a lower time point. In relaxation studies, the associated error is dependent on the number of increments acquired and the number of acquisitions per increment. Typically, an error of +/-10% is associated with these measurements. The initial time point is within this range, but well beyond the limits of every other measured time point in the experiment. For crystalline dexamethasone, oxygen gas has no observable effect on the ^{1}H and ^{19}F T_1 times.

6.4 Other Applications

There are many potential applications where the ability to control the relaxation time could be beneficial for sample analysis. A few of these potential applications are discussed below.

6.4.1 Difference-NMR technique

The selectivity enhancement in a difference-NMR experiment is directly related to the ratio of the relaxation rates of the components in a sample. In the case of detecting low levels of amorphous triamcinolone, purging with oxygen gas yields

an unquestionable advantage by reducing the ^{19}F T_1 time of the amorphous form and not affecting the ^{19}F T_1 of the crystalline form. To control the change in relaxation time, the samples were purged with oxygen gas and capped with O-ring sealed end caps. The increased partial pressure of oxygen gas reduced the 3.6 s ^{19}F T_1 relaxation time of amorphous triamcinolone to 1.2 s without significantly affecting the relaxation time of crystalline triamcinolone (105 s). The ratio of relaxation times between the crystalline and amorphous forms increased from 29 times to 88 times. Such a powerful effect has not been demonstrated for SSNMR magic-angle spinning applications. Spin-lattice relaxation time changes upon exposure to oxygen could allow for a multitude of research opportunities.

6.4.2 Processing of aspirin

In addition to the benefits from the difference-NMR technique, a brief study of aspirin is included to illustrate a potential application. As a pure powder, aspirin is known to have one stable crystalline form and remain crystalline despite conditions in which the material was processed. In our laboratory, the ^{1}H T_1 time of bulk aspirin and cryoground samples were measured.[12] After cryogryinding for 2 minutes, the T_1 time decreased to 42 s. Upon grinding for 60 minutes, it dropped to 14 s. The spectrum of each cryoground sample and the bulk sample were identical indicating no change in solid form.

In these studies, the ^{1}H T_1 times of bulk aspirin were compared to aspirin that had been cryoground for 20 minutes. Both samples were cycled between an oxygen

gas purge, a nitrogen gas purge, and another oxygen gas purge to observe the range of differences between the relaxation times. After each purge, the ^{1}H T_1 time was measured. In Figure 6.5, the T_1 times of bulk unprocessed aspirin were compared to the times for cryoground aspirin at each environment. Unprocessed aspirin shows a small change in relaxation from an oxygen-purged environment to a nitrogen-purged environment. Cryoground aspirin, which is the same crystalline form and has an identical SSNMR spectrum, had a relaxation time of 8.6 s. When purged with nitrogen gas, the relaxation time increased to 55.5 s. After the nitrogen purge, the relaxation time was much closer to the relaxation time (59.5 s) of the unprocessed aspirin.

In the case of processed lactose, the drastic changes in relaxation time were attributed to increased sites of high mobility, more specifically crystal defect sites, reduced particle size, and generation of amorphous material.[2] As mentioned before, an amorphous form cannot be generated from pure aspirin. Therefore, the reduction in relaxation time was likely due to an increased number of crystal defect sites and a reduction in particle size. Both a decrease in particle size and generation of crystal defects would allow oxygen to penetrate the crystal lattice more effectively. Oxygenating samples could potentially help study the presence of crystal defects in pharmaceutical solids.

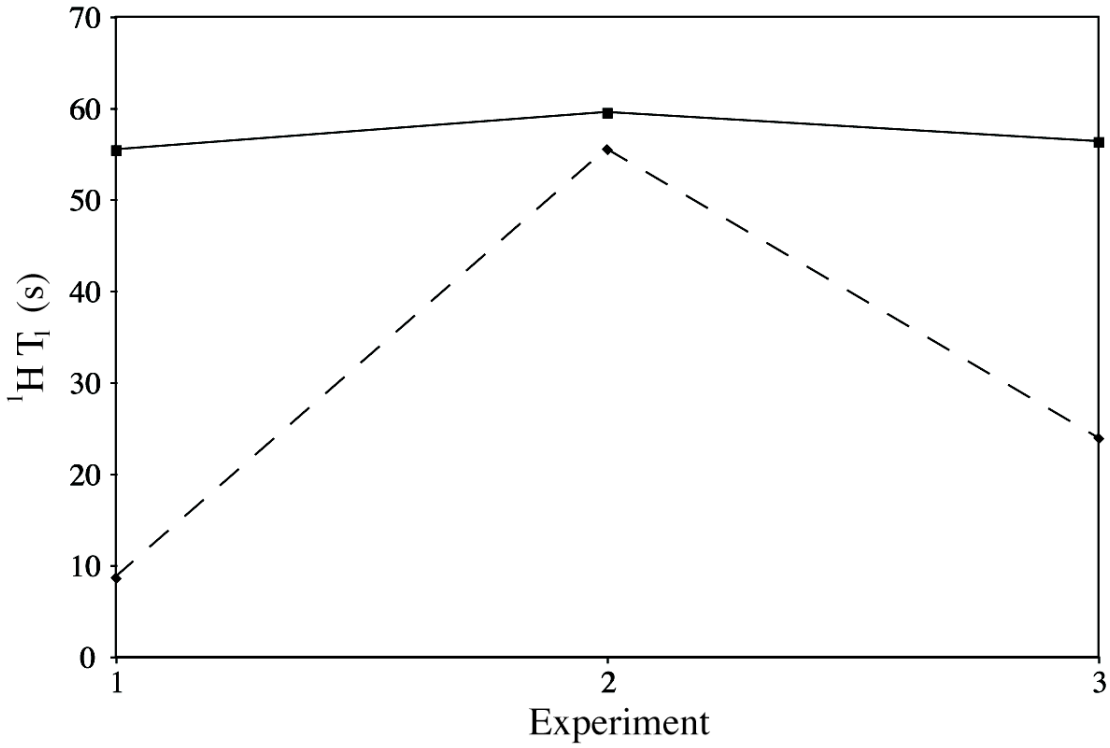

Figure 6.6. The ^{1}H T_1 times of as-received aspirin (solid line) and cryoground aspirin (dashed line) after (**1**) purging with oxygen, (**2**) purging with nitrogen, and (**3**) purging with compressed oxygen again.

6.5 Conclusions

The partial pressure of oxygen gas has been demonstrated to have a dramatic effect on the ^{19}F and ^{1}H spin-lattice relaxation times of several representative pharmaceutical compounds. The effect on relaxation should be well understood especially when acquiring SSNMR data while spinning with nitrogen gas. Changes in the level of oxygen could affect the sensitivity of your experiment, particularly important while quantitating.

The presence of oxygen has been demonstrated to dramatically effect both ^{1}H and ^{19}F relaxation times. Processing a material can affect the magnitude of the relaxation effect when oxygen is present, as was the case for aspirin.

Although there are potentially intriguing applications for the use of paramagnetic oxygen, the changes in relaxation time highlight the importance in understanding the physical environment of a material before and during SSNMR data collection.

6.6 References

1. Offerdahl TJ, Salsbury JS, Dong Z, Grant DJW, Schroeder SA, Prakash I, Gorman EM, Barich DH, Munson EJ 2005. Quantitation of crystalline and amorphous forms of anhydrous neotame using 13C CPMAS NMR spectroscopy. Journal of Pharmaceutical Sciences 94(12):2591-2605.

2. Lubach JW, Xu D, Segmuller BE, Munson EJ 2007. Investigation of the effects of pharmaceutical processing upon solid-state NMR relaxation times and implications to solid-state formulation stability. Journal of Pharmaceutical Sciences 96(4):777-787.

3. Barich DH, Davis JM, Schieber LJ, Zell MT, Munson EJ 2006. Investigation of solid-state NMR line widths of ibuprofen in drug formulations. Journal of Pharmaceutical Sciences 95(7):1586-1594.

4. Prosser RS, Luchette PA 2004. An NMR study of the origin of dioxygen-induced spin-lattice relaxation enhancement and chemical shift perturbation. Journal of Magnetic Resonance 171(2):225-232.

5. Prosser RS, Luchette PA, Westerman PW 2000. Using O2 to probe membrane immersion depth by 19F NMR. Proceedings of the National Academy of Sciences of the United States of America 97(18):9967-9971.

6. Prosser RS, Luchette PA, Westerman PW, Rozek A, Hancock REW 2001. Determination of membrane immersion depth with O2: a high-pressure 19F NMR study. Biophysical Journal 80(3):1406-1416.

7. Capitani D, De Rosa C, Ferrando A, Grassi A, Segre AL 1992. Polymorphism in syndiotactic polystyrene: a proton NMR relaxation study. Macromolecules 25(15):3874-3880.

8. Capitani D, Segre AL, Barsacchi M, Pentimalli M 1999. Poly-1-oxy-2-phenyltrimethylene as studied by 1H pulsed low resolution NMR: a possible oxygen scavenger. European Polymer Journal 35(4):681-690.

9. Capitani D, Segre AL, Blicharski JS 1995. Oxygen-Doped Polymers: An 1H NMR Spin-Lattice Relaxation Study. Macromolecules 28(4):1121-1128.

10. Capitani D, Segre AL, Grassi A, Sykora S 1991. Pulsed proton NMR relaxation in crystalline syndiotactic polystyrene. Macromolecules 24(2):623-624.

11. Capitani D, Sertge AL 1997. Relaxometric study of oxygen absorption on aromatic polymers. Polymer Preprints (American Chemical Society, Division of Polymer Chemistry) 38(1):792-793.

12. Lubach JW. 2007. Applications of Nuclear Magnetic Resonance Spectroscopy to Pharmaceutical Solids. Pharmaceutical Chemistry, ed., Lawrence: University of Kansas. p 259.